Ultrasound-induced polymer reaction engineering in high-pressure fluids

Ultrasound-Induced Polymer Reaction Engineering in High-Pressure Fluids

PROEFSCHRIFT

ter verkrijging van de graad van doctor aan de
Technische Universiteit Eindhoven, op gezag van de
Rector Magnificus, prof.dr. R.A. van Santen, voor een
commissie aangewezen door het College voor
Promoties in het openbaar te verdedigen
op dinsdag 2 november 2004 om 16.00 uur

door

Martijn Willem Anton Kuijpers

geboren te Breda

Dit proefschrift is goedgekeurd door de promotoren:
prof.dr.ir. J.T.F. Keurentjes
en
prof.dr. ir. M.M.C.G. Warmoeskerken

Copromotor:
dr.ir. M.F. Kemmere

Het leven bestaat, dus geniet ervan.

Summary

The chemical effects of ultrasound arise from cavitation, i.e. the collapse of microscopic bubbles in a liquid. Upon implosion of a cavity, extreme conditions in the bubble occur (5000 K and 200 bar) and high strain rates are generated outside the bubble (10^7 s^{-1}). Monomer molecules are dissociated by the high temperature inside the hot-spot, whereas polymer chains are fractured by the high strain rates outside the cavitation bubble. These two reactions lead to the formation of radicals, which can initiate a free-radical polymerization. Experimental results show that the majority of the radicals are generated by scission of polymer chains.

An important parameter in ultrasound-induced bulk polymerizations is the viscosity. Upon reaction the long chains formed cause a drastic increase in the viscosity. A high viscosity hinders cavitation and consequently reduces the production rate of radicals. Precipitation polymerization forms a potential solution to this problem, because a constant viscosity and hence a constant reaction rate can be maintained. In this perspective, high-pressure carbon dioxide (CO_2) is an interesting medium as most monomers have a high solubility in CO_2, whereas it exhibits an anti-solvent effect for most polymers.

Up till now ultrasound has rarely been studied at higher pressures, because in ordinary liquids a high static pressure hampers the growth of cavities. Unlike ordinary liquids, the higher vapor pressure of a dense-phase fluid (which is a gas at ambient conditions) allows cavitation to occur at increased static pressures. In this work, it has been proven experimentally that cavitation in CO_2-expanded methyl methacrylate (MMA) leads to the formation of hot-spots and subsequent radical formation from MMA.

In addition, the possibility to generate cavities and hot-spots in CO_2-expanded MMA has been modeled with the Blake threshold pressure and a dynamic bubble model based on the Rayleigh-Plesset equation. Still, these two models cannot explain the experimentally observed cavitation thresholds with increasing CO_2-pressure for the MMA/CO_2-system. Since these models are based on equilibrium conditions, they do not take mass transfer into account. Therefore, a mass transfer model has been employed to describe the growth of cavitation bubbles by ultrasound at increased static pressures. Modeling CO_2 transport in the liquid phase towards the bubble has shown that mass transfer is limiting in the CO_2/MMA-system when a bubble is growing.

Moreover, the influence of CO_2 on the viscosity and the reaction kinetics of the ultrasound-induced polymerization of MMA has been studied. The polymerization reactions have yielded high-molecular weight polymers. The phase behavior and the CO_2 fraction of the MMA/CO_2-system have been calculated with the Lee-Kessler-Plöcker equation of state. The required binary interaction parameter for these calculations has been determined by measuring the phase behavior of the high-pressure fluids. The influence of the CO_2 concentration on the viscosity of polymer solutions has been investigated by coupling the viscosity of the reaction mixtures to the overall heat transfer coefficient, as determined by temperature oscillation calorimetry. In contrast to polymerizations in bulk, a low viscosity is maintained during polymerization reactions in CO_2-expanded MMA. As a consequence, a constant or even increasing polymerization rate is experimentally observed when pressurized CO_2 is applied.

Besides polymerizations, ultrasound-induced polymer scission reactions have been investigated. Ultrasound-induced polymer scission is a well-controlled process, as fracture occurs approximately in the middle of the chain. A mechanism is proposed for this non-random fracture behavior, from which it can be concluded that complete stretching of the polymer chains is required before breakage can occur. The developed model, which is a combination of strain rate and drag force calculations, predicts a

limiting molecular weight and a quadratic dependence of the polymer molecular weight on the scission rate, which have experimentally been confirmed. The developed degradation model is also capable to describe the effects of various process variables on cavitation-induced polymer scission, such as the lower scission rate at a higher liquid viscosity.

At increasing polymer concentration, the scission process becomes less effective and eventually stops. This is a drawback for the development of a scission process based on ultrasound, as concentrated polymer systems are favored in industry. The addition of an anti-solvent for the polymer can prevent the increase in viscosity at higher polymer concentrations. To determine the influence of CO_2 as an anti-solvent on the ultrasound-induced scission rate, ultrasonic scission experiments of polymethyl methacrylate (PMMA) have been performed in bulk MMA as well as in CO_2-expanded MMA. Modeling the experimental time-dependent molecular weight distributions (MWD) has revealed the scission kinetics at different polymer concentrations and CO_2 fractions. From these results it can be concluded that it is possible to alter the MWD of polymers by ultrasound in concentrated polymer solutions, due to the CO_2 anti-solvent effect.

A challenge in ultrasound-induced reaction engineering is the relatively low energy efficiency (10^{-5} J/J) for the generation of radicals in the ultrasound process. For the development of an economically feasible bulk process (> 5000 kg/hr), the energy conversion still needs to be improved, for instance by using different liquids or ultrasound sources. For specialty products, however, it is expected that an ultrasound-based process can be already viable. Therefore, a preliminary process design has been made for the ultrasound-induced production of 10 kg/hr PMMA for application as specialty polymer in biomedical materials. This has resulted in a clean, closed-loop process to produce PMMA in CO_2-expanded MMA, without the use of initiators or organic solvents.

From this work can be concluded that ultrasound allows for polymer reaction engineering without additional chemicals, leading to the development of sustainable, well-controlled polymer processes. Furthermore, it is anticipated that the possibility of cavitation in high-pressure fluids is not limited to polymerization reactions. Other potential ultrasound applications in liquid CO_2 are ultrasound-induced phase transfer catalysis and ultrasound-assisted extraction of organic compounds, in which ultrasound can accelerate these processes due to micro-streaming. Moreover, gas-expanded liquids can be used in combination with ultrasound to carry out oxidation or hydrogenation reactions, because of the high solubility of hydrogen and oxygen in these types of fluids.

Samenvatting

De chemische effecten van ultrasoon geluid komen voort uit cavitaties, het imploderen van microscopische bellen in een vloeistof. Op het moment van implosie van een cavitatiebel ontstaan extreme omstandigheden in de bel (5000 K en 200 bar) en hoge afschuifsnelheden buiten de bel (10^7 s^{-1}). Monomeermoleculen dissociëren door de hoge temperaturen van de zogenaamde hot-spot, terwijl polymeerketens breken door de hoge afschuifsnelheden buiten de cavitatiebel. Deze twee reacties leiden tot de vorming van radicalen die een polymerisatiereactie kunnen initiëren. Experimentele resultaten laten zien dat de meerderheid van de radicalen gevormd wordt door het knippen van polymeerketens.

De vloeistofviscositeit is een kenmerkende grootheid van ultrasoon-geïnduceerde bulkpolymerisaties. De door reactie onstane lange polymeer-ketens veroorzaken een drastische stijging van de viscositeit. Deze hoge viscositeit hindert cavitatie en hierdoor de vorming van radicalen. Precipitatiepolymerisatie is een mogelijke oplossing voor dit probleem, doordat een constante viscositeit en derhalve een constante radicaalvormingssnelheid behouden kan worden. Vanuit dit oogpunt is hoge druk koolstofdioxide (CO_2) een interessant medium, doordat de meeste monomeren goed oplossen in CO_2 terwijl het een zeer slecht oplosmiddel is voor de meeste polymeren.

Tot nu toe is ultrasoon geluid zelden bestudeerd in hogedruksystemen, aangezien normaliter een hoge statische druk de groei van cavitatiebellen in vloeistoffen belemmert. In tegenstelling tot normale vloeistoffen, zorgt de hoge dampspanning van hoge druk vloeistoffen (een gas bij atmosferische condities) ervoor dat wel cavitatie bij verhoogde statische druk kan optreden. In dit werk is experimenteel aangetoond dat cavitaties in CO_2-geëxpandeerd methylmethacrylaat (MMA) leidt tot de vorming van hot-spots en de daaropvolgende radicaalvorming uit MMA.

Bovendien is de mogelijkheid om cavitaties en hot-spots te genereren in CO_2-geëxpandeerd MMA gemodelleerd met de Blake grenswaarde en een dynamisch belmodel dat gebaseerd is op de Rayleigh-Plesset vergelijking. Deze twee modellen kunnen niet de experimenteel waargenomen cavitatie-grenswaarden beschrijven met een toenemende CO_2 druk in het MMA/CO_2-systeem. Dit komt doordat de modellen gebaseerd zijn op evenwichtcondities, waardoor massatransport niet inbegrepen is. Modelering van het CO_2 transport naar de bel laat zien dat massatransport van CO_2 gelimiteerd is in het MMA/CO_2-systeem bij een groeiende bel. Massatransport van CO_2 dient dus in het dynamisch belmodel opgenomen te worden om cavitatie te beschrijven in gas-geëxpandeerde vloeistoffen.

Tevens is de invloed van CO_2 op de viscositeit en de reactiekinitiek van de ultrasoongeïnduceerde polymerisaties van MMA bestudeerd. De polymerisaties resulteren in polymeren met een hoog moleculair gewicht. Het fasegedrag en de CO_2 fractie van het MMA/CO_2-systeem zijn berekend met de Lee-Kessler-Plöcker toestandsvergelijking. De benodigde binaire interactie parameter voor deze berekeningen is bepaald door metingen aan het fasegedrag. De invloed van de CO_2-concentratie op de viscositeit is onderzocht door de viscositeit van het reactiemengsel te koppelen aan de totale warmteoverdrachtscoefficient die bepaald is met temperatuur oscillatie calorimetrie. In tegenstelling tot bulkpolymerisaties wordt een lage viscositeit behouden gedurende polymerisaties in CO_2-geëxpandeerd MMA, hetgeen tot gevolg heeft dat een constante of zelfs toenemende polymerisatiesnelheid wordt gevonden wanneer hoge druk CO_2 wordt gebruikt. Door de constante viscositeit is het mogelijk om hogere conversies te bereiken in CO_2-geëxpandeerd MMA vergeleken met bulk MMA.

Naast polymerisaties zijn ultrasoongeïnduceerde polymeerknipreacties onderzocht. Het knippen van polymeerketens geïnduceerd door ultrasoon geluid is een goed gecontroleerd proces, doordat breuk van de keten ongeveer in het midden van het polymeermolecuul plaats vindt. Een mechanisme voor dit niet willekeurig knipgedrag is ontwikkeld, waaruit geconcludeerd kan worden dat de keten volledig gestrekt dient te zijn

voordat deze gebroken kan worden. Het ontwikkelde model, dat een combinatie is van afschuifspannings- en weerstandsberekeningen, voorspelt een limiterend molecuulgewicht en een kwadratische afhankelijkheid van het polymeer molecuulgewicht op de knipsnelheid. Het limiterende molecuulgewicht en de kwadratische afhankelijkheid zijn beide experimenteel bevestigd. Het ontwikkelde model is tevens in staat om de invloeden van verschillende procescondities op het cavitatiegeïnduceerd knippen te beschrijven, zoals de lagere knipsnelheid bij hogere vloeistofviscositeiten.

Bij toenemende polymeerconcentraties wordt het knipproces minder effectief en stopt uiteindelijk. Dit is een nadeel voor de ontwikkeling van polymeerknipprocessen gebaseerd op ultrasoon geluid, omdat geconcentreerde polymeersystemen geprefereerd worden in de industrie. De toevoeging van een anti-solvent voor de polymeren kan de toename in viscositeit bij hogere polymeerconcentraties voorkomen. Om de invloed van CO_2 als een antisolvent op de ultrasoongeïnduceerde breuksnelheid vast te stellen, zijn knipexperimenten met polymethylmethacrylaat (PMMA) in MMA en CO_2-geëxpandeerd MMA uitgevoerd. Modelering van de tijdsafhankelijke molecuulgewichtsverdelingen (MWD) heeft geleid tot het ontrafelen van de knipkinetiek bij verschillende polymeer en CO_2-concentraties. Uit deze resultaten kan geconcludeerd worden dat het mogelijk is de MWD van polymeren te wijzigen in geconcentreerde polymeeroplossingen door middel van ultrasoon geluid dankzij het CO_2 antisolvent effect.

Een uitdaging in ultrasoongeïnduceerd polymeerreactietechnologie is de relatief lage energieconversie (10^{-5} J/J) van het ultrasoonproces. Voor de ontwikkeling van een economisch haalbaar bulkproces (> 5000 kg/uur), dient de energieconversie verbeterd te worden. Dit kan gerealiseerd worden door andere vloeistoffen of andere ultrasoonbronnen te gebruiken. Voor bijzondere producten wordt verwacht dat een op ultrasoon geluid gebaseerd proces haalbaar is. Daarom is een procesontwerp gemaakt voor de ultrasoongeïnduceerde productie van 10 kg/uur PMMA, met als toepassingsgebied biomedische materialen. Dit heeft geresulteerd in een

schoon closed-loop proces voor de productie van PMMA in CO_2-geëxpandeerd MMA, zonder gebruik te maken van initiatoren en organische oplosmiddelen.

Uit dit werk kan geconcludeerd worden dat ultrasoon geluid mogelijkheden biedt voor polymeerreactietechnologie zonder additionele toevoegingen. Dit leidt tot de ontwikkeling van duurzame, goed gecontroleerde polymeer processen. Bovendien wordt verwacht dat de mogelijkheid van cavitaties in hoge druk vloeistoffen niet gelimiteerd blijft tot polymerisaties. Andere potentiële ultrasoontoepassingen in vloeibaar CO_2 zijn de ultrasoongeïnduceerde faseoverdrachtkatalyse en ultrasoon-geassisteerde extractie van organische componenten, waarin de ultrasoon opgewekte microstroming deze processen kan versnellen. Verder kunnen gasgeëxpandeerde vloeistoffen in combinatie met ultrasoon geluid gebruikt worden om oxidaties of hydrogenaties uit te voeren, mede door de hoge oplosbaarheid van zuurstof en waterstof in deze vloeistoffen.

Contents

Chapter 9

Application Potential of Ultrasound Reaction Engineering **125**

1 Ultrasound-induced Polymerization and Polymer Scission

Polymers belong to the most important products of the chemical industry in modern society. Therefore, it is important that polymers can be produced in an environmentally safe and clean manner. Typically, in the production process catalysts or initiators are used to start the polymerization reaction, but may also contaminate the final product. These chemicals can be made redundant by using ultrasound, as it can produce radicals in situ from the reactants. An additional advantage of this technique is the intrinsic safe operation, because turning off the electrical power supply will immediately stop the radical formation and consequently the polymerization reaction. In this thesis, the possibility to produce polymers in high-pressure fluids via ultrasound-induced radical formation is studied. In this chapter the basics of ultrasound, cavitation and ultrasound-induced polymer reactions are discussed.

This chapter is partially based on: M.W.A. Kuijpers, M.F. Kemmere, J.T.F. Keurentjes Ultrasound-induced radical polymerization, *Encyclopedia of Polymer Science and Technology*, John Wiley & Sons, New York, 2004

1.1 Ultrasound

Sound passes through an elastic medium as a longitudinal wave, i.e. as a series of alternating compressions and rarefactions. This induces liquid to be displaced parallel to the direction of motion of the wave. Ultrasound is a sound wave with a frequency typically in the range of 20 kHz up to approximately 500 MHz.[1] The frequency (f) and the acoustic amplitude ($P_{A,max}$) are the most important properties to characterize the pressure wave. The variation of the acoustic pressure (P_A) of an ultrasound wave as a function of time (t) at a fixed frequency is described by Equation 1.1.[2]

$$P_A = P_{A,\max} \cdot \sin(2 \cdot \pi \cdot f \cdot t) \qquad (1.1)$$

Based on the applied frequency, the use of ultrasound can be broadly divided into two areas:

- Low intensity, high frequency ultrasound (2-500 MHz, 0.1-0.5 W/cm^2)
- Power ultrasound with a high intensity and a low frequency (20-900 kHz, >10 W/cm^2).

The first type of ultrasound does not alter the state of the medium through which it travels and is commonly used for non-destructive evaluation and medical diagnosis.[3] This type of ultrasound cannot be used for reactions. Contrarily, power ultrasound uses the energy to create cavitations, which involves the formation, growth, and implosive collapse of microscopic bubbles in a liquid.[4] These bubbles are generated when the "negative" pressure during the rarefaction phase of the sound wave is sufficiently large to disrupt the liquid, see Figure 1.1. The implosive collapse of the bubbles can locally produce extreme temperatures and pressures. These hot-spots can lead to irreversible changes. Power ultrasound is applied for cleaning purposes, treatment of kidney stones, plastic welding, and for chemical reactions. Table 1.1 summarizes the applications of the different types of ultrasound.[5]

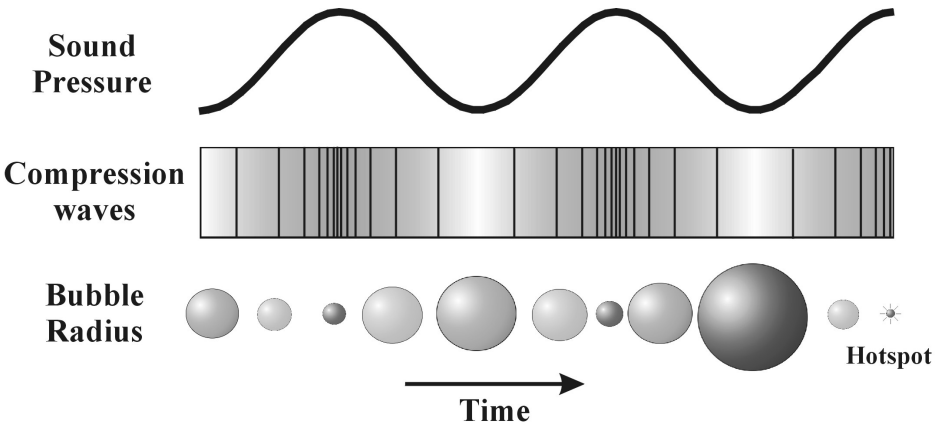

Figure 1.1. Schematic representation of bubble growth and collapse in a liquid irradiated with ultrasound and the resulting hot-spot.

Table 1.1. Overview of different types of ultrasound, including the various applications.

Power ultrasound 20 kHz - 900 kHz	Sonophoresis 20 kHz, low power	Therapeutic ultrasound 1 MHz, high power	Non-destructive ultrasound > 2 MHz, low power
- Sonochemistry - Welding - Cleaning - Cell disruption - Sterilization - Kidney stones	- Trans-dermal drug delivery	- Therapeutic massage - Controlled release	- Flaw detection - Medical diagnoses

1.2 Cavitation

Ultrasound waves in a liquid cause the molecules to oscillate around their mean position. During the positive-pressure cycle the distance between molecules decreases, while during the negative pressure period the distance increases. At a sufficiently high intensity a critical distance between the molecules is exceeded during the negative pressure period, and a cavity is formed.[6] Due to the presence of nuclei such as dissolved gases and solid impurities, cavities are formed at far lower sound pressures than theoretically predicted.[7] After the formation of a cavity, a critical acoustic pressure has to be overcome to initiate the explosive growth of this bubble. This explosive growth is followed by an implosive collapse (Figure 1.2). During this collapse, the content of the bubble is almost adiabatically heated, which leads to local short-lived hot-spots in the liquid. Depending on the specific conditions, bubble wall velocities, pressures and temperatures in the bubble can increase up to 1500 m/s, 200 bar and 5000 K, respectively.[8]

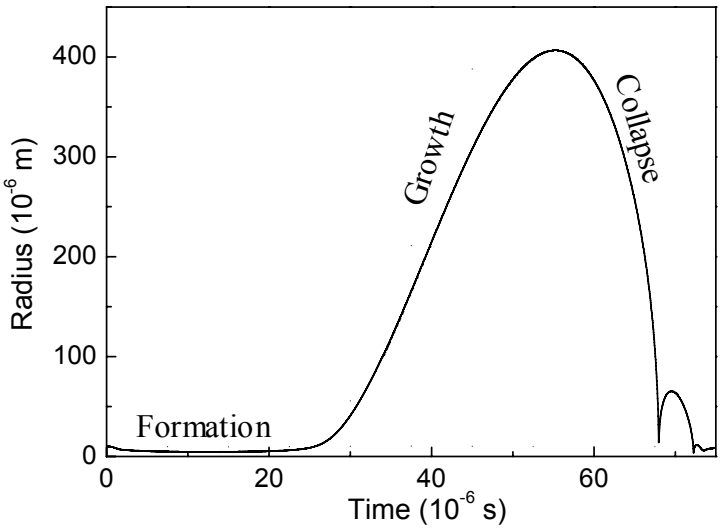

Figure 1.2. Radius-time curve of a cavitation bubble, including the three different phases of cavitation.

The acoustic pressure amplitude determines the growth of a cavitation bubble and consequently the chemical effects upon collapse. The amplitude of the pressure wave can be measured with a hydrophone or can be calculated using a calorimetric method,[9,10] in which it is possible to determine the ultrasound power (Q_{US}) that is transferred to the liquid. With the ultrasound power, the density of the liquid (ρ), the speed of sound in the medium (v) and the surface area of the ultrasound source (A_{US}), the acoustic amplitude can be calculated according to Equation 1.2. The ultrasound intensity is the power-input divided by the surface area of the source.[11]

$$P_{A,\max} = \sqrt{2 \cdot \rho \cdot v \cdot \frac{Q_{US}}{A_{US}}} = \sqrt{2 \cdot \rho \cdot v \cdot I_{US}} \quad (1.2)$$

1.3 Radical formation by cavitation

Radicals are generated by the extreme conditions in the bubble (5000 K and 200 bar)[12] and the high strain rates outside the bubble (10^7 s^{-1})[13] generated upon implosion. Volatile molecules are dissociated by the high temperatures in the hot-spot, whereas significantly large molecules, e.g. polymer chains, are fractured by the high strain rates.[14,15] The rate at which ultrasound-induced reactions occur depends on the molecules present in the bubble during collapse, the speed of collapse, the hot-spot temperature and the number of cavities. The effects of all these parameters can be reduced to the physical properties of the liquid and the physical and chemical processes occurring around and inside the cavity.[16] The most important properties and processes occurring in one single bubble are schematically depicted in Figure 1.3. In general a higher implosion velocity leads to more extreme conditions inside and outside the bubble and consequently a higher ultrasound-induced chemical activity.[17] The number of cavities is determined by the impurities in the liquid, the static pressure, the ultrasound intensity and the vapor pressure. This emphasizes that the overall ultrasound-induced reaction rate is influenced in a complex way.[18,19] In the following, the effects of the most important parameters will be discussed.

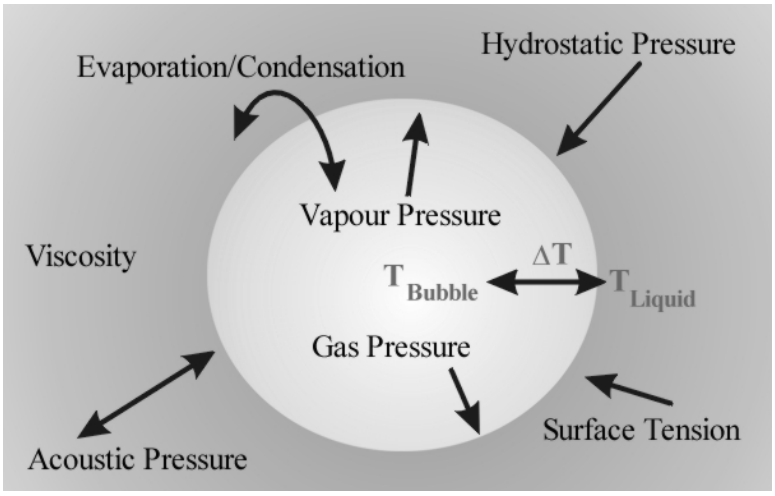

Figure 1.3. Physical properties and processes that determine the bubble growth due to ultrasound.

Temperature. When the reaction temperature is altered, the liquid properties will change. Although these properties (viscosity, surface tension, sound velocity, vapor pressure, etc.) all have an influence on the chemical effect of cavitation, the change in vapor pressure dominates the other liquid properties. As the temperature is raised, the vapor pressure in the bubble is increased, which cushions the implosion of the cavity. This results in a lower local temperature inside the cavity at higher overall temperatures. Consequently, fewer radicals are formed per cavitation bubble. On the other hand, a higher vapor pressure can lead to easier bubble formation. In most cases, however, an increase in reaction temperature will result in an overall decrease in the radical formation rate. Therefore, ultrasound-induced reactions exhibit opposite behavior as compared to common radical reactions.[20]

Static pressure. A high static pressure can prevent the formation of cavitation bubbles. This implies that less or no cavitations are formed at higher static pressures. To counteract this effect a higher acoustic pressure

is required, which will result in a more violent collapse of a cavitation bubble.[21]

Viscosity. At increasing viscosities the growth and collapse of a cavitation bubble is retarded, due to the higher drag force of the liquid. At a certain viscosity the drag force becomes too high and the bubble has insufficient time to grow to a critical radius.[22] If this radius is not reached, no collapse will occur. Additionally, the higher viscosity slows down the collapse, which makes it possible for heat to be transferred to the liquid. Due to this heat transfer, lower hot-spot temperatures are reached and consequently less radicals are being generated.[23]

Ultrasound intensity. At first the radical formation rate will increase to a maximum with increasing ultrasound intensity.[24] This is caused by the higher cavitation intensity per bubble and the larger number of cavitation bubbles. At too high ultrasound intensities, however, a cloud of cavitation bubbles is formed near the ultrasound source, due to which the pressure wave is no longer transmitted efficiently to the liquid. As a result, the cavitation intensity and consequently the radical formation rate decrease with a continued increase in intensity.[24] An optimum radical formation rate with ultrasound intensity can thus be found.

1.4 Cavitation-induced radical polymerizations

Generally, free-radical polymerization consists of four elementary steps; initiation, propagation, chain-transfer and termination.[25] When ultrasound is used to initiate polymerization, radicals can be formed both from monomer and from polymer molecules.[26] This implies that due to radical formation by polymer scission an additional elementary step is introduced in ultrasound-induced polymerization as indicated in Figure 1.4.

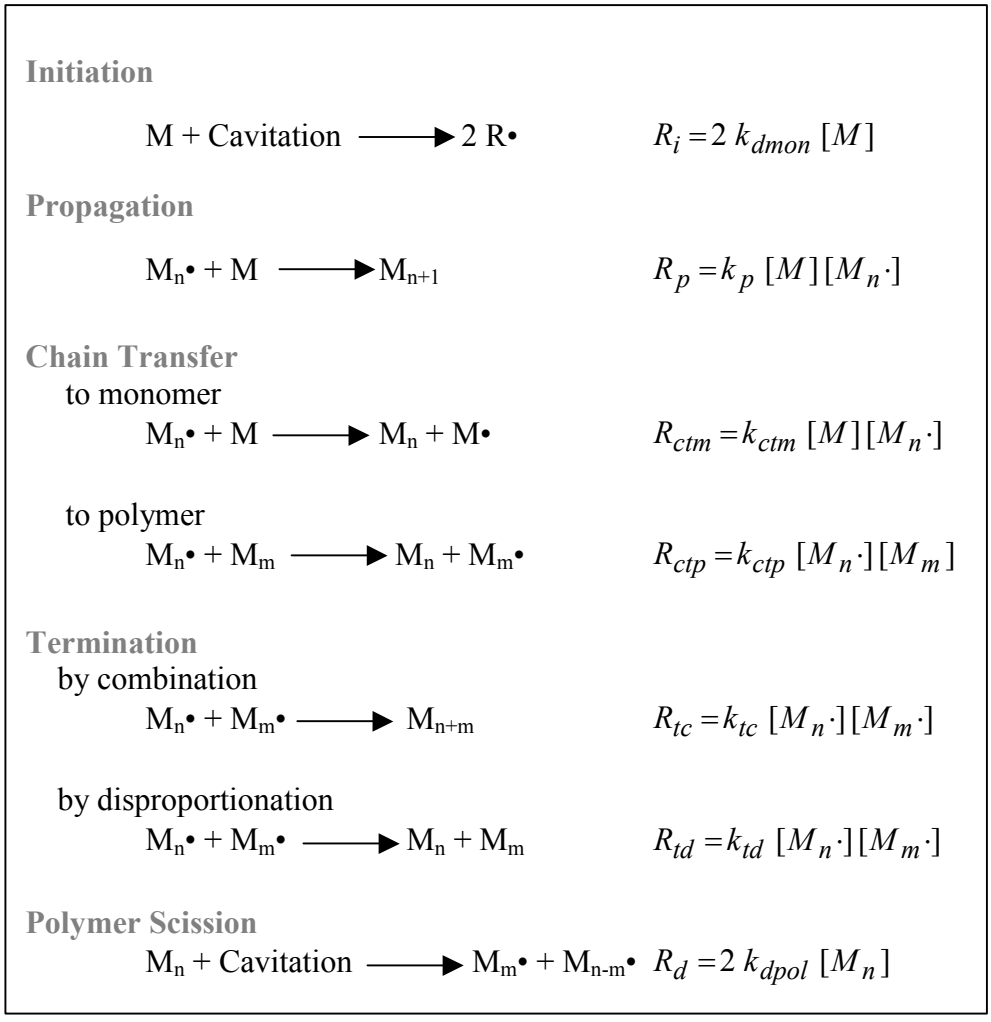

Figure 1.4. Reaction mechanism of ultrasound-induced radical polymerization, assuming intrinsic polymerization and avoiding thermal initiation.

The radicals from polymer and monomer are generated by two different mechanisms. The monomer molecules are dissociated by the high temperatures inside the hot-spot, whereas the polymer chains are fractured by the high strain rates outside the bubble.[27] The majority of the radicals in an ultrasound-induced polymerization reaction originate from the polymer chains.[28] In Figure 1.5, the ultrasound-induced radical formation rate constants from polymer and monomer are shown at different polymer concentrations. The produced radicals by ultrasound can initiate a radical polymerization. It has to be noted that the radicals are only formed in the immediate vicinity of the ultrasound source where cavitation occurs. Subsequently, these radicals are dispersed throughout the reactor.

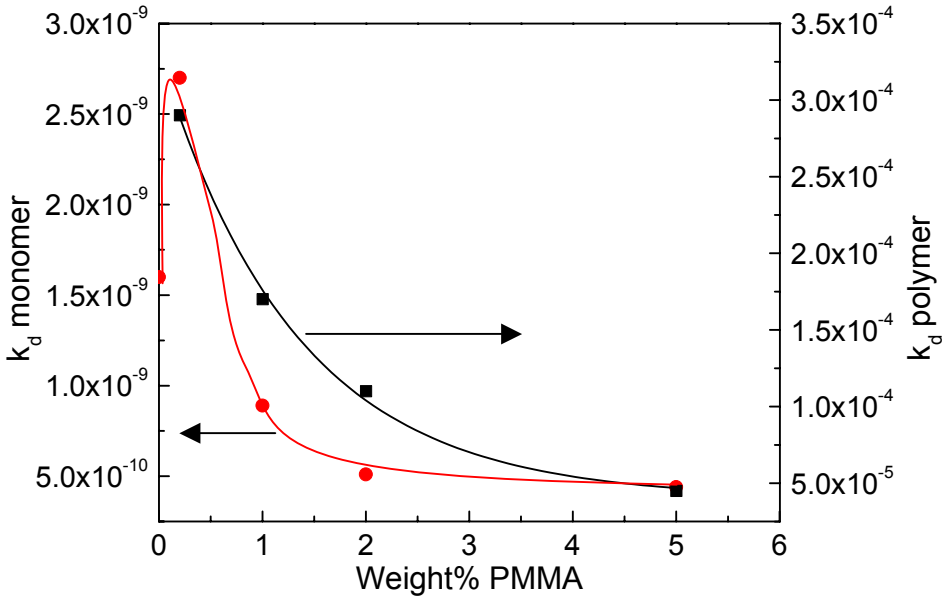

Figure 1.5. Radical formation rate constants from MMA and PMMA as a function of the weight% polymer dissolved at a temperature of 20 ºC.

Ultrasound-induced bulk polymerizations are usually performed at room temperature.[31] This low temperature is chosen because radical formation induced by ultrasound is more efficient at lower temperatures.[32]

In contrast to conventional thermal initiators such as potassium persulfate, ultrasound can initiate a polymerization reaction at ambient temperatures. It should be noted, however, that the propagation rate increases with an increasing temperature. Therefore, a suitable temperature in terms of propagation rate constant and radical formation rate has to be chosen to optimize ultrasound-induced polymerization. Since the basic reaction kinetics of the polymerization of MMA are well known,[29,30] the ultrasound-induced polymerization of MMA is the far most studied system. Typically, the resulting molecular weight of the obtained PMMA is in the range of $1*10^5$ to $6*10^5$ g/mol.

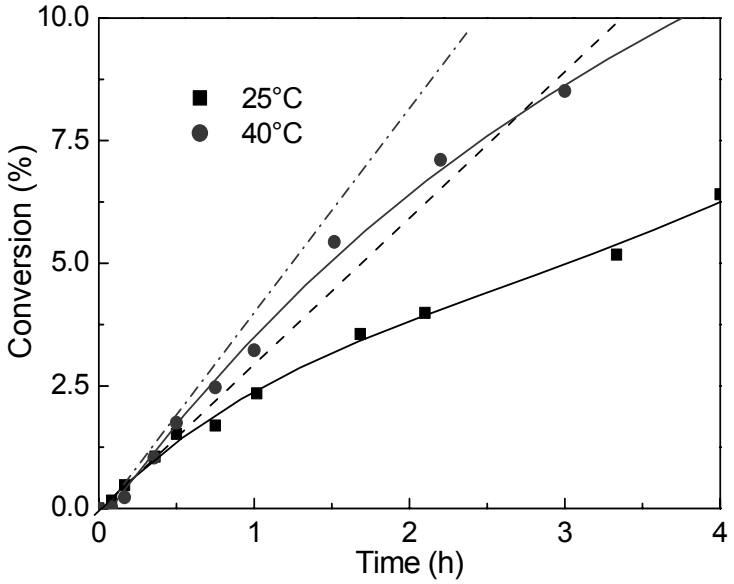

Figure 1.6. Conversion development of an ultrasound-induced bulk polymerization of MMA and the initial reaction rates at 25°C and 40°C.

An important parameter during ultrasound-induced bulk polymerizations is the viscosity.[23] As the reaction proceeds, the formed polymer chains cause a drastic increase in the viscosity, resulting in slower growth and collapse of the cavity. Since the cavitations become less

effective, the radical formation rate both from monomer and from polymer will decrease. Consequently the reaction rate decreases, as is shown in Figure 1.6. At a conversion of approximately 20% the collapse is no longer sufficiently strong to induce hot-spot temperatures that are able to generate monomeric radicals.[33] Moreover, the strain rates outside the collapsing bubble are not high enough to produce polymeric radicals by polymer scission. As a consequence, the polymerization ultimately stops at this conversion, which represents a serious drawback for the development of ultrasound-induced bulk polymerization towards industrial application. Possible solutions for this viscosity problem are emulsion and precipitation polymerizations. In emulsion polymerizations a heterogeneous reaction system is involved. The polymers are insoluble in the continuous aqueous phase, and therefore the viscosity of the water phase does not increase upon reaction. Ultrasound-induced emulsion polymerization is a well-studied system in which indeed high conversions can be obtained.[34-36] During precipitation polymerizations, the polymer precipitates from the reaction mixture, resulting in a constant viscosity and thus a constant radical formation rate by ultrasound. Section 1.6 discusses ultrasound-induced precipitation polymerization in more detail.

1.5 Ultrasound-induced polymer scission

In terms of product properties, the molecular weight distribution is an important characteristic of polymers. In the polymer industry often a post-processing step is applied to alter the molecular weight of the polymers, e.g. the peroxide-induced degradation of polypropylene.[37] In this process, fracture of the polymer chain occurs at a random site. An alternative method is ultrasound-induced polymer scission, which involves a much better controlled, non-random process.[38]

It has been shown that ultrasound-induced polymer breakage is a direct consequence of cavitation, because under conditions that suppress cavitation, no degradation is observed. In this non-random scission process

the polymer is fractured at the center of the chain.[39-41] This is clearly shown in Figure 1.7, in which a polymer with a peak molecular weight value of 90 kg/mol is produced from the initial molecular weight distribution with a peak value of 180 kg/mol. It is often thought that the extreme temperatures inside the bubble upon implosion contribute to the degradation. However, temperature degradation implies a random process and thus does not explain the scission at the middle of the chain.

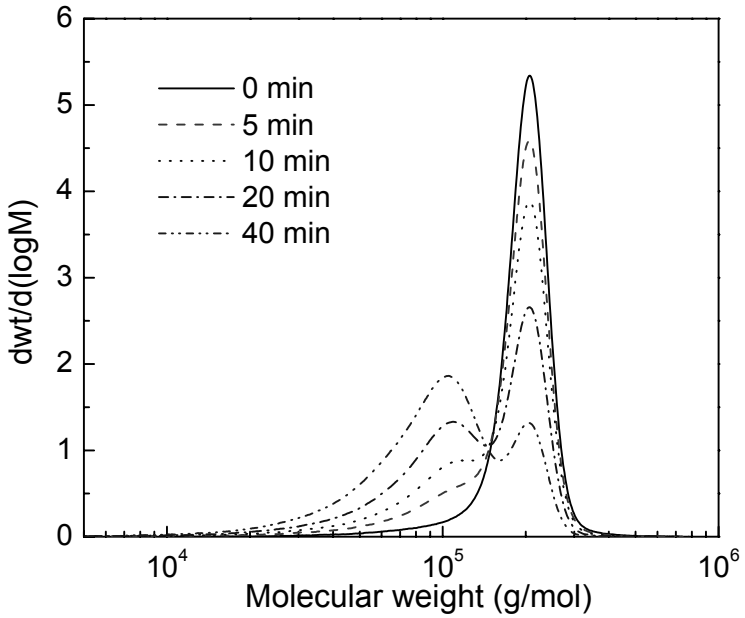

Figure 1.7. Molecular weight distributions of an ultrasound-induced polymer scission experiment of PMMA with an initial M_n of $18.0*10^4$ g/mol and a polydispersity of 1.05.

Ultrasound-induced chain fracture arises from the high strain rates on the polymer chain upon implosion. The non-random fracture in the middle of the chain by cavitation can only occur when the polymer chain is in a non-random conformation: It needs to be completely stretched.[42] In the absence of an external force a polymer chain in solution is randomly coiled. Upon bubble collapse, the entire molecule will move along with the fluid. However, due to the velocity profile near the cavities, friction between the

polymer chain and the liquid will occur. Under sufficiently strong flow conditions, the solvent drag force causes extension of the polymer molecule and finally full stretching. If the polymer chain is stretched the maximum stress due to the drag force will be in the center of the polymer chain, which is in analogy with flow-induced polymer scission.[43] If the drag force on the stretched polymer molecule exceeds the bond strength, scission will occur in the middle of the chain; otherwise the chain is not fractured and a limiting molecular weight is reached.[44] This limiting molecular weight depends on the implosion velocity of a cavitation bubble and is thus influenced by the ultrasonic wave and the solvent properties.

One of the applications of ultrasound-induced polymer scission is the production of block copolymers. Block copolymers are used in many applications where different polymers are connected to yield a material with hybrid properties,[45] for instance as compatibilizing agent between immiscible polymers.[46] The synthesis of block copolymers by ultrasound starts with the dissolution of a homo-polymer in a different monomer.[47] Subsequently, ultrasonic scission of the polymer chains generates polymeric radicals, which initiate the polymerization reaction with the monomer present. In this way ultrasound provides the controlled formation of block copolymers. Solvation of two different polymers in a non-reactive solvent can also lead to the formation of block co-polymers.[48] In this case, the generated polymeric radicals have to undergo termination by cross combination.

1.6 Polymerizations in high-pressure fluids

As described in section 1.4, ultrasound-induced bulk polymerizations are limited to relatively low conversions, because a strong viscosity increase upon reaction hinders cavitation. In order to obtain higher conversions, the addition of an anti-solvent forms a potential solution. The viscosity of a polymer solution is dependent on the gyration radius of the polymer and the polymer concentration. At low anti-solvent concentrations

the polymer will still be soluble in the solvent, however, the gyration radius will be smaller (Figure 1.8), which results in a viscosity reduction.[49] At higher anti-solvent concentrations the polymer precipitates and a second phase is formed, thus reducing the amount of polymer that is dissolved.[50] Due to these two effects, the viscosity increase will be smaller during an ultrasound-induced polymerization with an anti-solvent present, as compared to a bulk polymerization. Consequently, the radical formation rate decrease is expected to be less drastic by the addition of an anti-solvent.

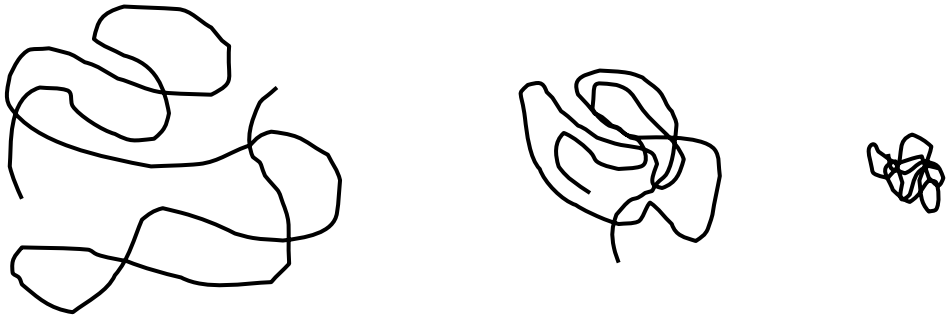

Figure 1.8. Schematic representation of polymer coils in solution; a good solvent (A), a mediocre solvent (B) and an almost precipitated polymer in a poor solvent (C).

In this perspective high-pressure carbon dioxide (CO_2) is a suitable reaction medium, because most monomers have a high solubility in CO_2, whereas it exhibits an anti-solvent effect for most polymers.[51] Moreover, CO_2 is regarded as an environmentally friendly compound, which is non-toxic, non-flammable and naturally abundant.[52,53] However, sonochemical studies have been limited to atmospheric conditions as an increased static pressure hampers the formation of cavities in a liquid.[54] This increased static pressure is necessary for high-pressure fluids (Figure 1.8). In ordinary liquids a high acoustic pressure is required to have cavitation at these high pressures. In the case of high-pressure fluids and gas-expanded liquids,

this static pressure is counteracted by the higher vapor pressure, which makes it possible to have cavitation at relatively low acoustic pressures.[55]

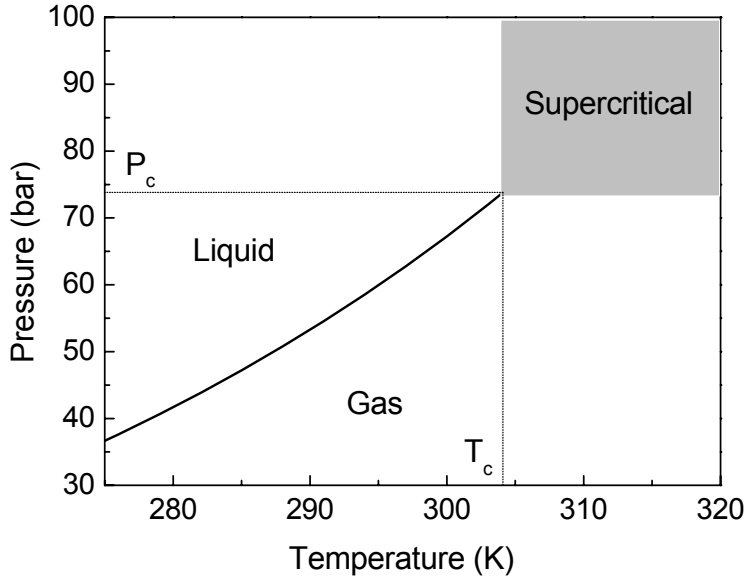

Figure 1.9. Phase diagram of pure carbon dioxide, with its critical temperature (T_c) and critical pressure (P_c) of 304.1 K and 73.8 bar, respectively.[56]

1.7 Aim and outline of this thesis

The combination of ultrasound with carbon dioxide is very interesting from an environmental point of view, as it enables a clean and safe route to produce polymers in a well-controlled way. The objective of this thesis is to study ultrasound-induced reactions in high-pressure fluids, especially polymerization and polymer scission reactions in pressurized CO_2. Physical aspects such as, static pressure, viscosity, ultrasound intensity and mass transfer influence the cavitation intensity. To provide a thorough understanding, the effects of these physical parameters on the cavitation-induced reaction have to be known.

The possibility to perform ultrasound-induced reactions in high-pressure fluids is addressed in Chapter 2. Chapter 3 deals with the physical aspects of cavitation in ordinary liquids and high-pressure fluids. Additionally, the influence of pressurized CO_2 on ultrasound-induced polymerizations is presented in Chapter 4. The polymer scission reaction, which also occurs during an ultrasound-induced polymerization, is addressed in Chapter 5 and 6. The energy conversion of ultrasound-induced radical formation is discussed in Chapter 7. Based on the obtained results, a process design using ultrasound-induced initiation for the production of PMMA in CO_2-expanded MMA has been developed in Chapter 8. Finally, opportunities for ultrasound-induced reactions in high-pressure fluids are given in Chapter 9. It has been chosen to set-up this thesis in such a way that each individual chapter provides enough information to be read independently from the other chapters. Consequently, some information is repeated in different chapters.

1.8 References

1. M.W.A. Kuijpers, M.F. Kemmere, J.T.F. Keurentjes, Ultrasound-induced radical polymerization, *Encyclopedia of Polymer Science and Technology*, John Wiley & Sons: New York, 2004
2. J.P. Lorimer, T.J. Mason, *Chem Soc Far.* **1987**, 16, 239
3. L. Kornet, A.P. Hoeks, B.J. Janssen, J.M. Willigers, R.S. Reneman, *J. Hypertension* **2002**, 20, 1165
4. K.S. Suslick, *Science* **1990**, 247, 1439
5. A. Shoh, Ultrasonics, *Kirk-Othmer Encyclopedia of Chemical Technology*, Wiley: New York, 1983
6. M.P. Brenner, S. Hilgenfeldt, D. Lohse, *Rev. Modern Physics* **2002**, 74, 425
7. W.P. Mason, *Physical Acoustics; Principles and methods Vol. IB*, Academic Press: New-York, 1964

8. K.S. Suslick, Y. Didenko, M.M. Fang, T. Hyeon, K.J. Kolbeck, W.B. McNamara III, M.M. Mdeleleni, M. Wong, *Phil. Trans. Roy. Soc. A.* **1999**, 335

9. M.W.A. Kuijpers, M.F. Kemmere, J.T.F. Keurentjes, *Ultrasonics* **2002**, 40, 675

10. J.-M. Löning, C. Horst, U. Hoffmann, *Ultrason. Sonochem*. **2002**, 9, 169

11. U. Hoffmann, C. Horst, U. Wietelmann, S. Bandelin, R. Jung, Sonochemistry, *Ullmann's Encyclopedia of Industrial Chemistry*, Wiley-VCH: Weinheim, 2003

12. Y.T. Didenko, K.S. Suslick, *Nature* **2002** 407, 877

13. T.Q. Nguyen, Q.Z. Liang, H.-H. Kausch, *Polymer* **1997**, 38, 3783

14. P. Kruus, T.J. Patraboy, J. Phys. Chem. **1985**, 89, 3379

15. G.J. Price, *New Methods of Polymer Synthesis, vol. II*, Blackie: Glasgow, 1995

16. Y.T. Shah, A.B. Pandit, V.S. Moholkar, *Cavitation Reaction Engineering,* Plenum: New-York, 1999

17. Y.T. Didenko, W.B. Mcnamara III, K.S. Suslick *Nature* **2000**, 407, 877

18. J.-L. Luche, *Synthetic Organic Chemistry*, Plenum, New-York, 1998

19. S. Majumdar, P.S. Kumar, A.B. Pandit, *Ultrason. Sonochem.* **1998**, 5, 113

20. M. Ibisi, B. Brown, *J. Acoust. Soc. Am.*, **1967**, 41, 568

21. J.M. Pestman, J.B.F.N. Engberts, F. de Jong, *Recl. Trav. Chim. Pays-Bas* **1994**, 113, 533

22. S. Hilgenfeldt, M.P. Brenner, S. Grossmann, D. Lohse, *J. Fluid Mech.* **1998**, 365, 171

23. G.J. Price, P.F. Smith, *Eur. Polym. J.* **1993**, 29, 419

24. L.H. Thompson, L.K. Doraiswamy, *Ind. Eng. Chem. Res.* **1999**, 38, 1215

25. A. Rudin, *The elements of Polymer Science and Engineering*, Academic Press: San Diego, 1999

26. D. Feldman, *Polymer News* **1995**, 20, 138

27. G. Madras, S. Kumar, S. Chattopadhyay, *Polym. Degrad. Stab.* **2002**, 69, 73

28. M.W.A. Kuijpers, M.F. Kemmere, J.T.F. Keurentjes, Annual AIChE-meeting, November **2001**, 341B

29. P. Kruus, J.A.G. Lawrie, M.L. O'Neill, *Ultrasonics* **1988**, 26, 352

30. G.J. Price, D.J. Norris, P.J. West, *Macromolecules* **1992**, 25, 6447

31. T.J. Mason, J.P. Lorimer, *Sonochemistry: theory, applications and uses of ultrasound in chemistry*, Ellis Horwood Ltd.: Chichester, 1988

32. P. Kruus, M. O'Neill, D. Robertson, *Ultrasonics* **1990**, 28, 304

33. G.J. Price, *Ultrason. Sonochem.* **1996**, 3, S229

34. H.C. Chou, J.O. Stoffer, *J. Appl. Pol. Sci*. 1999, 72, 797

35. G. Cooper, F. Grieser, S. Biggs *J. Colloid Interface Sci*. **1996**, 184, 52

36. C. Zhang, Q. Wang, H. Xia, G. Qiu, *Eur. Pol. J*. **2002**, 38, 1769

37. A.V. Machado, J.A. Covas, M. van Duin, *J. Appl. Pol. Sci*. **2001**, 81, 58

38. J. Niezette, A. Linkens, *Polymer* **1978**, 19, 939

39. P.A.R. Glyn, B.M.E. van der Hoff, P.M. Reilly, *J. Macromol. Sci.-Chem.* **1972**, A6, 1653

40. B.M.E. van der Hoff, C.E. Gall, *J. Macromol. Sci.* **1977**, A11, 1739

41. G. Madras, S. Kumar, S. Chattopadhyay, *Pol. Degr. Stab.* **2000**, 69, 73

42. M.W.A. Kuijpers, P.D. Iedema, M.F. Kemmere, J.T.F. Keurentjes, submitted

43. A.M. Basedow, K.H. Ebert, *Adv. Pol. Sci.* **1977**, 22, 83

44. J.A. Odell, A. Keller, *J. Pol. Sci. B* **1986**, 24, 1889

45. I.W. Hamley, Block copolymers, *Encyclopedia of Polymer Science and Technology*, John Wiley & Sons: New York, 2002

46. T.J. Mason, Sonochemistry, *The Uses of Ultrasound in Chemistry*, CRC Press, 1990

47. H. Fujiwara, J. Tanaka, A. Horiuchi, *Polymer Bulletin* **1996**, 36, 723

48. G.J. Price, P.J. West, *Polymer* **1996**, 37, 3975

49. K.A. Shaffer, J.M. DeSimone, *Trends Polym. Sci.* **1995**, 3, 146

50. M.F. Kemmere, M.W.A. Kuijpers, L.J.M. Jacobs, J.T.F. Keurentjes, *Macromol. Symp.* **2004**, 206, 321

51. C.F. Kirby, M.A. McHugh, *Chem. Rev.* **1999**, 99, 565

52. A.I. Cooper, *J. Mater Chem.* **2000**, 10, 207

53. M.A. Abraham, L. Moens, *Clean Solvents, Alternative Media for Chemical Reactions and Processing*; ACS Symposium Series 819: Washington, 2002

54. J. Berlan, F. Trabelsi, H. Delmas, A.M. Wilhelm, J.F. Petrignani, *Ultrason. Sonochem.* **1994**, 1, S97

55. M.W.A. Kuijpers, D. van Eck, M.F. Kemmere, J.T.F. Keurentjes, *Science* **2002**, 298, 1969

56. P.G. Jessop, W. Leitner, *Chemical Synthesis using Supercritical Fluids*; Wiley-VCH: Weinheim, 1999

2 Cavitation-induced Reactions in High-Pressure Carbon Dioxide

The feasibility of ultrasound-induced in situ radical formation in liquid carbon dioxide was demonstrated. The required threshold pressure for cavitation could be exceeded at a relatively low acoustic intensity, as the high vapor pressure of CO_2 counteracts the hydrostatic pressure. With the use of a dynamic bubble model, the formation of hot spots upon bubble collapse was predicted. Cavitation-induced radical formation was used for the polymerization of methyl methacrylate in CO_2, yielding high-molecular-weight polymers. These results show that sonochemical reactions can be performed in dense-phase fluids, which allows the environmentally benign CO_2 to replace conventional organic solvents in many reaction systems.

This chapter is based on: M.W.A. Kuijpers, D. van Eck, M.F. Kemmere, J.T.F. Keurentjes *Science* **2002**, 298, 1969.

2.1 Introduction

Sonochemistry comprises all of the chemical effects that are induced by ultrasound, including the formation of radicals and the enhancement of reaction rates at ambient temperatures.[1,2] The chemical effects of ultrasound are caused by cavitation: the collapse of microscopic bubbles in a liquid,[3,4] a phenomenon that does not occur in boiling liquids. Cavities are generated when the "negative" pressure during the rarefaction phase of the sound wave is sufficiently large to disrupt the liquid. In water, the implosions of these cavities generate temperatures up to 5000 K and pressures up to 200 bar, because of the compression of the gas phase inside the cavity.[5,6] These conditions lead to the formation of excited states, bond breakage, and the generation of radicals. As compared to the use of initiators or catalysts, cavitation-induced radical reactions allow for clean and safe operation, because no separation is required afterward and the formation of radicals can be controlled externally. On the other hand, electrical energy is required to generate cavitation.

Dense-phase fluids (with a strong emphasis on CO_2) are expected to provide a powerful means for the development of processes based on green chemistry.[7,8] To generate sufficient solvent power in dense-phase fluids, high densities and hence high pressures are required. In ordinary solvents, cavitation does not occur at elevated pressures.[9] As a result, sonochemical studies have been limited to atmospheric conditions. The use of dense-phase fluids in sonochemical reactions could open up the use of pressure as a process variable to control solubility during ultrasound-induced reactions. As an example, in polymerizations, high-pressure CO_2 will act as an antisolvent[10] and will precipitate the polymer, thus enabling a viscosity reduction that would lead to high conversions.

2.2 Results and discussion

Cavitation in high-pressure systems

To initiate the growth of a cavitation bubble, an acoustic pressure above the so-called Blake threshold pressure has to be applied.[11,12] During pressurization of a liquid, the Blake threshold pressure increases, which implies that higher acoustic pressures are needed to produce cavitations. The maximum acoustic pressure P depends on the intensity provided by the ultrasonic device (I_{US}), the density of the liquid (ρ), and the velocity of sound (c).

$$P_A = \sqrt{2 \cdot \rho \cdot c \cdot I_{US}} \qquad (2.1)$$

Because the velocity of sound is a function of the compressibility of the medium,[13] the attainable acoustic pressure for a given ultrasound intensity is a function of pressure and temperature. Unlike ordinary liquids, the high vapor pressure of a dense-phase fluid (which is a gas at ambient conditions) allows cavitation to occur. As a result, the Blake threshold is reduced, which enables cavitation in liquid CO_2 at higher pressures. Figure 2.1 shows the calculated Blake threshold pressure for CO_2 and water at 58.2 bar. At 58.2 bar and 293 K, the Blake threshold pressure of liquid CO_2 equals the threshold pressure in water at 1 bar and 293 K. For water at 58.2 bar, a very high acoustic pressure is required to create cavitation.

The threshold pressure in water is determined only by the static pressure and the surface tension of the liquid, because of its low vapor pressure. Because the vapor pressure does not change significantly with increasing temperature, the threshold pressure of water is approximately constant. Because CO_2 condenses at a substantially higher pressure, its vapor pressure has a substantial influence. Liquid CO_2 has a relatively low surface tension σ [at 293 K and 57.2 bar, σ equals $3.3*10^{-3}$ N/m].[13] This leads to a contribution of the Laplace pressure ($2\sigma/R_0$) to the Blake threshold pressure of only 0.0066 bar at a bubble radius R_0 of 10^{-5} m, whereas the vapor pressure contribution equals 57.2 bar. The occurrence of cavitation in

high-pressure CO_2 has been shown at 75 bar and 283 K, at which CO_2 is in the liquid state, although above its critical pressure. It is important to stay below the critical point of the mixture, because above the critical point no phase boundaries exist, hence prohibiting cavitation. At an acoustic intensity below the Blake threshold pressure (25 W/cm^2), the liquid remains transparent (Figure 2.2A), whereas at an ultrasound intensity of 125 W/cm^2, cavitation occurs (Figure 2.2B).

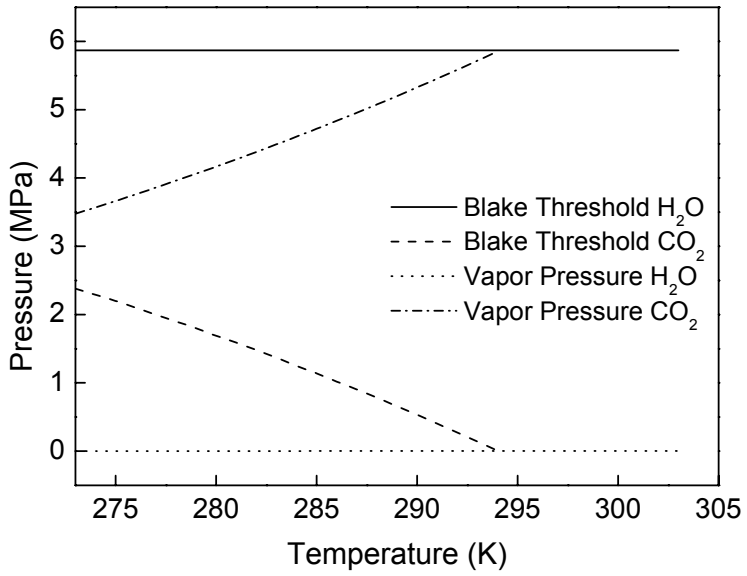

Figure 2.1. Calculated Blake threshold pressure and vapor pressure for water and CO_2 at 58.2 bar. The Blake threshold pressure is calculated as

$$P_B = P_0 - P_v + \frac{4}{3}\cdot\sigma\cdot\sqrt{\frac{2}{3}\cdot\frac{\sigma}{\left(P_0 + 2\cdot\frac{\sigma}{R_0} - P_v\right)\cdot R_0^{\,3}}} \qquad (2.2)$$

This equation assumes that the external pressure P_o, the vapor pressure P_v, the surface tension σ and the equilibrium radius of the bubble R_0 determine the required negative pressure in the liquid to start explosive growth of a cavity. Using $P_{v,\,water}$=0.023 bar, σ_{water}=72*10^{-3} N/m, $P_{v,CO2}$=57.2 bar, σ_{CO2}=3.3*10^{-3} N/m, and R_o=10^{-5} m, the Blake threshold pressure equals 1 bar for water at atmospheric conditions, so that in CO_2 a hydrostatic pressure of 58.2 bar is required for a threshold pressure of 1 bar.

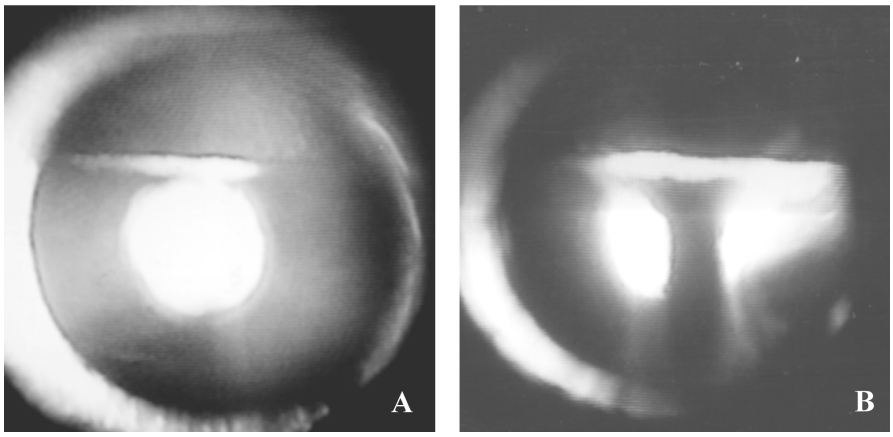

Figure 2.2. Ultrasound-induced cavitation in liquid CO_2 at 283 K and 75 bar. The experiments were performed in a high-pressure cell of 175 ml provided with quartz windows. The tip of the ultrasound horn is located at the top and provides 20 kHz ultrasound with an intensity of 25 W/cm^2 (**A**) and 125 W/cm^2 (**B**). In (**A**), no cavitation occurs and the liquid remains transparent, whereas in (**B**) indeed cavitation occurs, visible by the presence of dispersed gas bubbles underneath the ultrasound horn. Additionally, the cavitation threshold can simply be determined by ear.

Assuming a sound velocity of 800 m/s,[13] the measured threshold intensity of 125 W/cm^2 corresponds with an acoustic pressure of 12.5 bar, which is below the calculated Blake threshold pressure of 30 bar. Because of the inhomogeneous temperature distribution close to the probe, however, a lower threshold pressure is expected because the threshold pressure strongly decreases at higher temperatures. A dynamic model is required to describe the motion of the bubble and to calculate the temperature and pressure at bubble collapse.[14]

We used the Kyuchi-Yasui model,[15,16] which is based on the Rayleigh-Plesset equation combined with mass and energy balances over the bubble, and we assumed that evaporation and condensation at the bubble wall are in equilibrium. The variation of the bubble radius with time is shown in

Figure 2.3. No bubble formation or growth occurs in water at elevated pressures. The maximum bubble radius before collapse is on the same order of magnitude for water at atmospheric conditions and in liquid CO_2 at high pressure.

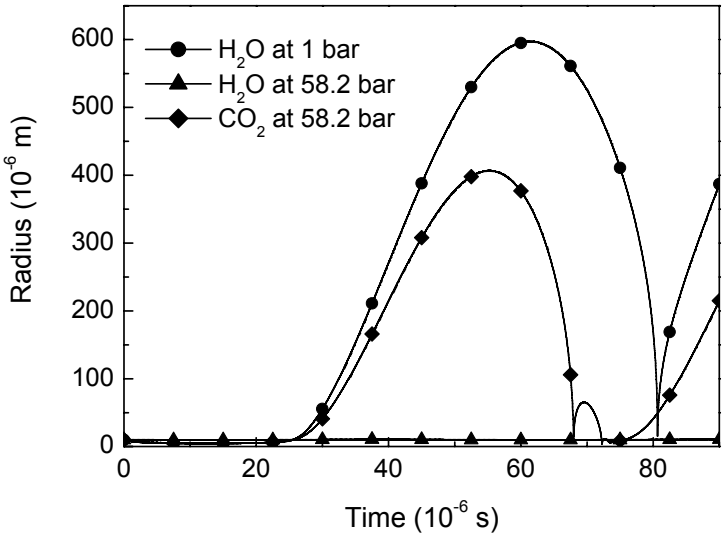

Figure 2.3. Calculated radius of a cavitation bubble as a function of time in water and high-pressure CO_2 at 293 K. Initially, a small cavity with a radius of 10^{-5} m is present, which consists of argon and the corresponding vapor of the liquid phase. In the calculations an ultrasound wave with an acoustic pressure of 10 bar and a frequency of 20 kHz is imposed on this bubble.

The calculated maximum attainable temperatures are 722 K for water (at 1 bar) and 585 K for liquid CO_2 at 58.2 bar. To show that bubble collapse in liquid CO_2 is sufficiently strong to induce radical formation, measurements were done in CO_2-methyl methacrylate (MMA) systems at high pressure. Mixing MMA with CO_2 will increase the Blake threshold pressure, so that the system will behave more like an ordinary liquid.[17] Using the reaction calorimetry technique during ultrasound application as described in our earlier work,[18] we found that the threshold intensity for CO_2-MMA mixtures at 293 K was 23 and 68 W/cm^2 for CO_2 mole fractions of 0.27 and 0.64, respectively. Although both systems are near their boiling points, the CO_2-MMA system with a high mole fraction of CO_2 requires an additional argon head pressure to avoid boiling and to allow for cavitation.

Radical formation in high-pressure systems

Radical formation has been measured in CO_2-MMA systems using a radical scavenger (Figure 2.4A). From these results, a radical formation rate of $1.5*10^{14}$ s^{-1} is determined, for which no noticeable difference between the three systems is found. Additionally, polymerization experiments have been performed in the same CO_2-MMA system without the radical scavenger. In Figure 2.4B, the molecular weight distribution of the formed poly (methyl methacrylate) (PMMA) is given, which shows that high molecular-weight material is formed with a weight-averaged and number-averaged molecular weight of 100,000 and 21,000, respectively, leading to a polydispersity of about 4.9. In pure MMA, no cavitation occurs at this pressure and ultrasound intensity and hence no polymerization was observed. In ultrasound-induced bulk polymerizations at ambient pressures, a strong viscosity increase is observed, which hinders cavitation, and hence radical formation, which limits the conversion to low values.[2]

Because high-pressure CO_2 acts as an anti-solvent, the polymer will precipitate from the CO_2-monomer phase, so that even at high conversions a low solvent viscosity and a high radical formation rate can be maintained. Because cavitation can also cause chain scission, the attained molecular weight can be limited by this effect.[2] To allow for chain scission, the polymer needs to be in solution and has to be above a certain molecular weight to experience sufficient strain on the polymer chain. Depending on the cavitation intensity and the viscosity of the system, an upper limit for the molecular weight of approximately 30,000 g/mol can be expected as a result of polymer scission. The solubility of PMMA in the system is strongly dependent on the CO_2:MMA ratio: At a CO_2:MMA ratio of 0.71:0.29, the solubility of PMMA with a number-averaged molecular weight of 46,400 g/mol is approximately 5%.[19] Increasing the CO_2:MMA ratio, however, results in a sharp decrease in solubility. This would provide an additional means to control the molecular weight of the polymer and to obtain multimodal molecular weight distributions.

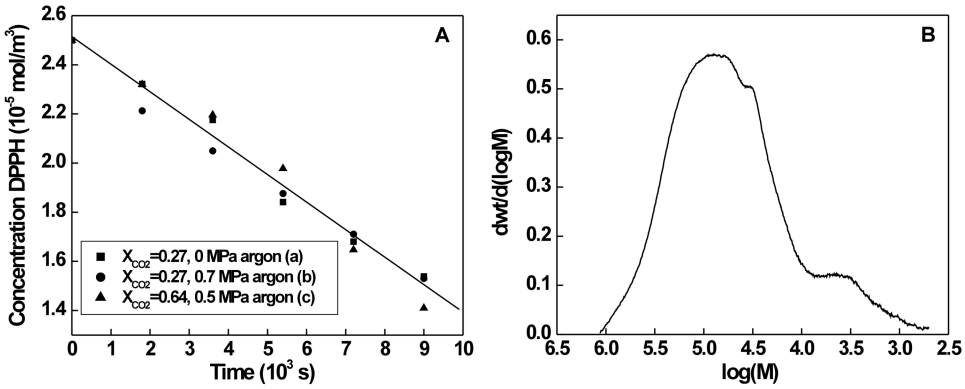

Figure 2.4. (**A)** Cavitation-induced radical formation in liquid CO_2. Displayed is the concentration of the radical scavenger 1,1-diphenyl-2-picrylhydrazyl (DPPH) in time as determined by ultraviolet-visible spectroscopy analysis at 520 nm.[18] A 175 ml high-pressure vessel was filled with MMA, which was distilled before use to remove the hydroquinone inhibitor. Argon was bubbled through the liquid and carbon dioxide was added to total the liquid volume to 150 ml. The measurements were performed at 293 K for two CO_2-MMA ratios, i.e. 0.27/0.73 mole/mole (**a** and **b**) and 0.64/0.36 mole/mole (**c**), leading to pressures of 12 and 30 bar, respectively. Additionally, 7 and 5 bar argon was added for systems **b** and **c**, respectively. Subsequently, the ultrasound probe (1.24 cm^2) was switched on with a frequency of 20 kHz and an intensity of 118 W/cm^2 (**a** and **b**). In (**c**) a limiting intensity of 72 W/cm^2 was observed. (**B)** Molecular weight distribution of the polymer obtained from the cavitation-induced polymerization of MMA after 2 hours of sonication. The experiments were performed at a molar CO_2-MMA ratio of 0.27/0.73 at 293 K. The polymer was characterized via gel permeation chromatography, which was calibrated against polystyrene standards.

2.3 Conclusions

These experiments demonstrate the feasibility of ultrasound-induced in situ radical formation in liquid CO_2, thereby substantially broadening the application potential for sonochemistry as it allows for the use of environmentally benign CO_2 to replace conventional organic solvents in many reaction systems.

2.4 References

1. L. H. Thompson, L. K. Doraiswamy, *Ind. Eng. Chem. Res.* **1999**, 38, 1215

2. G. J. Price, *Ultrason. Sonochem.* **1996**, 3, S229

3. K. S. Suslick, *Science* **1990**, 247, 1439

4. Y. T. Didenko, K. S. Suslick, *Nature* **2002**, 418, 394

5. K. S. Suslick, *Sci. Am.* 1989, 260, 80

6. J-L. Luche, *Synthetic Organic Sonochemistry*; Plenum: New York, 1998

7. P. G. Jessop, W. Leitner, Eds., *Chemical Synthesis Using Supercritical Fluids*; Wiley-VCH: Weinheim, 1999

8. M. A. Abraham, L. Moens, Eds., *Clean solvents, alternative media for chemical reactions and processing, ACS Symposium Series 819*; ACS: Washington, 2002

9. J. Berlan, F. Trabelsi, H. Delmas, A. M. Wilhelm, J. F. Petrignani, *Ultrason. Sonochem.* 1994, 1, S97

10. K. A. Shaffer, J. M. DeSimone, *Trends Polym. Sci.* **1995**, 3, 146

11. T. J. Leighton, *The Acoustic Bubble*; Academic Press: London, 1994

12. S. Hilgenfeldt, P. M. Brenner, S. Grossmann, D. Lohse, *J. Fluid Mech.* **1995**, 365, 171

13. D. P. Singh, M. Lal, B. Singh, *Acoust. Lett.* **1992**, 15, 235

14. J. P. Lorimer, T. J. Mason, *Chem. Soc. Rev.*, **1987**, 16, 239

15. K. Yasui, *J. Acoust. Soc. Am.* **1995**, 98, 2772

16. K. Yasui, *Ultrasonics* **1998**, 36, 575

17. D. L.Goldfarb, H. R. Corti, F. Marken, G. J. Compton, *J. Phys. Chem. A*. **1998**, 102, 8888

18. M. W. A. Kuijpers, M. F. Kemmere, J. T. F. Keurentjes, *Ultrasonics* **2002**, 40, 675

19. M. Lora, M. A. McHugh, *Fluid Phase Equilibria* **1999**, 157, 285

3 Cavitation Thresholds in Gas-expanded Liquids at Elevated Pressures

Recently, we have shown that it is possible to induce cavitation in gas-expanded liquids. In this paper, cavitation threshold intensities have experimentally been determined for methyl methacrylate (MMA) pressurized with argon or carbon dioxide (CO_2) using calorimetry. When MMA is pressurized with argon, the threshold intensities at elevated pressures can be calculated with the Blake threshold model as well as with a dynamic bubble model. For the CO_2-expanded MMA system, however, these two models cannot explain the experimentally observed threshold maximum with increasing CO_2-pressure. Therefore, a mass transfer model has been employed to describe the growth of cavitation bubbles by ultrasound at increased static pressures. Modeling CO_2 transport in the liquid phase towards the bubble has shown that mass transfer is limited in the CO_2/MMA-system when a bubble is growing. This results in a lower vapor pressure inside the bubble and hence a higher acoustic threshold pressure is observed to induce cavitation in liquid mixtures, which coincides with the experimental results.

This chapter is partially based on: M.W.A. Kuijpers, D. v. Eck, M.F. Kemmere, J.T.F. Keurentjes *J. Phys. Chem. A*., submitted.

3.1 Introduction

Ultrasound is known to enhance chemical reactions as well as mass transfer at ambient temperatures and pressures. The chemical effects of ultrasound include the formation of radicals and the enhancement of reaction rates at ambient temperatures.[1,2] The enhanced dissolution of a solid reactant or catalyst caused by renewal of the liquid at the solid-liquid interface illustrates a mechanical effect induced by ultrasound.[3] Most of these effects are caused by cavitations, i.e. the collapse of microscopic bubbles in a liquid. The cavitation process can generate temperatures and pressures of approximately 5000 K and 200 bar,[4] respectively, due to compression of the gas phase inside the cavity upon implosion. Before implosion of a bubble can occur, an explosive growth of a gas nucleus has to occur. To initiate this growth, a minimum acoustic pressure has to be applied. The Blake threshold pressure (Equation 3.1) describes this critical pressure, which assumes that the external pressure (P_0), the vapor pressure (P_v), the surface tension (σ) and the equilibrium radius of the bubble (R_0) determine the required negative pressure in the liquid to produce an explosive growth of a cavity.[5,6]

$$P_B = P_0 - P_v + \frac{4}{3} \cdot \sigma \cdot \sqrt{\frac{2}{3} \cdot \frac{\sigma}{\left(P_0 + 2 \cdot \frac{\sigma}{R_0} - P_v \right) \cdot R_0^3}} \qquad (3.1)$$

During pressurization of a liquid the Blake threshold pressure increases, which implies that higher acoustic pressures are needed to produce cavitations. Obviously, no cavitation occurs when the Blake pressure exceeds the maximum acoustic pressure that can be produced with the available ultrasound equipment.

When a liquid is pressurized with a gas that does not dissolve, cavitation does not readily occur.[7] This is due to the fact that the static pressure is not counteracted by the gas pressure inside the cavity during bubble growth. As a result, the Blake threshold increases linearly with the static pressure (Figure 3.1). However, when large amounts of gas dissolve,

a gas-expanded liquid is formed and the vapor pressure of the liquid is equal to the static pressure. This theoretically implies that the threshold pressure is constant with an increase in static pressure, see Figure 3.1. In that case, the Laplace pressure (the last term in Equation 3.1) only determines the Blake threshold. Recently, we have shown experimentally that cavitation is possible in dense-phase fluids.[8] The high vapor pressure of these fluids counteracts the high static pressure allowing the cavitation bubble to grow and subsequently implode at elevated pressures.

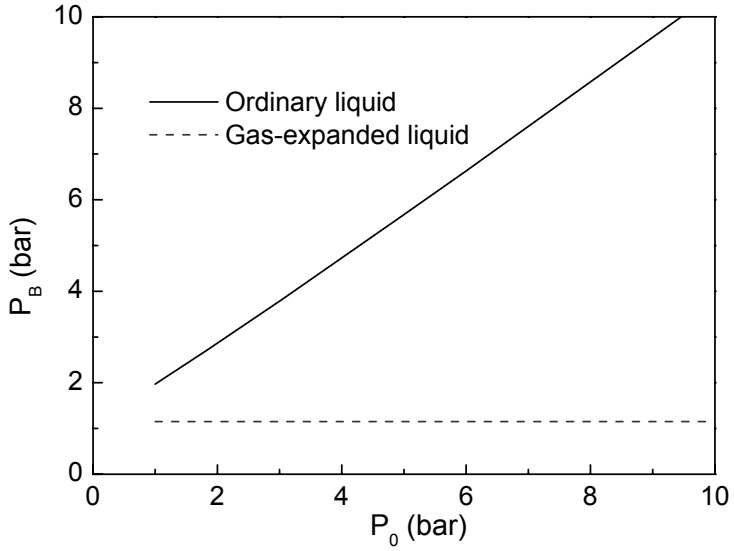

Figure 3.1. Theoretical Blake threshold pressure as a function of the static pressure for an ordinary liquid and a gas-expanded liquid ($R_0 = 1*10^{-6}$ m, $\sigma = 1.5*10^{-2}$ N/m).

In this study, the cavitation threshold intensities of ordinary liquids (MMA pressurized with argon) and gas-expanded liquids (MMA pressurized with CO_2) have been experimentally determined by calorimetry. To calculate the phase behavior of the liquids at increased static pressures requires the use of an equation of state. In this work, the Lee-Kessler-Plöcker equation of state is used to correlate the liquid temperature and static pressure with the liquid and gas composition. The Blake threshold calculations, a dynamic bubble model and a mass transfer model are used to determine if mass transfer limitations in the liquid phase occur and whether these limitations are able to explain differences in

cavitation threshold measurements between ordinary and gas-expanded liquids.

3.2 Dynamic bubble simulations

The Blake threshold pressure is a static quantity, as no time-dependent variables are taken into account.[5] This implies that the Blake threshold pressure cannot predict the onset of the growth of a cavitation bubble, when liquid viscosity or mass transfer play a role. In these cases, a dynamic model is required to calculate the actual required acoustic threshold pressure ($P_{A,max}$), which can be calculated from the threshold intensity (I_{US}), the liquid density (ρ) and the sound velocity (v):[6]

$$P_{A,\max} = \sqrt{2 \cdot \rho \cdot v \cdot I_{US}} \qquad (3.2)$$

The dynamic bubble model used in this study is based on the Rayleigh-Plesset equation (Equation 3.3),[12,13] which includes the surface tension, the gas pressure in the bubble (P_{gas}), the liquid viscosity (η) and the acoustic pressure (P_A). The pressure inside the bubble is simply calculated with the Van der Waals equation[14] (Equation 3.4) in combination with a mass balance over the bubble. This pressure depends on the temperature (T), the gas constant (R_{gas}), the molar volume (V_m), the hard sphere volume (b) and the attractive pressure term (a). The parameters a and b can be calculated from the critical constants of the compounds involved.[14] During the initial stage of the growth of a cavitation bubble, the temperature in the bubble is almost constant.[5] Because of these isothermal conditions, no energy balance over the bubble is required to calculate the threshold intensity.

$$R\frac{d^2}{dt^2}R + \frac{3}{2}\left(\frac{d}{dt}R\right)^2 = \frac{1}{\rho}\left(P_{gas} - \frac{2\sigma}{R} - \frac{4\eta\frac{d}{dt}R}{R} - P_0 - P_A(t)\right) \qquad (3.3)$$

$$P_{gas} = \frac{R_{gas}\,T}{V_m - b} - \frac{a}{V_m^2} \qquad (3.4)$$

3.3 Mass transfer towards the bubble

The applied acoustic pressure wave drives the motion of the bubble, as shown in Figure 3.2. During the rarefaction phase, the bubble grows and liquid has to evaporate to obtain the equilibrium vapor pressure. If a liquid mixture is used, the vapor composition most likely differs from the liquid composition, because of the different volatilities of the pure components. As a result, one component will evaporate faster during bubble growth, which results in a lower concentration at the bubble interface in the liquid. This deficiency has to be restored by mass transfer from the bulk liquid. In fast processes such as cavitation, in which bubble growth occurs in 30 μs (Figure 3.2), mass transfer can be limited.[15,16]

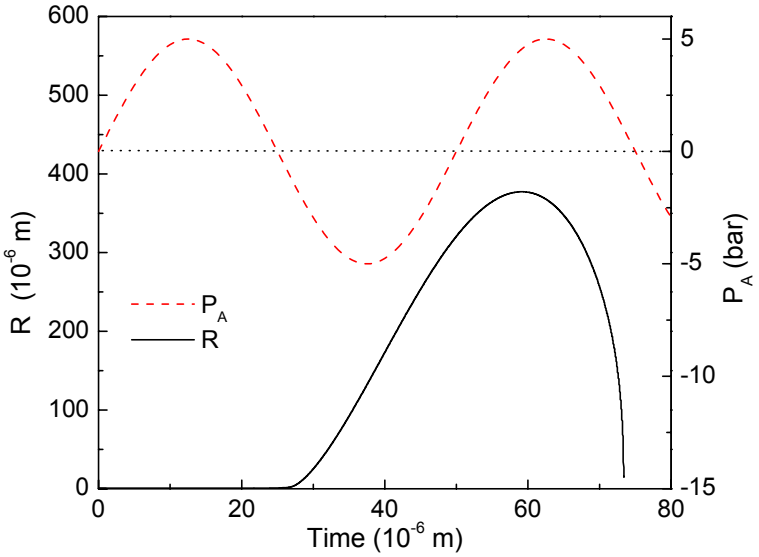

Figure 3.2. Calculated radius of a cavitation bubble in MMA with an initial radius of 10^{-6} m (1 bar, 293 K, P_A = 5 bar and f = 20 kHz).

Due to these mass transfer limitations in the liquid phase, the concentration of the most volatile component will be lower at the bubble interface than in the bulk liquid (Figure 3.3). As the concentration at the interface is in equilibrium with the bubble content, the vapor pressure

inside the growing bubble will be lower than expected without the mass transfer limitations. Consequently, the threshold pressure will be higher than theoretically predicted by the Blake threshold pressure (Equation 3.1). Inside the bubble, no concentration gradients are present during its growth.[5]

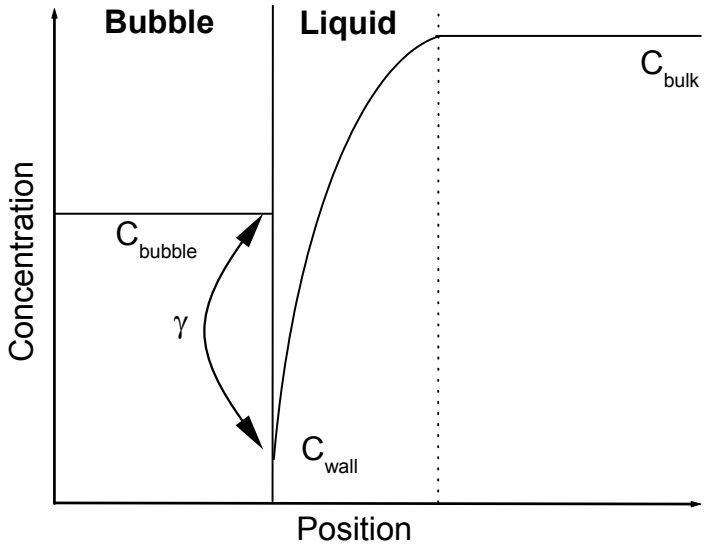

Figure 3.3. A schematic presentation of the concentration profile around a growing cavitation bubble.

This mass transfer effect is especially important for liquids in which large amounts of gas are dissolved, e.g. gas-expanded liquids. The liquid composition (x_i) of gas-expanded liquids can be correlated to the vapor composition (y_i) by the activity coefficient (γ_i) and the fugacity (f_i) at a certain temperature and pressure (Equation 3.5).[14]

$$\gamma_i = \frac{y_i P_0}{x_i f_i} \qquad (3.5)$$

Equation 3.6 describes the mass transfer of the most volatile component from the bulk liquid towards the cavity. The mass flux for this component can be calculated based on the concentration in the bulk liquid (C_{bulk}), the concentration at the interface in the liquid (C_{wall}), the surface area of the

bubble (A_{bubble}) and the mass transfer coefficient (k).[17] The mass transfer coefficient can be estimated using the penetration theory (Equation 3.7)[17] with a diffusion coefficient D and ultrasound frequency f.

$$\frac{dN(t)}{dt} = k\, A_{bubble} \left(C_{bulk} - C_{wall}\right) \qquad (3.6)$$

$$k = 1.13 \sqrt{½\, f\, D} \qquad (3.7)$$

3.4 Experimental

Cavitation thresholds were determined in a gas-expanded liquid (MMA with CO_2) and in an ordinary liquid (MMA with argon). As almost no argon (Ar) dissolves in MMA, no equation of state was necessary to calculate the liquid composition for the Ar/MMA-system. However, for the CO_2/MMA-system, an equation of state is required to correlate the liquid composition to the gas composition at different temperatures and pressures.[18] The Lee-Kessler-Plöcker (LKP) equation of state[19] was used to describe the phase behavior of the CO_2/MMA-system. This equation of state applies to hydrocarbon systems, which include light gases such as CO_2. The LKP-model uses pure component parameters, such as the critical temperature, the critical pressure and the acentric factor, and one binary interaction parameter. The temperature independent interaction parameter for the CO_2/MMA-system appears to be 1.08.[20] In addition to the liquid composition, the activity coefficients and the densities were also calculated with the LKP-equation of state.

The ultrasound threshold intensities were determined using a 1.8 L commercially available reaction calorimeter RC1e (Mettler-Toledo GmbH, HP60 reactor, Switzerland).[21,22] Ultrasound with a frequency of 20 kHz was produced by a Sonics and Materials VC-750 ultrasonic generator. A ½-inch full-wave titanium probe was applied to couple the piezoelectric transducer to the liquid. To allow for an accurate comparison, the total configuration of the RC1e was exactly kept constant during all the experiments. The RC1e was operated in isothermal mode, i.e., the jacket temperature (T_j) was automatically adjusted to keep the reactor temperature (T_r) constant. Both the jacket temperature and the reactor

temperature can be measured very accurately, which allows for the calculation of the heat-flow through the reactor wall (Q) (Equation 3.8). The ultrasonic power input equals the calculated heat-flow through the reactor-wall. Subsequently, the ultrasound intensity (I_{US}) was calculated by dividing the heat flow by the surface area of the ultrasound horn (A_{US}), according to Equation 3.8.[5] For the continuous determination of the overall heat-transfer coefficient (U) and the wetted surface area (A_r), a small sine wave temperature modulation was superimposed on the jacket temperature. From the resulting sine-amplitude of the reactor temperature and the phase shift between T_j and T_r the UA_r-factor was constantly calculated during the experiments.[23,24]

$$I_{US} = \frac{Q}{A_{US}} = \frac{U\,A_r\,(T_r - T_j)}{A_{US}} \qquad (3.8)$$

The experimental procedure of the threshold experiments was as follows. The reactor was filled with 1.5 L MMA, obtained from Aldrich. The liquid was sonicated for 15 minutes at an intensity just above the cavitation threshold, from which the mean cavitation threshold intensity was calculated. Cavitation could clearly be determined by ear. Subsequently, carbon dioxide or argon (Hoekloos) was added, until the desired pressure was reached. The LKP equation of state was used to calculate the composition and the density of the liquid. With these calculations, the amount of MMA was adjusted to keep the liquid volume constant at exactly 1.5 L. The cavitation thresholds with argon were determined at 293 K until the maximum attainable ultrasound intensity was reached. The experiments with the CO_2/MMA-system were performed in a pressure range of 0 to 40 bar at temperatures of 293 K, 303 K and 313 K, respectively.

3.5 Results and discussion

Experimental cavitation thresholds have been determined for an ordinary liquid (MMA with argon) and a gas-expanded liquid (MMA with CO_2). Additionally, the threshold intensities have been calculated with the Blake threshold and a dynamic bubble model. The experimental and

simulation results are used to determine if mass transfer limitation in the liquid phase occurs and whether this mass transfer limitation has to be taken into account to calculate the threshold intensities for ordinary and gas-expanded liquids.

Ordinary liquids

In normal liquids, cavitation is hampered at increased static pressures, as the external pressure is not counteracted during bubble growth by the internal gas pressure. Almost no diffusion of gas from the liquid to the bubble occurs when the bubble grows, due to the low gas solubility. The result is that the cavitation threshold increases with an increase in static pressure (Figure 3.4). To calculate the threshold pressure ($P_{A,max}$) from the experimental determined threshold intensity (I_{US}), the density and sound velocity in MMA are required, for which values of 0.937 kg/L and $1.2*10^3$ m/s have been used, respectively.[25] From the experimental threshold pressure at 3 bar the initial bubble radius (R_0) is calculated, which appears to be $R_0 = 1.7*10^{-8}$ m. This value is used as initial radius in the Blake threshold pressure calculations and the dynamic bubble model, in order to calculate the acoustic pressure required to induce cavitation. The difference in slope of the experimental threshold pressures as compared to the Blake threshold model (Figure 3.4) is probably caused by the smaller size of the nuclei at higher pressures, which is not taken into account by the model.

Additionally, the threshold pressure has been determined with the dynamic bubble model. For instance, a cavitation bubble at 293 K and 1 bar explosively grows at an acoustic pressure of 7.75 bar (Figure 3.5), which corresponds with the Blake threshold pressure. The threshold pressure of MMA pressurized with argon can thus be calculated with both the Blake threshold pressure and the dynamic bubble model.

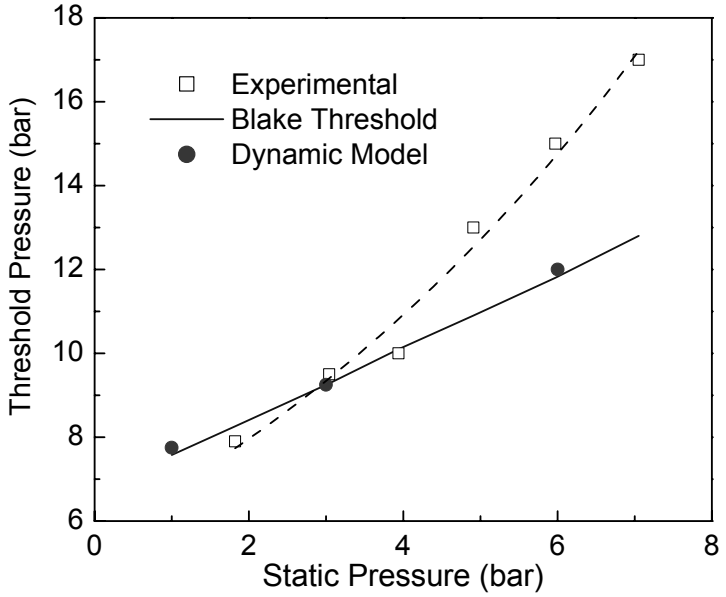

Figure 3.4. Experimental and calculated threshold intensities for the MMA/Ar-system at 293 K ($\sigma = 1.5*10^{-2}$ N/m).[26]

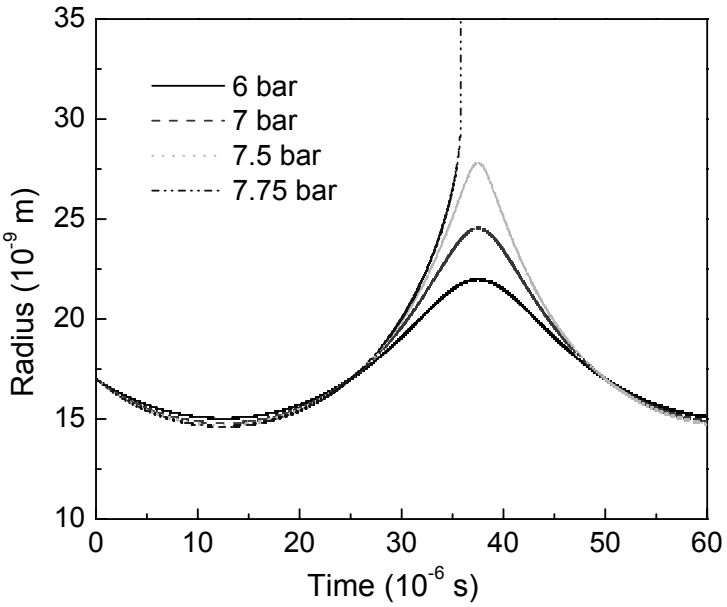

Figure 3.5. Determination of the cavitation threshold in the MMA/Ar-system with the dynamic bubble model at 1 bar and 20°C.

Gas-expanded liquids

The Blake threshold is not able to calculate the required threshold intensities if mass transfer limitation influences the growth of a cavity. This is probably the case for the CO_2/MMA system, as large amounts of CO_2 can dissolve in MMA. The two intensities that can be calculated with the Blake threshold equation are for the pure components, MMA and CO_2, and occur at 0.04 bar and 57 bar, respectively. Obviously, in these two cases mass transfer limitations cannot occur. At every other CO_2 fraction the liquid composition differs from the vapor composition and mass transport can be limiting. To illustrate the large difference in composition between liquid and vapor, the composition of both phases have been calculated with the LKP equation of state. Figure 3.6 shows the distribution of CO_2 and MMA over the two phases at 293K, 303K and 313K. In general, the equilibrium molar fraction of CO_2 in the bubble will approximately be 0.99.

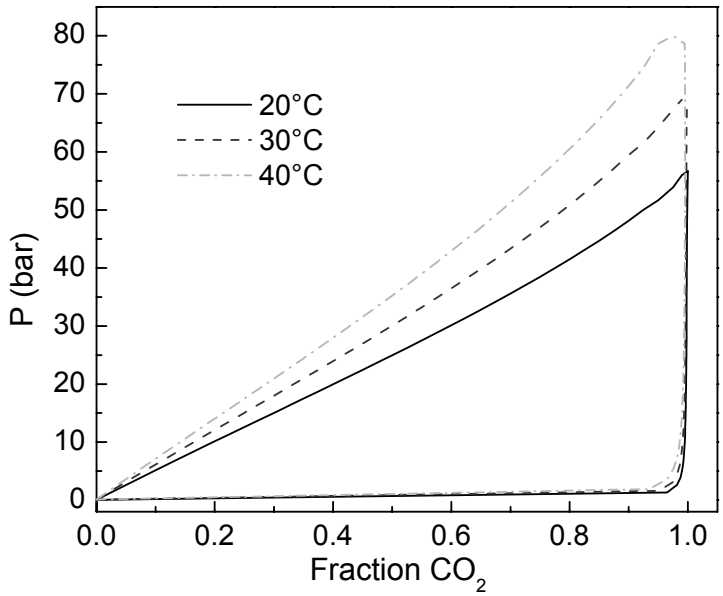

Figure 3.6. Calculated phase diagram of the CO_2/MMA system with the LKP equation of state at 293 K, 303 K and 313 K, respectively.

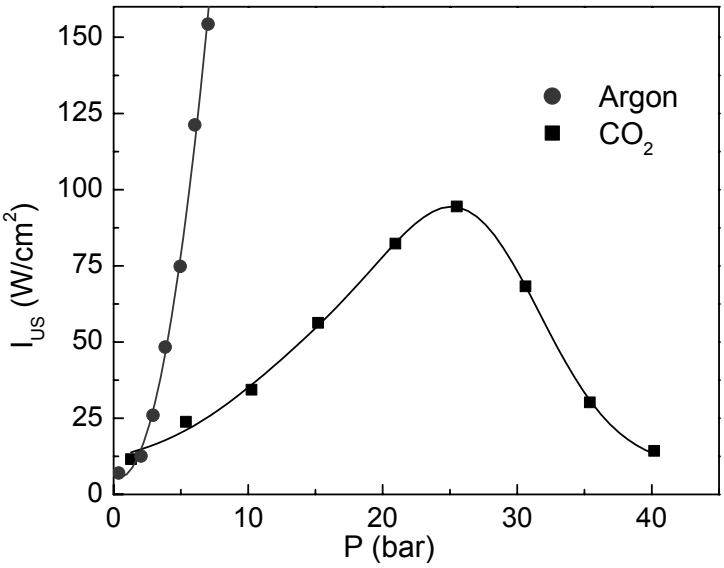

Figure 3.7. Experimental cavitation intensities as a function of pressure for MMA, pressurized with argon or carbon dioxide.

In Figure 3.7, the experimental threshold intensities are given as a function of pressure for MMA, pressurized with Ar or CO_2. Comparison of Figure 3.7 with Figure 3.1 shows a large deviation between the Blake threshold pressure and the experimental threshold pressure for the CO_2-expanded MMA system, especially the trend. Goldfarb et al.[27] have observed similar results for water that was pressurized with argon or CO_2. They ascribed this maximum for water pressurized with CO_2 to a decrease in the surface tension of the liquid at higher CO_2 fractions. As a result of this lower surface tension, however, the Blake threshold pressure only decreases by approximately 2 bar. This effect, therefore, cannot explain the large deviation in threshold pressure that is observed.

Figure 3.8 shows the experimental threshold intensities of the CO_2/MMA-system at three different temperatures. The lines represent the trend of the cavitation threshold as a function of the CO_2 fraction. In all three cases a maximum is observed, which moves to lower CO_2 fractions for higher temperatures.

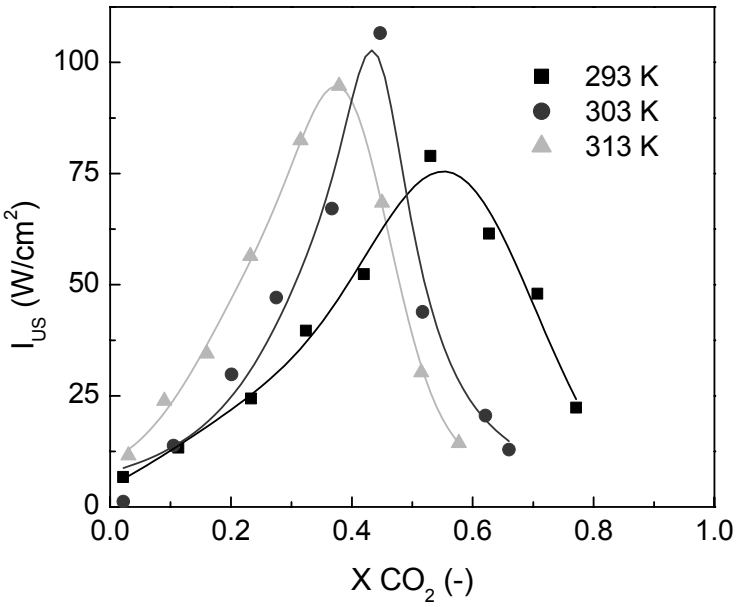

Figure 3.8. Experimental cavitation intensities for CO_2-expanded MMA at 293 K, 303 K and 313 K, respectively.

To determine whether mass transfer limitations can explain the deviation between the theoretical and experimental threshold intensities, the concentration profiles around a growing cavity have been calculated. Figure 3.9 shows the CO_2-concentration profiles in the liquid surrounding a bubble at 10 bar and 293 K (X_{CO_2} = 0.2) when it grows from an initial radius of $1*10^{-6}$ m with a velocity of 0.1 m/s. The diffusion coefficient of CO_2 in MMA has been estimated with the Wilke-Chang equation.[17] According to Figure 3.9, a strong decrease in the CO_2 fraction at the interface is found and consequently a lower vapor pressure in the bubble, as explained in the theoretical section. For this reason, mass transport limitation results in a much higher threshold pressure as theoretically predicted by the Blake threshold (Figure 3.1).

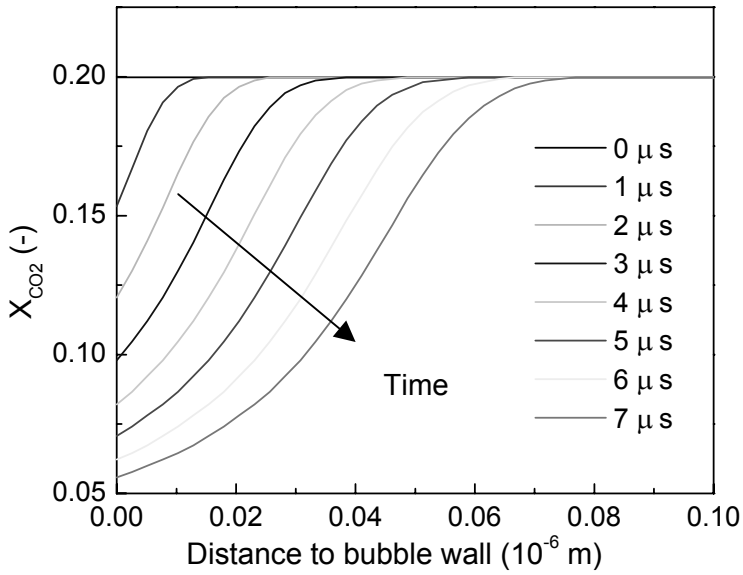

Figure 3.9. CO_2 concentration profiles around a cavity when a bubble with an initial radius of $1*10^{-6}$ m grows with a velocity 0.1 m/s ($D = 5*10^{-9}$ m^2/s, f = 20 kHz).

Therefore, mass transport limitations explain the maximum that is experimentally observed in this study as well as the results obtained by Goldfarb et al.[25] The fact that the threshold maximum moves to lower CO_2 fractions at higher temperatures (Figure 3.8) is possibly caused by the higher mass transfer rate. From the foregoing it can be concluded that mass transfer in the liquid phase has thus a significant influence on the threshold intensity and hence on the initial growth of a cavity at elevated pressures. Consequently, the growth and implosion of a cavitation bubble and the resulting hot-spot are significantly affected by mass transfer.

3.6 Conclusions

In this work, cavitation thresholds have been experimentally determined for an ordinary liquid (MMA with argon) and a gas-expanded liquid (MMA with CO_2) by calorimetry. The Blake threshold pressure as well as the dynamic bubble model are able to predict the onset of cavitation in MMA pressurized with argon. However, for the CO_2/MMA-system, a maximum threshold intensity has been measured when the pressure is increased, which cannot be explained with the Blake threshold equation. Therefore, a mass transport model has been employed to investigate the influence of mass transfer on the growth of cavities. The results show that mass transfer limitation of CO_2 in the liquid towards the bubble explains the observed acoustic threshold pressures.

3.7 References

1. L. H. Thompson, L. K. Doraiswamy, *Ind. Eng. Chem. Res.* **1999**, 38, 1215

2. K. S. Suslick, *Science* **1990**, 247, 1439

3. C. Horst, U. Kunz, A. Rosenplänter, U. Hoffmann, *Chem. Eng. Sci.* **1999**, 54, 2849

4. K. S. Suslick, *Sci. Am*. **1989**, 2, 62

5. T. J. Leighton, *The Acoustic Bubble*; Academic Press: London, 1994

6. S. Hilgenfeldt, P. M. Brenner, S. Grossmann, D. Lohse, *J. Fluid Mech.* **1998**, 365, 171

7. J. Berlan, F. Trabelsi, H. Delmas, A. M. Wilhelm, J. F. Petrignani, *Ultrason. Sonochem.* **1994**, 1, S97

8. M. W. A. Kuijpers, D. v. Eck, M. F. Kemmere, J. T. F. Keurentjes, *Science* **2002**, 298, 1969

9. M. A. Abraham, L. Moens, *Clean solvents, alternative media for chemical reactions and processing*; ACS Symposium Series: Washington, 2002

10. P. G. Jessop, W. Leitner, *Chemical synthesis using supercritical fluids*; Wiley-VCH: Weinheim, 1999

11. T.J. de Vries, M. A. G. Vorstman, J. T. F. Keurentjes, *Chem. Commun*. **2000**, 4, 263

12. A. Harkin, A. Nadim, T. J. Kaper, *Physics of Fluids* **1999**, 11, 274

13. M. S. Plesset, A. Prosperetti, *Annu. Rev. Fluid. Mech.* **1977**, 9, 145

14. J. M. Smith, H. C. van Ness, M. M. Abbott, *Introduction to Chemical Engineering Thermodynamics*; Mcgraw-Hill: Singapore, 1996

15. R. Toegel, D. Lohse, *J. Chem. Phys.* **2003,** 118, 1863

16. M. P. Brenner, S. Hilgenfeldt, D. Lohse, *Reviews of Modern Physics* **2002**, 74, 425

17. J. R. Welty, C. E. Wicks, R. E. Wilson, *Fundamentals of Momentum, Heat and Mass Transfer*; John-Wiley & Sons: New York, 1984

18. M. Lora, M. A. McHugh, *Fluid Phase Equilibria* **1999**, 157, 285

19. U. Plöcker, H. Knapp, J. Prausnitz, *Ind. Eng. Chem. Process Des. Dev.* **1978**, 17, 324

20. M. W. A. Kuijpers, L. J. M. Jacobs, M. F. Kemmere, J. T. F. Keurentjes, submitted

21. L. Varela de la Rosa, E. D. Sudol, M. S. El-Aasser, A. Klein, *J. Polym. Sci.* **1996**, *34*, 461

22. M. W. A. Kuijpers, M. F. Kemmere, J. T. F. Keurentjes, *Ultrasonics* **2002**, 40, 675

23. R. Carloff, A. Prob, K.-H. Reichert, *Chem. Eng. Tech.* **1994**, 17, 406

24. A. Tietze, A. Prob, K.-H. Reichert *DECHEMA Monogr*. **1995**, 131, 673

25. S. L. Oswal, B. M. Patel, A. M. Patel, N. Y. Ghael, *Fluid Phase Equilibria* **2003**, 206, 313

26. C. L. Yaws, *Chemical Properties Handbook*; McGraw-Hill: New York, 1999

27. D. L. Goldfarb, H. R. Corti, F. Marken, G. Compton, *J. Phys. Chem. A.* **1998**, 102, 8888

4 Influence of CO_2 on Ultrasound-induced Polymerizations in High-Pressure Fluids

A strong viscosity increase upon polymerization hinders cavitation and subsequent radical formation during an ultrasound-induced bulk polymerization. In this work, ultrasound-induced radical polymerizations of methyl methacrylate (MMA) have been performed in CO_2-expanded MMA as well as in bulk MMA. For this purpose, the phase behavior of CO_2/MMA systems has been determined. With temperature oscillation calorimetry, the influence of CO_2 on the viscosity and on the reaction kinetics of ultrasound-induced polymerizations of MMA has been studied. In contrast to polymerizations in bulk, this technique shows that a low viscosity is maintained during polymerization reactions in CO_2-expanded MMA. As a consequence, a constant or even increasing polymerization rate is observed when pressurized CO_2 is applied.

This chapter is based on: M.W.A. Kuijpers, L.J.M. Jacobs, M.F. Kemmere, J.T.F. Keurentjes, AIChE-Journal, submitted.

4.1 Introduction

Ultrasound-induced cavitation is known to enhance chemical reactions as well as mass transfer at ambient temperatures and pressures. The chemical effects of cavitation arise from the extreme conditions in the bubble (10.000 K and 200 bar)[1] and the high strain rates outside the bubble (10^7 s^{-1})[2] generated upon implosion. Monomer molecules are dissociated by the high temperatures in the hot-spot, whereas polymer chains are fractured by the high strain rates.[3,4] These two effects lead to the formation of radicals, which can initiate a polymerization reaction. The majority of the radicals in an ultrasound-induced polymerization reaction originate from the polymer chains.[5] Since the radicals are generated in-situ by ultrasound, no initiator or catalyst is required to perform an ultrasound-induced polymerization. An additional advantage of this technique is the intrinsic safe operation, because turning off the electrical power supply will immediately stop the radical formation and consequently the polymerization reaction.

An important factor during ultrasound-induced bulk polymerizations is the viscosity.[6] Upon reaction the long chains formed cause a drastic increase in the viscosity. A high viscosity hinders cavitation and consequently reduces the production rate of radicals.[7] In order to obtain a constant viscosity and hence a constant radical formation rate, an anti-solvent for the polymer can be used. Two effects then lead to a lower liquid viscosity at a given polymer concentration. First, the gyration radius of a polymer chain in solution is smaller as compared to bulk systems, resulting in less entanglements of polymer chains. Secondly, at high polymer and/or anti-solvent concentrations, the polymer precipitates from the solution. Consequently, the viscosity and hence the radical formation rate is expected to remain virtually constant. In this perspective, high-pressure CO_2 is an interesting medium as most monomers have a high solubility in CO_2, whereas it exhibits an anti-solvent effect for most polymers.[8] However, up till now ultrasound is rarely studied at higher pressures, because in most cases a high static pressure hampers the growth of cavities. Recently, we have shown that cavitation is possible in pressurized CO_2.[9]

Unlike ordinary liquids, carbon dioxide has a high vapor pressure, which counteracts the static pressure. Cavitation is possible if the difference between the static and vapor pressure is smaller than the maximum acoustic pressure that can be applied.[10] Dense-phase fluids (with a strong emphasis on CO_2) provide possibilities for the development of sustainable polymer processes.[11,12] Additionally, ultrasound combined with high-pressure carbon dioxide allows the development of clean routes to produce polymers with specific properties, since no organic anti-solvents are required.

In this work, the anti-solvent effect of CO_2 on the ultrasound-induced polymerization of MMA is studied. First, phase equilibrium measurements are presented, which give the composition and the density of the CO_2/MMA system at different conditions. With these data, the liquid volume can be calculated, allowing for a proper comparison of the ultrasound-induced polymerization experiments. Based on a combination of phase equilibrium data and temperature oscillation calorimetry, the influence of the CO_2 fraction and polymer concentration on the viscosity of the solution is determined. With temperature oscillation calorimetry, the overall heat transfer coefficient is measured, which can be coupled to the viscosity. Finally, the results of ultrasound-induced polymerization experiments are given, in which the influence of the CO_2 fraction on the produced polymer and the reaction kinetics is investigated.

4.2 Experimental

Phase equilibrium measurements

Phase equilibrium and density measurements were performed by two different techniques: using a high-pressure view-cell in combination with a CO_2-buffer cylinder and with a so-called Cailletet apparatus.[13]

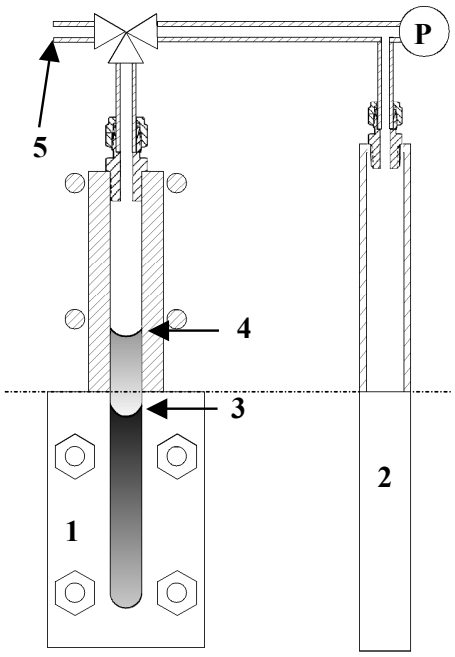

Figure 4.1. A schematic representation of the view-cell/CO_2-buffer cylinder apparatus, with: 1. High-pressure view cell, 2. CO_2-buffer cylinder, 3. Starting liquid volume, 4. Expanded liquid volume, 5. Vacuum/CO_2 .

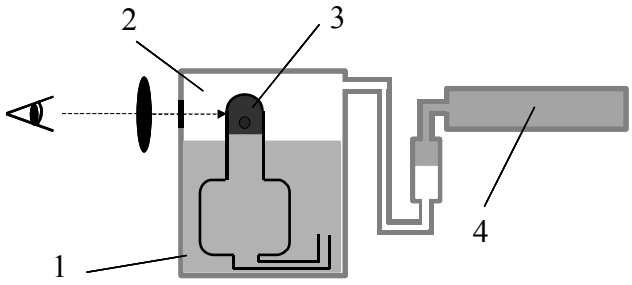

Figure 4.2. A schematic representation of the Cailletet apparatus, with: 1. Mercury, 2. Water, 3. Sample, 4. Pressure System.

Figure 4.1 shows the set-up of the view-cell and CO_2-buffer cylinder used for the equilibrium measurements. The whole apparatus was submerged in a water bath, which was thermostated within 0.1°C. The measurements in the view-cell were performed by filling the cell to a certain height with MMA (Merck) and evacuating all the air. After pressurization of the buffer cylinder with a known amount of CO_2 (grade 5.0, Hoekloos), it was connected with the view-cell. When equilibrium was reached, the expansion of the liquid was calculated from the rise of the meniscus. Using the known initial and final gas volume as well as the pressure decrease in the system, the amount of CO_2 that dissolved in MMA was calculated with a modified Benedict-Webb-Rubin equation.[14] This equation calculates accurately the density of CO_2 as function of temperature and pressure. With the dissolved amount of CO_2 and the final liquid volume, the CO_2 fraction in the liquid phase and the liquid density were calculated. It was assumed that the amount of MMA in the gas phase is negligible.

In the Cailletet apparatus (Figure 4.2) the phase behavior of mixtures of constant composition can be determined visually by varying the pressure at constant temperature. A sample of the mixture with known composition was confined over mercury in the sealed top of a glass capillary tube. The static pressure on the CO_2/MMA system was increased until the vapor phase had disappeared. The pressure at which this occurs is the bubble point of the system. The mercury served as a sealing fluid and pressure transmitting fluid between the sample and the hydraulic system. The glass tube was thermostated with an accuracy of 0.01°C by circulating water of constant temperature.

Modeling phase equilibria

The Lee-Kessler-Plöcker (LKP) equation of state[15] is used to describe the phase behavior of the CO_2/MMA system. This equation of state applies to hydrocarbon systems, which include light gases such as CO_2. The LKP-model uses pure component parameters, such as the critical temperature, the critical pressure and an acentric factor (ω), and a single binary

interaction parameter. The LKP equation of state can be described in terms of compressibility factors (Z) in which *ref1* is a reference fluid with an acentric factor of zero and *ref2* is a fluid with a high acentric factor, i.e. n-octane (Equation 4.1). The compressibility factors of the reference fluids are a function of the reduced temperature and pressure of the mixture of interest. To obtain the mixture parameters, mixing rules are applied using a binary interaction parameter for the critical temperature. The binary interaction parameter for LKP was determined by fitting the model to the experimental points at all temperatures.

$$Z = Z_{ref1} + \frac{\omega_m - \omega_{ref1}}{\omega_{ref2} - \omega_{ref1}}\left(Z_{ref2} - Z_{ref1}\right) \quad (4.1)$$

Evaluation of the CO_2 anti-solvent effect

In ultrasound-induced polymerization reactions, the viscosity has a large influence on the radical formation rate. Therefore it is important to monitor the viscosity during these reactions. By coupling the overall heat transfer coefficient U to the viscosity of the reaction mixture, the influence of the CO_2-concentration on the viscosity of polymer solutions was determined.

$$\frac{1}{U} = \frac{1}{h_i} + \frac{D_i}{2\,k_w}\ln\frac{D_0}{D_i} + \frac{1}{h_0}\frac{D_i}{D_0} \quad (4.2)$$

In Equation 4.2 the heat transfer coefficient is based on the inside area of the reactor, for which h_i and h_o represent the partial heat transfer coefficients in the vessel and in the jacket, respectively; k_w stands for the thermal conductivity coefficient of the wall; D_i and D_o are the inner and outer diameter of the vessel.[16] The last two terms of Equation 4.2 remain constant during a polymerization reaction, because the properties of the reactor wall and cooling liquid will not change during the experiments. Therefore, U is an indirect measure of the viscosity of the reaction mixture, since the empirical relation for the Nusselt number (Nu) as a function of the Reynolds (Re) and Prandtl number (Pr) can be applied to couple h_i to the viscosity. Equation 4.6, which is derived from Equations 4.3, 4.4 and 4.5, shows the influence of the viscosity on the overall heat-transfer coefficient.

An increase in the viscosity (μ) thus results in a decrease of the overall heat transfer coefficient.[17]

$$Nu = \frac{h_i D_i}{k_i} = 0.75\,\mathrm{Re}^{2/3}\,\mathrm{Pr}^{1/3} \qquad (4.3)$$

Where the Reynolds and the Prandtl number stand for:

$$\mathrm{Re} = \frac{\rho N D^2}{\mu} \qquad (4.4)$$

$$\mathrm{Pr} = \frac{\mu C_p}{k_i} \qquad (4.5)$$

$$\frac{1}{U} \sim \sqrt[3]{\mu} + \mathrm{Constant} \qquad (4.6)$$

The experiments to determine the influence of the CO_2 fraction and polymer concentration on the viscosity were performed in a commercially available reaction calorimeter RC1e (Figure 4.3, Mettler-Toledo GmbH, HP60 reactor, Switzerland). A detailed description of this equipment is given by Varela de la Rosa et al.[18] The reactor was filled with 1.5 L CO_2-expanded MMA, in which polymethyl methacrylate (PMMA, Aldrich) with a M_n of 141 kg/mol and a polydispersity of 2.2 was dissolved. A radical scavenger (1,1-diphenyl-2-picrylhydrazyl, Aldrich) was added to prevent polymerization. U was continuously calculated by temperature oscillation calorimetry[19,20] during the experiments with different polymer and CO_2-concentrations. The RC1e was operated in isothermal mode at 20°C, i.e. the jacket temperature (T_j) of the reactor was automatically adjusted to keep the reactor temperature (T_r) constant.

Ultrasound-induced polymerizations

Ultrasound with a frequency of 20 kHz was produced using a Sonics and Materials VC750 ultrasonic generator. A ½-inch full-wave titanium probe was applied to couple the piezoelectric transducer to the liquid. To allow an accurate comparison, the total configuration of the reactor was exactly kept constant during all the experiments. The experiments were performed in the RC1e in isothermal mode at 20°C. Throughout the

experiments the heat flow (Q) was calculated, based on the surface area of the reactor wall (A), the overall heat transfer coefficient and the difference between jacket and reactor temperature (Equation 4.7). The ultrasound intensity (I_{US}), which is a measure of the acoustic pressure amplitude ($P_{A,max}$, Equation 4.8), was calculated by dividing the heat flow by the surface area of the ultrasound horn (A_{US}).[10]

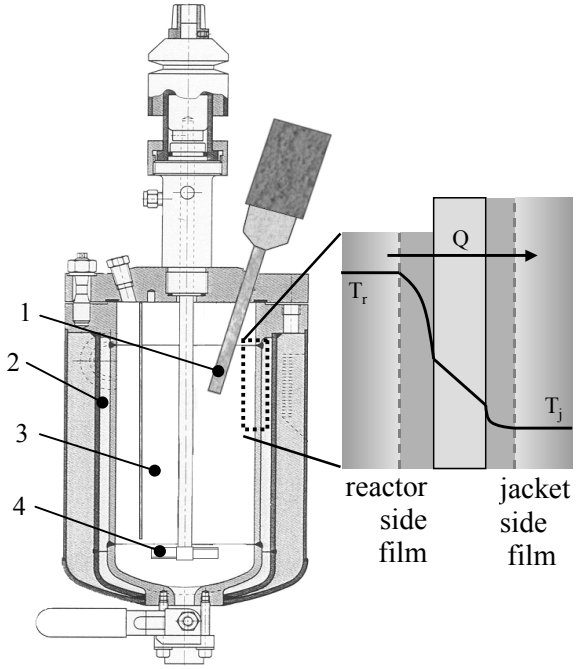

Figure 4.3. Schematic representation of the reactor set-up and the resistances for heat transfer through the reactor wall, with; 1. Full-wave horn, 2. Jacket, 3. Reactor contents, 4. Impeller.

$$Q = U\,A\,(T_r - T_j) \qquad (4.7)$$

$$P_{A,\max} = \sqrt{2\,\rho\,v\,\frac{Q}{A_{US}}} = \sqrt{2\,\rho\,v\,I_{US}} \qquad (4.8)$$

For the polymerization reactions, the reactor was filled with 1.5 L CO_2-expanded MMA, in which 0.5 weight% PMMA with a M_n of 141 kg/mol and a polydispersity of 2.2 was dissolved. By the addition of polymer the inhibition period due to oxygen was minimized. The MMA was distilled under vacuum to remove the hydroquinone inhibitor before use. During

the reaction CO_2 (grade 5.0) or argon (grade 5.0, Hoekloos) was bubbled through a 3 mm tube into the reaction mixture with a flow rate of 2.0 mL/s. These Ar or CO_2 bubbles served as nuclei for the cavities. Samples were taken during the experiments from which the conversion and the molecular weight distribution (MWD) of the polymer were obtained. Additionally, U was determined in time to monitor the viscosity. The MWDs were measured by gel permeation chromatography, calibrated against polystyrene standards. The molecular weight distributions of the PMMA samples were calculated with the appropriate Mark-Houwink parameters (a=0.719 and $K=9.44*10^{-5}$ m^3).[21]

4.3 Results and Discussion

In this study the influence of the CO_2 anti-solvent effect on the viscosity and on the kinetics of an ultrasound-induced polymerization reaction have been studied. First, the phase behavior of the applied CO_2/MMA system has been determined and modeled. Next, the influence of the CO_2-concentration and polymer concentration on the liquid viscosity has been measured without polymerization. Finally, the anti-solvent effect of CO_2 on the ultrasound-induced polymerization kinetics has been determined.

Phase behavior of the reaction mixture

The phase behavior of the CO_2-expanded MMA system is required to determine the influence of CO_2 on the viscosity during ultrasound-induced polymerization experiments. In Figure 4.4 several phase equilibrium measurements in the CO_2/MMA-system are presented. The phase equilibrium data of the experiments in the high-pressure view-cell (closed symbols) and in the Cailletet apparatus (open symbols), which are based on two different measurement principles, are in good agreement. The three isotherms in Figure 4.4 are obtained by modeling the bubble points with the LKP equation of state[15] with an interaction parameter of 1.08. With this temperature-independent interaction parameter, the measurements at 20°C, 30°C and 40°C are accurately modeled. In principle, the use of such a model also allows for extrapolation to higher CO_2 fractions.

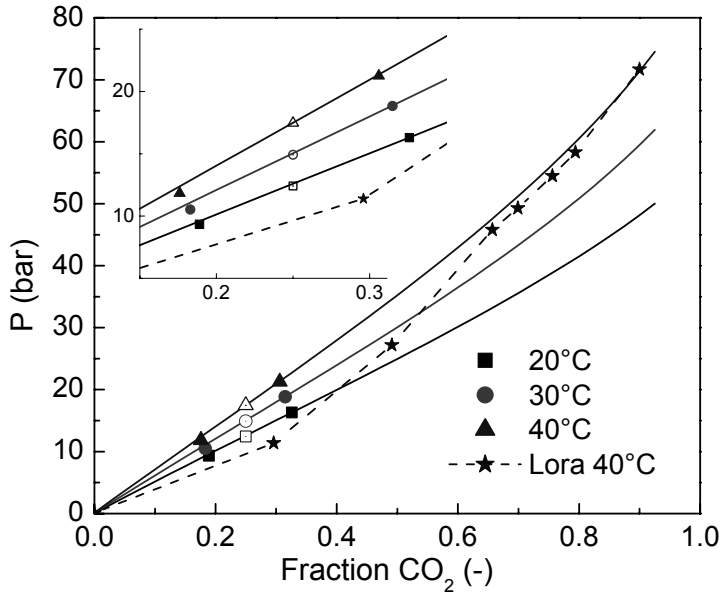

Figure 4.4. Measured bubble points of the CO_2/MMA system and the calculations based on the Lee-Kessler-Plöcker equation of state. Open symbols are measurements with the Cailletet apparatus.

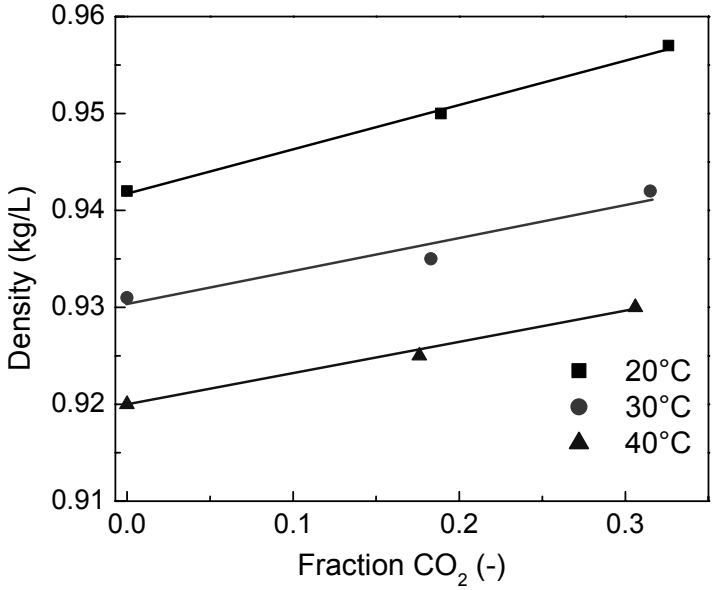

Figure 4.5. Density of the CO_2-expanded MMA system at 20°C, 30°C and 40°C.

Our measurements at 40°C as obtained in the two described apparatuses show substantially higher values at low CO_2 fractions as compared to the experimental data reported by Lora and McHugh.[22] However, the data from Lora and McHugh do coincide with the Lee-Kessler model at 40°C above a CO_2 fraction of 0.65. This deviation at low pressures probably originates from the plunger apparatus used by Lora and McHugh. This system is less accurate at low pressures caused by friction of the plunger, due to which a lower equilibrium pressure is observed at a given CO_2 fraction.

Subsequently, the density of the CO_2-expanded MMA system has been calculated from the view-cell experiments. The density increases when more CO_2 dissolves, see Figure 4.5, in which the lines show the trend However, a reduction of the density is expected at higher CO_2 fractions as pure CO_2 at 20°C and 30°C has a density of 0.776 kg/L and 0.595 kg/L, respectively. This implies that the density is not a linear function between the two pure components.

Anti-solvent effect of CO_2

The liquid viscosity has a major influence on the implosion velocity and consequently on the polymerization rate. To quantify the influence of the CO_2 fraction on the liquid viscosity, the overall heat transfer coefficients are determined for polymer solutions in which no polymerization occurs. Figure 4.6 shows the influence of the polymer concentration (C_{pol}) and CO_2 fraction on U and consequently on the liquid viscosity. The plotted difference (ΔU) is calculated by subtracting U with polymer ($U(C_{pol})$) from U without polymer (U(0)) at a given CO_2 fraction (Equation 4.9). The curves in Figure 4.6 give the trend of the heat transfer decrease and consequently the viscosity increase (Equation 4.6).

$$\Delta U = U(0) - U(C_{pol}) \qquad (4.9)$$

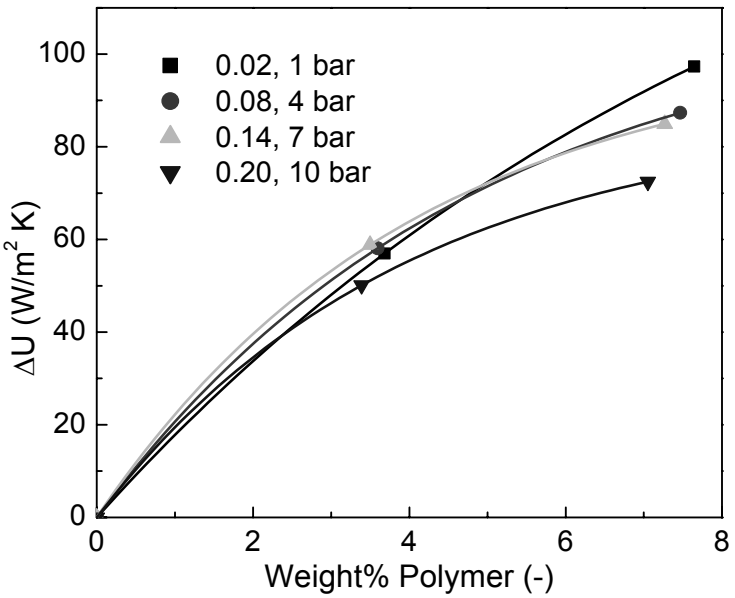

Figure 4.6. Heat transfer coefficient difference as a function of the polymer weight percentage at different CO_2 fractions.

At polymer concentrations above 4 weight percent, a distinct difference between the overall heat transfer coefficients at different CO_2 fractions is obtained. This is a clear evidence for the anti-solvent effect of CO_2. It is not a dilution effect due to the expansion of MMA, as this is taken into account by the calculation of the polymer concentration. The anti-solvent effect at lower concentrations is not apparent, since the polymer coils start overlapping at a polymer concentration of approximately 4 weight percent. Moreover, the anti-solvent effect is expected to be more distinct with higher molecular weight polymer as the chains will overlap at lower concentrations. In view-cell experiments of a solution of 7.5 weight% PMMA in MMA at 13 bar CO_2 and 20°C, no second phase (polymer phase) has been observed, which implies that the lower viscosity is due to the smaller gyration radius of the polymer chains, so that higher polymer concentrations or CO_2 fractions are required to induce precipitation of the polymer.

Table 4.1. Results of ultrasound-induced polymerizations of MMA at 20°C and different CO_2-pressures.

CO_2-pressure (bar)	Fraction CO_2 (-)	Ultrasound amplitude (μm)	Ultrasound intensity (W/cm^2)	Conversion (%)	Initial Rate (mol/m^3 s)	Final Rate (mol/m^3 s)	M_n (kg/mol)
0	0	74	31	3.1	0.037	0.018	110
1.0*	0.02	74	31	3.3	0.019	0.019	471
4.5	0.09	99	102	3.9	0.019	0.040	474
7.0	0.14	74	69	2.5	0.023	0.023	428

*Reaction started with 1.0 weight% polymer.

Ultrasound-induced polymerizations

The results of the ultrasound-induced polymerizations in CO_2-expanded MMA are given in Table 1. For a proper comparison of the overall heat transfer coefficients, it is important to use polymers with the same molecular weight, since the viscosity is a function of both the polymer concentration and molecular weight. For this reason the polymerization in which argon is used as nucleation source (0 bar CO_2), is not given in Figure 4.7 and a higher amplitude is used at 4.5 bar in order to obtain polymers with similar molecular weights. Figure 4.7 shows U, which is determined by temperature oscillation calorimetry, as a function of the conversion. It can clearly be seen that the decrease in U is smaller and hence the increase in viscosity is lower for higher CO_2 fractions during polymerization. This is a result of the smaller gyration radius of the polymer coils as no precipitated polymer has been found at the final conversion. This positive influence of CO_2 on the solution viscosity has also been seen in the previous section in which no polymerization occurred. To couple the viscosity to U, the viscosity at 0% and 1.2% conversion at 1 bar CO_2 have been measured, which are $1.0*10^{-3}$ and $2.8*10^{-3}$ Pa s, respectively. The

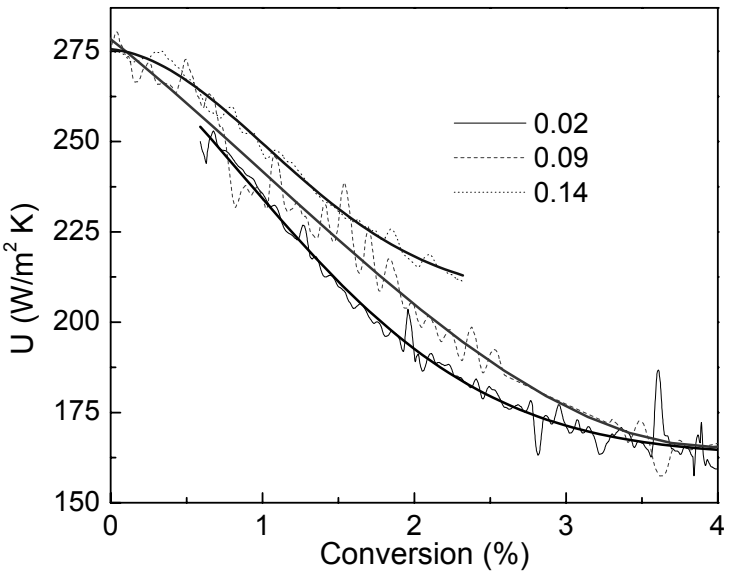

Figure 4.7. Development of the overall heat transfer coefficient during the polymerization reactions at three different CO_2-pressures.

corresponding overall heat transfer coefficients are 275 and 225 W/m^2 K (Figure 4.7) at 0% and 1.2% conversion, respectively. The polymerization reaction with a CO_2 fraction of 0.14, reaches this U-value of 225 W/m^2 K and hence the viscosity of $2.8*10^{-3}$ Pa s, at a conversion of 1.9%. This theoretically implies that the cavitation intensity and hence the radical formation rate at 1.9% conversion and a CO_2 fraction of 0.14 is similar to the radical formation rate at 1.2% conversion and a CO_2 fraction of 0.02.

The polymerizations in CO_2 show a reaction rate in the same order of magnitude as compared to the bulk experiment at ambient pressure with argon (Figure 4.8A and Table 4.1). The initial reaction rates with CO_2 are slightly lower as compared to the bulk experiment. This is probably caused by the lower polytropic index of CO_2 as compared to Ar,[10] due to which the implosion of the cavitation bubbles is less violent. Although the reaction rates are similar, the polymer produced at 1, 4.5 and 7 bar CO_2-pressure have much a higher molecular weight than the reference polymer in bulk MMA with argon. Kruus et al.[23] found a similar result during an ultrasound-induced polymerization when CO_2 was bubbled through the reaction mixture instead of another gas. A possible reason for the higher molecular weight would be a decrease in the chain transfer rate to monomer or an increase in the chain transfer rate to polymer. These transfer reactions only influence the produced molecular weight and not the reaction rate. All other reactions, e.g. polymer scission, propagation, initiation and termination, affect both the MWD and the polymerization rate.

Figure 4.8B and Table 4.1 show that in the experiment with argon the reaction rate decreases whereas the polymerization rate is constant or even increases when CO_2 is used. This is a result of the viscosity reduction by the anti-solvent behavior of CO_2 at higher polymer concentrations. Consequently, the radical formation rate by cavitation is not decreased when CO_2 is applied. The initial negative influence of CO_2 on the implosion intensity at low polymer concentrations (0.5 wt%) is thus more than compensated at higher polymer concentrations by the anti-solvent effect.

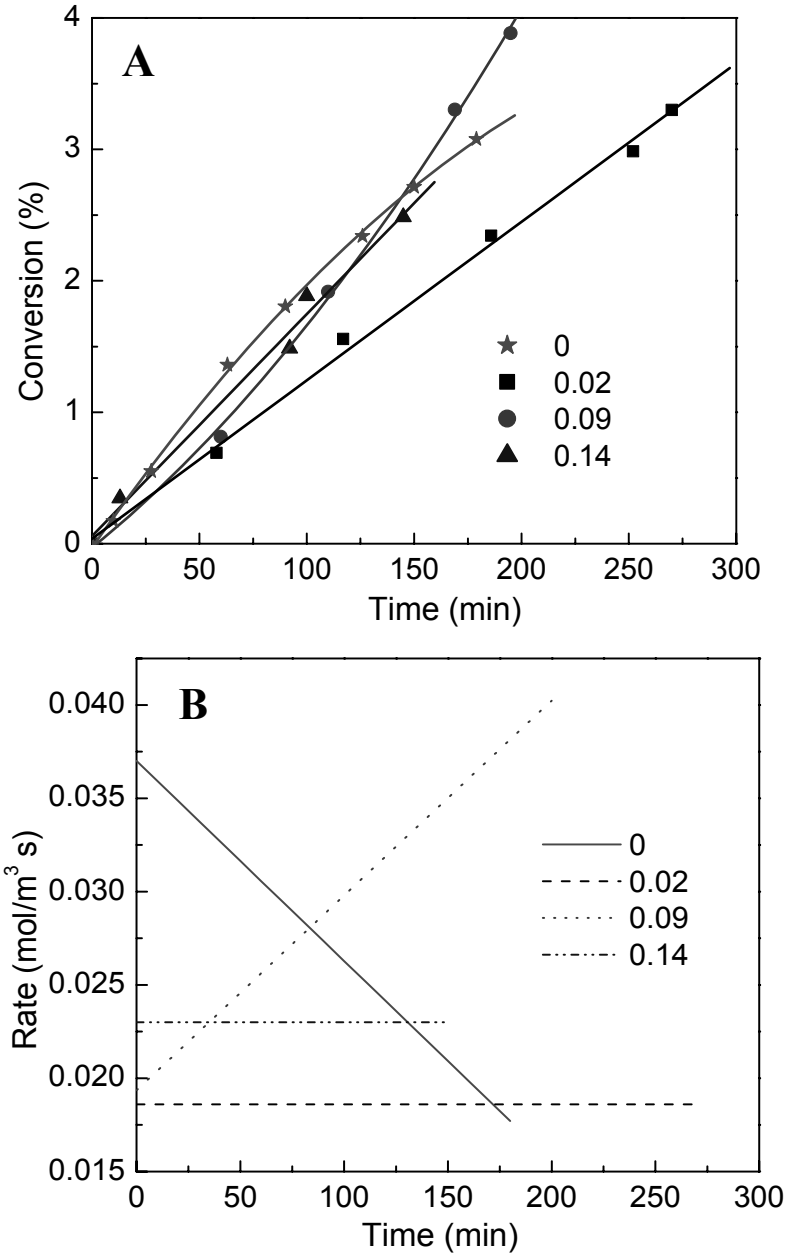

Figure 4.8. Conversion-time history (A) and reaction rates (B) of ultrasound-induced polymerizations of MMA at various CO_2 pressures.

Typically, in ultrasound-induced bulk polymerizations a maximum conversion of approximately 15% can be achieved.[7] At this conversion the collapse of cavitation bubbles is no longer sufficiently strong to generate radicals by ultrasound, due to the high viscosity. The decrease in viscosity by the CO_2 anti-solvent effect implies that higher conversions in CO_2-expanded MMA as compared to bulk MMA would be possible. Moreover, at higher conversions the polymer will precipitate in the presence of an anti-solvent, due to which a constant viscosity is maintained and even higher conversions are expected.

4.4 Conclusions

In this work, the influence of the CO_2 fraction on the viscosity and the resulting reaction kinetics of the ultrasound-induced polymerization of MMA have been studied. For this purpose, phase equilibrium and density measurements in a high-pressure view-cell and a Cailletet apparatus have been performed. The obtained phase equilibria are accurately modeled with the Lee-Kessler-Plöcker equation of state with an interaction parameter of 1.08. Based on these data, the influence of CO_2 and polymer concentration on the viscosity has been determined by temperature oscillation calorimetry. With this technique, the overall heat transfer coefficient has been measured, which can be coupled to the viscosity. By calibration of the calorimeter, it is shown that the viscosity is significantly reduced at polymer concentrations at which the coils would overlap in bulk systems without CO_2 present. Due to this anti-solvent effect of CO_2, the reaction rate does not decrease and even increases during ultrasound-induced polymerization in CO_2-expanded MMA. As a result of the reduction in viscosity as compared to ultrasound-induced bulk polymerization, it will be possible to obtain higher conversions in CO_2-expanded MMA systems.

4.5 Nomenclature

- μ Viscosity (Pa s)
- ρ Density (kg/m^3)
- ω Acentric factor (-)
- A Heat transfer area (m^2)
- A_{US} Area ultrasound probe (m^2)
- C_p Specific heat capacity (J/kg K)
- D Impeller diameter (m)
- D_0 Outer diameter of reactor (m)
- D_i Inner diameter of reactor (m)
- h_i Partial heat transfer coefficient reactor (W/m^2 K)
- h_0 Partial heat transfer coefficient jacket (W/m^2 K)
- k_i Conductivity of liquid inside reactor (W/m K)
- k_0 Conductivity of liquid inside jacket (W/m K)
- k_w Conductivity of reactor wall (W/m K)
- N Stirrer speed (s^{-1})
- Nu Nusselt number (-)
- Pr Prandtl number (-)
- Q Heat flow (W)
- Re Reynolds number (-)
- T_j Jacket temperature (K)
- T_r Reactor temperature (K)
- U Overall heat transfer coefficient (W/m^2 K)
- v Sound velocity (m/s)
- Z Compressibility (-)

4.6 References

1. Y.T. Didenko, W.B. Mcnamara III, K.S. Suslick, *Nature* **2000**, 407, 877

2. T.Q. Nguyen, Q.Z. Liang, H.-H. Kausch, *Polymer* **1997**, 38, 3783

3. P. Kruus, *Ultrasonics*, **1987**, 25, 20

4. G.J. Price, P.J. West, P.F. Smith, *Ultrason. Sonochem.* **1994**, 1, S51

5. M.W.A. Kuijpers, M.F. Kemmere M.F., J.T.F. Keurentjes, "*Ultrasound-induced radical polymerization*", in Encyclopedia of Polymer Science and Technology; John Wiley & Sons: New York, 2004

6. J.M. Pestman, J.B.F.N. Engberts, F. de Jong, *Recl. Trav. Chim. Pays-Bas* **1994**, 113, 533

7. G.J. Price, *Ultrason. Sonochem.* **1996**, 3, S229

8. D.A. Canelas, J.M. DeSimone, *Adv. Pol. Sci.* **1997**, 133, 103.

9. M.W.A. Kuijpers, D. van Eck, D., M.F. Kemmere, J.T.F. Keurentjes, *Science* **2002**, 298, 1969

10. T.J. Leighton, *The Acoustic Bubble;* Academic Press: London, 1994

11. P.G. Jessop, W. Leitner, *Chemical Synthesis using Supercritical Fluids;* Wiley-VCH: Weinheim, 1999

12. M.A. Abraham, L. Moens, *Clean Solvents, Alternative Media for Chemical Reactions and Processing*; ACS Symposium Series 819: Washington, 2002

13. Th.W. de Loos, H.J. van der Kooi, P.L. Ott,.*Chem. Eng. Data* **1986**, 31, 166

14. M. Benedict, G.B. Webb, L.C. Rubin, *J. Chem. Phys.* **1940**, 8, 334

15. U. Plöcker, H. Knapp, J. Prausnitz, *Ind. Eng. Chem. Process Des. Dev.* **1978**, 17, 324

16. M.F. Kemmere, J. Meuldijk, A.A.H. Drinkenburg, A.L. German, *Polymer Reaction Engineering* **2000**, 8, 271

17. M.F. Kemmere, M.W.A. Kuijpers, L.J.M. Jacobs, J.T.F. Keurentjes, *Macromol. Symp.* **2004**, 206, 321

18. L. Varela de la Rosa, E.D. Sudol, M.S. El-Aasser, A. Klein, *J. Polym. Sci.* **1996**, 34, 461

19. R. Carloff, A. Proβ, K.-H. Reichert, *Chem. Eng. Tech.* **1994**, 17, 406

20. A. Tietze, A. Proβ, K.-H. Reichert, *DECHEMA Monogr.* **1995**, 131, 673

21. L. Xue, U.S. Agarwal, P.J. Lemstra, *Macromolecules* **2002**, 35, 8650

22. M. Lora, M.A. McHugh, *Fluid Phase Equilibria* **1999**, 157, 285

23. P. Kruus, M. O'Neill, D. Robertson, *Ultrasonics* **1990**, 28, 304

5 The Mechanism of Cavitation-induced Polymer Scission

In this paper we describe qualitatively and quantitatively the non-random scission of polymers by ultrasound. Scission experiments have been performed using monodisperse polymethyl methacrylate dissolved in methyl methacrylate, showing that fracture occurs close to the center of the polymer chain. A mechanism is proposed for this non-random fracture, from which it can be concluded that complete stretching of the polymer chains is required before breakage can occur. The developed model, which is a combination of strain rate and drag force calculations, predicts a limiting molecular weight, which has experimentally been confirmed. The scission rate depends almost quadratically on the molecular weight, which is derived by modeling the experimental time-dependent molecular weight distributions. This dependence supports the requirement of complete stretching of the polymer chain before breakage. The developed degradation model is also capable to describe the effects of various process variables on cavitation-induced polymer scission.

This chapter is partially based on: M.W.A. Kuijpers, P.D. Iedema, M.F. Kemmere, J.T.F. Keurentjes *Polymer*, submitted

5.1 Introduction

The molecular weight distribution (MWD) is an important characteristic of polymers. In the polymer industry often a post-processing step is applied to alter the MWD, e.g. peroxide-induced degradation of polypropylene, thus producing polymers with tailored properties.[1] An alternative method is ultrasound-induced polymer scission, which can either be used as a post-processing step or can be used during ultrasound-induced polymerizations, thus providing an accurate method to control the molecular weight of the obtained polymers by tuning both the scission and polymerization rate.[2]

Ultrasound is known to enhance chemical reactions as well as mass transfer at ambient temperatures and pressures. Most of these effects are caused by cavitations, i.e. the collapse of microscopic bubbles in a liquid. The chemical effects of cavitation arise from the extreme conditions in the bubble (5000 K and 200 bar)[3] and the high strain rates outside the bubble (10^7 s^{-1})[4] generated upon implosion. It has been shown that ultrasound-induced polymer breakage is a direct consequence of cavitation, because no degradation is observed under conditions that suppress cavitation.[5] Similar to flow-induced chain scission, chain fracture upon cavitation arises from the high strain rates on the polymer chain. In the past, much insight has been gained on the flow-induced stretching and scission behavior of linear polymers.[6-8] However, the concentric flow patterns occurring during the collapse of a cavitation bubble differ substantially from the flow patterns studied in flow-induced polymer scission. Moreover, the time scale of cavitation bubble collapse is in the order of microseconds. These effects make the comparison with flow-induced scission not straightforward. Although, significant research efforts have been performed on the ultrasound-induced degradation of polymers, the exact mechanism of polymer scission is still unclear.[8-12] It has been shown that ultrasound-induced polymer scission is a non-random process, as scission occurs approximately in the center of the chain.[4,13,14] Moreover, the scission process stops at a certain limiting molecular weight.[15] This non-random fracture

behavior has been modeled,[4,16,17] however, until now a satisfactory model which fully explains the scission process has not been developed.

In this work ultrasound-induced polymer scission has been studied using monodisperse polymethyl methacrylate (PMMA), for which the relation between molecular weight and scission rate as well as the scission distribution over the polymer chain has been determined experimentally. Additionally, a model is proposed which describes the occurring breakage events, based on models available from flow-induced polymer scission. These models require knowledge of the strain rates around a cavity, which have been calculated using a dynamic bubble model. This general degradation model provides insight in the mechanism and the kinetics of cavitation-induced polymer scission, which can effectively be used to explain various results described in literature.[18-20]

5.2 Theory

Bead-rod model

In the absence of an external force a polymer chain in solution is randomly coiled. Under sufficiently strong flow conditions, however, the solvent drag force causes extension of the polymer molecule. The effects of this drag force have extensively been studied in the flow-induced stretching and scission of linear polymers.[6-8] If a polymer chain is stretched, it can be represented as a chain of beads and rods in the fluid.[6] To completely stretch a polymer chain in solution, the total strain (ε) exerted on the chain has to exceed approximately 3.5 to 6.5, depending on the molecular weight.[21,22]

$$\frac{d\varepsilon}{dt} = -2\frac{R^2\frac{dR}{dt}}{r^3} \qquad (5.1)$$

The strain rate can be calculated from the distance of the polymer chain from the center of the cavity (r), the bubble wall velocity (dR/dt) and the

radius of the bubble (R) (Equation 5.1).[23] During the implosion, the volume between the bubble wall and the polymer molecule is taken constant.

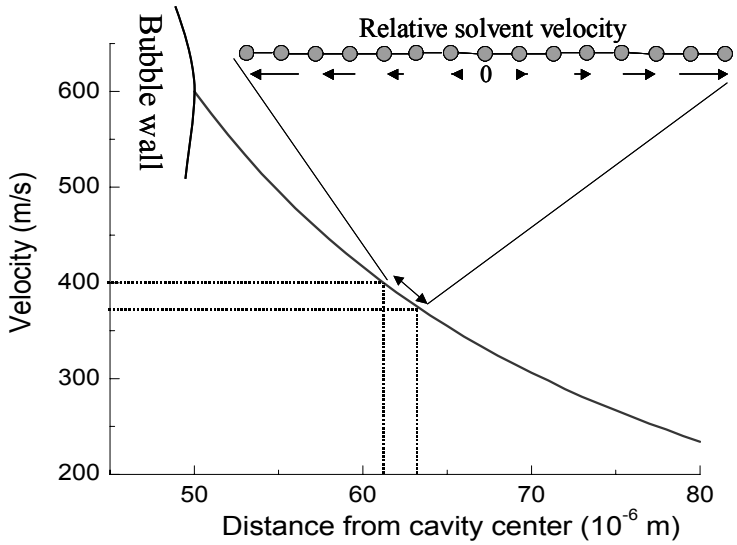

Figure 5.1. Schematic representation of the velocity profile near an imploding bubble and the resulting relative liquid velocity near a stretched polymer chain.

Upon bubble collapse, the entire molecule will move along with the fluid, however, due to the radial velocity profile near the cavity, friction between the polymer chain and the liquid will occur. The drag force per bead resulting from this friction will accumulate in the middle of the chain (Figure 5.1). The force exerted on the center of the chain F_c (Equation 5.2) is dependent on the radius of the bead (a), the length of the repeat unit along the chain (b), the shielding factor (S), the solvent viscosity (η), the strain rate and the number of repeat units (n).[6] Since the accumulative drag force has its maximum in the center of the chain, this will lead to a breakage distribution around the middle. Obviously, the polymer chain will only fracture if the tensile force in a stretched chain segment is larger than the force needed to break a bond.

$$F_c = \frac{6 \cdot \pi}{8} \eta \; a \; b \; S \frac{d\varepsilon}{dt} n^2 \qquad (5.2)$$

Bubble dynamics

The main parameters determining the scission process are the strain rate caused by cavitation and implosion time. A dynamic model is required to calculate the strain rate as a function of time during the implosion of a cavitation bubble. In this study the Kyuichi-Yasui model[24] is used to describe the dynamic movement of the bubble. The model is based on the Rayleigh-Plesset equation (Equation 5.3),[25] which includes the surface tension (σ_{liq}), the vapor pressure (P_v), the liquid viscosity (η), the polytropic index of the gas phase (κ), the static pressure (P_0), the initial bubble radius (R_0) and the acoustic pressure (P_A).

$$R\frac{d^2}{dt^2}R+\frac{3}{2}\left(\frac{d}{dt}R\right)^2=\frac{1}{\rho}\left(P_{gas}+P_v-\frac{2\sigma_{liq}}{R}-\frac{4\eta\frac{d}{dt}R}{R}-P_0-P_A(t)\right) \quad (5.3)$$

The temperature and the vapor and gas pressure inside the bubble are derived from the Rayleigh-Plesset equation in combination with mass and energy balances. The energy balance comprises thermal conduction, the energy of condensation and evaporation, and compression of the non-ideal gas phase in the bubble. For the calculation of the vapor and gas pressure inside the bubble, it is assumed that the vapor phase is in equilibrium with the liquid. Viscosity, vapor pressure and acoustic pressure mainly determine the bubble motion. Consequently, the type of polymer, the polymer concentration, the solvent, the liquid temperature and the acoustic pressure define the degradation rate and the limiting molecular weight.

Molecular weight distribution

The development of the molecular weight distribution has been described using a model based on population balances.[26] Assuming first-order scission kinetics, the scission rate can be determined as function of molecular weight and liquid properties. The kinetic scheme of scission by ultrasound reads as follows:[27]

Scission: $P_n \xrightarrow{k_d(n,m)} P_m \bullet + P_{n-m} \bullet$

Termination by recombination: $P_m \bullet + P_{n-m} \bullet \xrightarrow{k_{tc}} P_n$

Termination by disproportionation: $P_m \bullet + P_{n-m} \bullet \xrightarrow{k_{td}} P_m + P_{n-m}$

If a radical scavenger is present, the termination reaction occurs instantaneously and only between a macroradical fragment and a scavenger molecule. Thus, the scheme reduces to:

$$P_n \xrightarrow{k_d(n,m)} P_m + P_{n-m}$$

where $k_d(n,m)$ is an effective scission rate constant. The scission rate constant k_d is chosen as a function of the original chain length n and fragment length m to allow for the non-random character of the scission process. According to the overall scission reaction, the population balance than becomes:

$$\frac{dP_n}{dt} = \sum_{m=n+1}^{\infty} k_d(n,m) P_m - P_n \sum_{m=1}^{n} k_d(n,m) \qquad (5.4)$$

This balance equation is solved with the Galerkin finite element (FEM) package PREDICI®.[26] By manipulating the shape of $k_d(n,m)$ – which is anticipated to be Gaussian with a width (σ) – it is possible to obtain a best fit between the MWD predicted by Equation 5.5 and the measured MWD. The overall dissociation constant k_d consists of a Gaussian distribution function and a molecular weight dependent scission function (k_{MW}):

$$k_d(n,m) = \frac{k_{MW}(n)}{\sqrt{2\pi}\,\sigma(n)} e^{\left(-\frac{1}{2\sigma(n)^2}\left(m-\frac{n}{2}\right)^2\right)} \qquad (5.5)$$

5.3 Experimental

Scission of linear monodisperse polymethyl methacrylate (PMMA) was studied in a thermostated 200 mL vessel at 20°C (Figure 5.2). Sonification of the solution was performed using 20 kHz ultrasound, which was produced by a Sonics and Materials VC-750 generator. A ½-inch full-wave titanium

probe was applied to couple the piezoelectric transducer to the liquid. To allow for an accurate comparison, the total configuration and the experimental conditions of the reactor were kept constant during all experiments. This ensured that the ultrasonic power input, 55 W, was constant for all experiments at an amplitude of 75 μm.

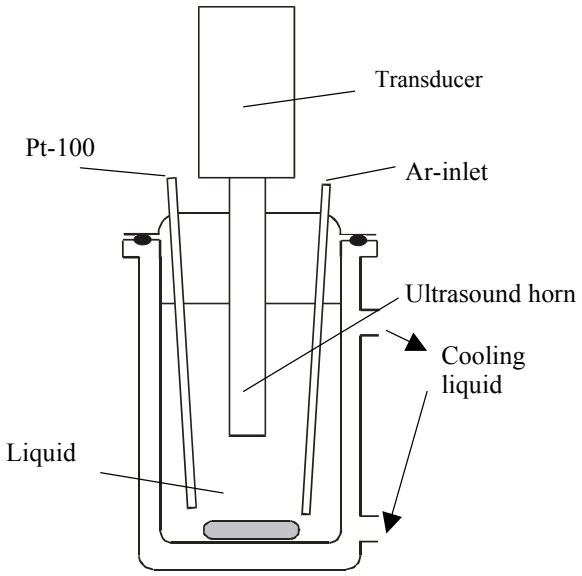

Figure 5.2. Schematic view of the experimental sonification set-up.

Monodisperse linear PMMA (Fluka) was dissolved in methyl methacrylate (MMA, Merck), which was distilled before use to remove the inhibitor. The polymers had a number average molecular weight of $18.0*10^4$, $27.0*10^4$, $45.5*10^4$ and $64.5*10^4$ g/mol, with a polydispersity of approximately 1.05. To avoid entanglements between polymers and to reduce the influence of molecular weight on viscosity, the polymer concentration used was 0.1 weight%. To ensure that no reaction or recombination of polymer radicals could occur during the ultrasound experiments, a radical scavenger (1,1-diphenyl-2-picrylhydrazyl, Aldrich) was added to the solution. During the experiments argon 6.0 (Hoekloos) was bubbled through a 3 mm tube into the reaction mixture with a flow rate of 2.0 mL/s. Samples were taken during the reaction and were analyzed by gel permeation chromatography (GPC), which was calibrated

against polystyrene standards. The molecular weight distribution of the PMMA samples was calculated with Mark-Houwink parameters (a=0.719 and $K=9.44*10^{-5}$ m^3).[28]

5.4 Results and discussion

Ultrasound-induced scission experiments

The development of the number-averaged molecular weight (M_n) in time for scission experiments with different initial molecular weights is shown in Figure 5.3. For the conditions applied, scission stops at a molecular weight of $5*10^4$ g/mol for all starting molecular weights. At this limiting molecular weight the overall dissociation constant (k_d) equals zero. The experimental time-dependent MWDs for the scission of PMMA with a starting molecular weight of $18.0*10^4$ g/mol are given in Figure 5.4. As an example, at 40 minutes a polymer with a peak value of $10*10^4$ g/mol is formed from the initial MWD with a peak value of $20*10^5$ g/mol, clearly showing non-random fracture in the middle of the chain.

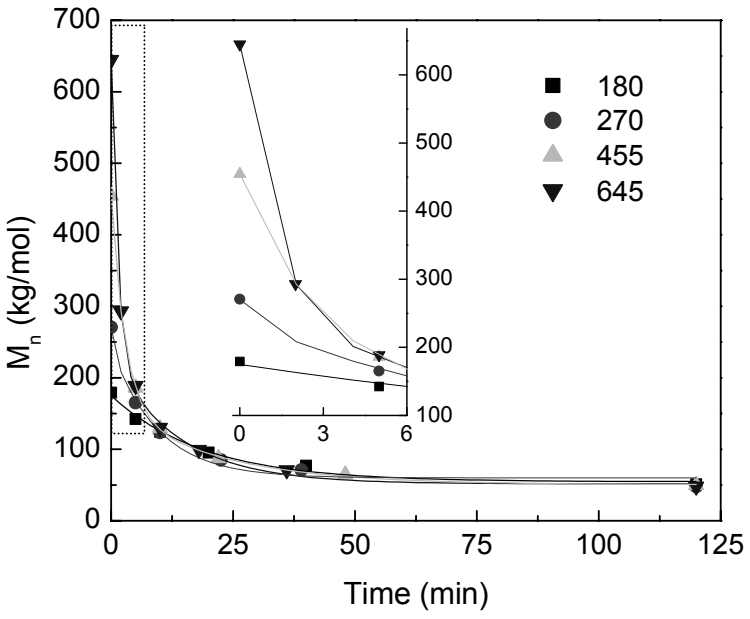

Figure 5.3. Ultrasound-induced polymer scission of 0.1 wt% PMMA in MMA for different initial molecular weights (kg/mol).

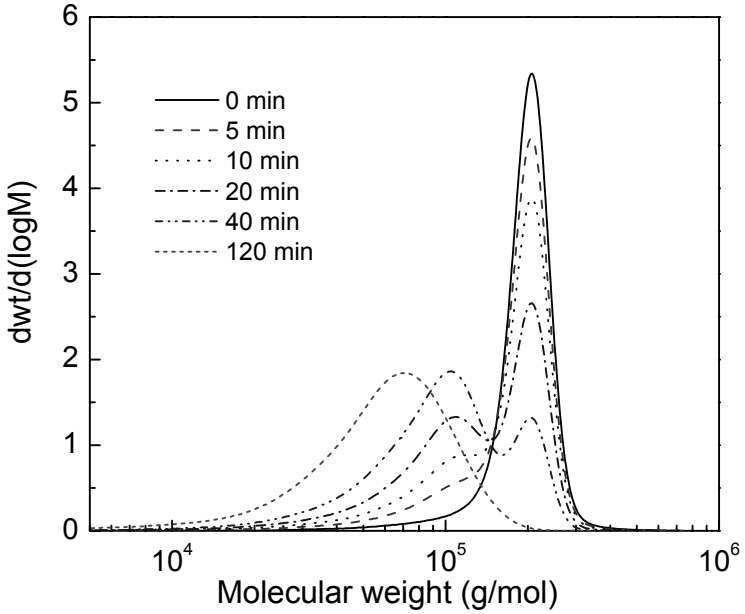

Figure 5.4. MWDs of the ultrasound-induced polymer scission experiments of PMMA with an initial M_n of $18.0*10^4$ g/mol.

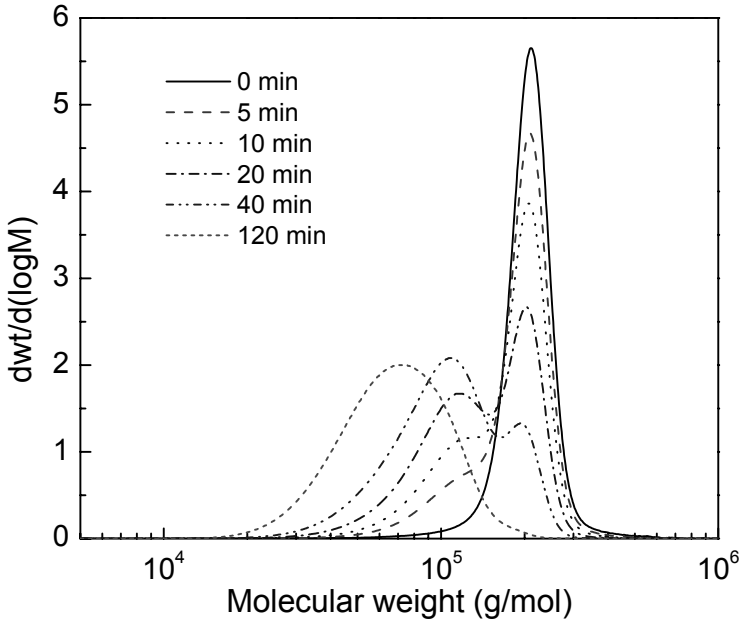

Figure 5.5. Simulation results of the polymer scission of PMMA with an initial M_n of $18.0*10^4$ g/mol.

The scission probability along the polymer chain ($\sigma(n)$) and the effect of the molecular weight on the dissociation rate ($k_d(n,m)$) are determined from the experimental MWDs using PREDICI®. The first is obtained from the width of the produced bimodal distribution, the latter by modeling the entire MWDs in time. The modeled MWDs for the scission reaction are shown in Figure 5.5. In general, the model fully describes the scission reaction, as only a minor difference between the experimental and the model results can be observed for low molecular weights. This deviance, the tailing of the peak at lower molecular weights in the experiments, can be related to multiple chain breakage upon one single implosion, which is not taken into account by the model. From the bimodal distributions the width of the sigmoidal distribution is obtained: $\sigma(n)=0.13*n$. This implies that a higher chance of scission exists next to the center of the polymer chain for higher molecular weights. Fracture occurs closer to the middle of the chain for polymers with a molecular weight not too far above the limiting molecular weight.

The dependence of the dissociation rate ($k_{MW}(n)$) on the molecular weight is shown in Figure 5.5 and can be described by Equation 5.6. This equation is only valid for polymer chains with a molecular weight higher or equal to the limiting molecular weight.

$$k_{MW}(n) = -1 \cdot 10^{-5} + 7.5 \cdot 10^{-11} \cdot n^{2 \cdot e^{-n/(2 \cdot 10^5)}} \qquad (5.6)$$

As the force in the middle of the chain has a squared dependence in the number of beads (Equation 5.2), we have initially chosen to use a quadratic function to describe the dissociation rate as a function of the molecular weight (Figure 5.6). Although this is correct for low molecular weights, from the simulations it is concluded, however, that at higher molecular weights (10^6 g/mol) the scission rate is dependent on the chain length to the power 1.9. This implies that the polymer chain does not have to be completely stretched to break at higher molecular weights. This also follows from the molecular weight dependence of the width of the sigmoidal distribution, from which it can be concluded that the chain has

to be fully stretched to break when it has a molecular weight close to the limiting molecular weight.

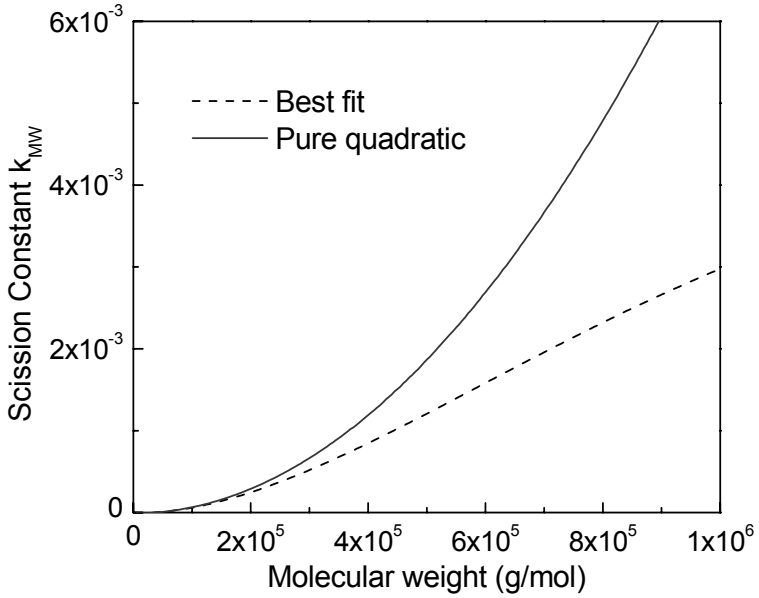

Figure 5.6. Degradation coefficients of PMMA as a function of molecular weight.

Strain rate calculations

The experiments described above indicate that the polymer chain has to uncoil completely before fracture. To support this hypothesis, strain rate simulations have been performed. The dynamic movement of the bubble wall, needed for the strain rate calculations, has been modeled as described in the theoretical section. Initially, a small cavity with a radius of 10^{-5} m is present in the liquid, which consists of argon and methyl methacrylate. In the simulations, an ultrasound wave with an acoustic pressure of 5 bar and a frequency of 20 kHz is imposed on the bubble. The variation of the radius of the bubble in time is shown in Figure 5.7, from which it follows that growth and implosion start after 25 and 59 μs, respectively.

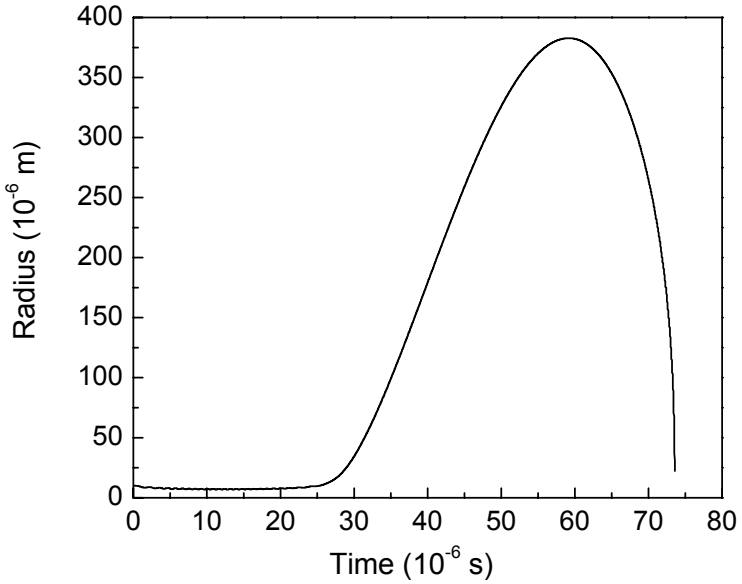

Figure 5.7. Calculated radius of a cavitation bubble in methyl methacrylate at atmospheric pressure and 20°C.

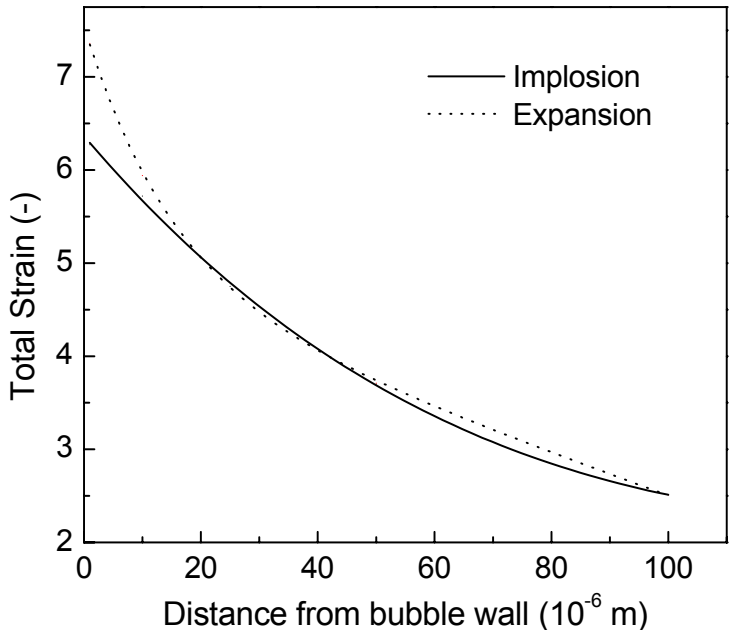

Figure 5.8. Total strain on a polymer chain as a function of the distance from the bubble wall, calculated from the bubble radius in time.

The total strain exerted on the polymer by cavitation determines the configuration of the chain. For complete stretching of PMMA with a molecular weight of $18.0*10^4$ and $64.5*10^4$ g/mol, the total strain has to exceed values of 4.0 to 4.2, respectively. Figure 5.8 shows that a polymer molecule can be completely stretched by the implosion if situated within approximately 40 μm from the bubble wall. Moreover, the cumulative strain of implosion and expansion can stretch a chain that is situated within 100 μm.

The force required to break a PMMA-chain is approximately 10^{-8} N.[6] This corresponds with a strain rate of 10^6 s^{-1} for a PMMA molecule with a molecular weight of $5*10^5$ g/mol. The constants for the drag force calculations a, b and S are taken from literature data for polystyrene, which are 0.20 nm, 0.25 nm and 1, repectively.[6] Since polystyrene has similar dimensions as compared to PMMA, similar values are expected for PMMA. The strain rates obtained from the simulations are shown in Figure 5.9, from which it is obvious that a maximum value is obtained at the bubble-liquid interface. This strain rate determines the minimum molecular weight of a polymer that can still be degraded. The maximum strain rate that follows from the simulations is 10^8 s^{-1}, which will result in a limiting molecular weight for 0.1wt% PMMA in MMA of approximately $6*10^4$ g/mol. This value is in good agreement with the experimental limiting molecular weight of $5*10^4$ g/mol.

Effect of system characteristics on scission process

With the model various influences on the scission rate and limiting molecular weight can be understood. At higher polymer concentrations the dissociation rate will decrease, as can be seen from Figure 5.10. This is caused by the increase in viscosity, leading to a slower collapse of the bubble, which results in a lower strain rate and a lower total strain. Additionally, the model predicts a higher limiting molecular weight due to the slower bubble collapse at higher viscosities. A similar influence of polymer concentration is reported by Price et al.,[18] investigating the ultrasound-induced scission of polystyrene in toluene and methyl butyrate.

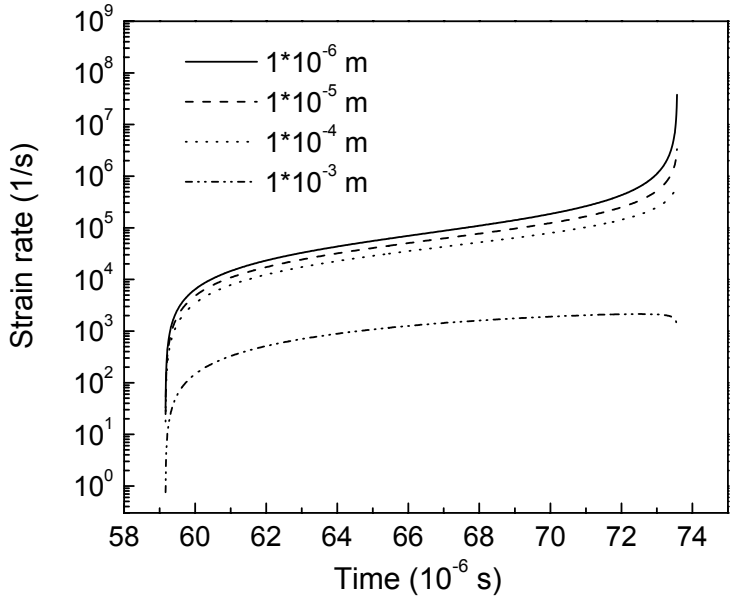

Figure 5.9. Strain rates around a cavity in MMA during collapse for different distances to the bubble wall.

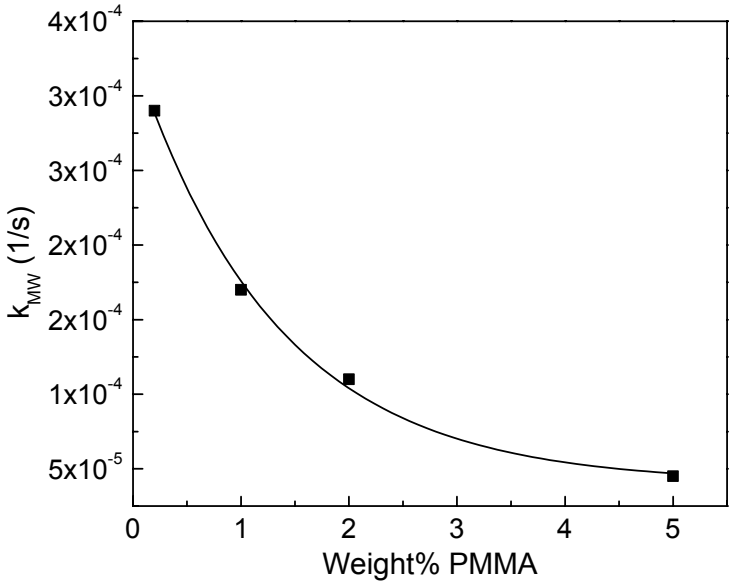

Figure 5.10. Dissociation constant as function of the concentration of PMMA dissolved in MMA.

Some reports describe the influence of ultrasound intensity and liquid temperature on the degradation rate and limiting molecular weight.[18,19] Generally, a higher intensity results in a higher scission rate and in a lower limiting molecular weight. Similar effects have been observed for scission at lower temperatures. Our scission model ascribes these two effects to the higher implosion velocity at higher intensity and lower temperatures, the latter effect being induced by the lower vapour pressure inside the cavitation bubble at lower temperatures.

An increase in degradation rate and a decrease in limiting molecular weight have been observed when better solvents are used.[18] In the literature, these effects have been ascribed to the configuration of the polymer chain, which becomes more open in better solvents. By changing the solvent, however, numerous essential parameters are changed, including the vapor pressure, the viscosity of the solution and the ultrasound intensity. From experimental degradation results of polyvinyl acetate of Madras et al.[20], it can be concluded that these effects dominate the polymer-solvent interactions. The model proposed in this paper can effectively be used to determine which parameter prevails, for which only the physical properties of the solution are required.

5.5 Conclusions

Ultrasound-induced polymer scission has been studied experimentally and a model describing the scission mechanism has been proposed. The model is composed of a dynamic bubble simulation and a bead-rod model. The dynamic cavitation calculations predict that total stretching of the polymer chain is possible during explosive growth and collapse of a cavitation bubble in microseconds. This is a prerequisite for scission at the polymer chain center. With the bead-rod model a limiting molecular weight of $6*10^4$ g/mol is calculated for PMMA dissolved in MMA, which has been experimentally confirmed. An almost squared dependence of the molecular weight on the scission rate is obtained from the measured time-dependent molecular weight distributions. Moreover, the general degradation model is capable to describe the effects of various process variables on cavitation-induced polymer scission.

5.6 Nomenclature

- a Mark-Houwink parameter [-]
- ε Strain [-]
- η Liquid viscosity [Pa s]
- κ Polytropic index of the gas phase [-]
- ϱ Liquid density [kg/m^3]
- σ Width of Gaussian distribution [-]
- σ_{liq} Liquid surface tension [N/m]
- a Radius of bead [m]
- b Repeat unit along chain [m]
- F_c Force at the center of chain [N]
- K Mark-Houwink Parameter [m^3/g]
- k_d Overall dissociation constant [1/s]
- k_{MW} Molecular weight dependent dissociation constant [1/s]
- m Number of monomer units in chain [-]
- n Number of monomer units in original chain [-]
- P_0 Static pressure [Pa]
- P_A Acoustic pressure [Pa]
- P_v Vapor pressure [Pa]
- R Bubble radius [m]
- r Distance between polymer and bubble center [m]
- S Shielding factor [-]
- t time [s]

5.7 References

1. Machado, A. V.; Covas, J. A.; Van Duin, M. *J. Appl. Pol. Sci.* **2001**, 81, 58-68.

2. Kuijpers, M. W. A.; Van Eck, D.; Kemmere, M. F.; Keurentjes, J. T. F. *Science* **2002**, 298, 1969-1971.

3. Didenko, Y. T.; Mcnamara III, W. B.; Suslick, K. S. *Nature* **2000**, 407, 877-879.

4. Nguyen, T. Q.; Liang, Q. Z.; Kausch, H.-H. *Polymer* **1997**, 38, 3783-3793.

5. Basedow, A.M.; Ebert, K. H. *Adv. Pol. Sci.* **1977**, 22, 83

Odell, J. A.; Keller, A. *J. Pol. Sci. B* **1986**, 24, 1889-1916.

7. Glynn, P. A. R.; Van der Hoff, B. M. E.; Reilly, P. M. J. *Macromol. Sci.-Chem.* **1972**, A6, 1653-1664.

8. Smith, D. E.; Chu, S. *Science* **1998**, 281, 1335-1340.

9. Tayal, A.; Khan S. A. *Macromolecules* **2000**, 33, 9488-9493.

10. Kanwal, F.; Liggat J. J.; Pethrick, R. A. *Pol. Degrad. Stab.* **2000**, 68, 445-449.

11. Grönroos, A.; Pirkonen P.; Ruppert O. *Ultrason. Sonochem.* **2004**, 11, 9-12.

12. Miyazaki T.; Yomota C.; Okada S. *Pol. Degrad. Stab.* **2001**, 74, 77-85.

13. Glynn, P.A.R.; Van der Hoff, B. M. E. *J. Macromol. Sci.-Chem.* **1974**, A8, 429-449.

14. Price, G.J.; Smith, P.F. *Polym. Int.* **1991**, 24, 159-164.

15. Kuijpers, M.W.A.; Kemmere, M. F.; Keurentjes, J.T.F. *Encyclopedia of Polymer Science and Technology*; John Wiley & Sons: New York, **July 2004**.

16. Madras, G.; Kumar, S.; Chattopadhyay S. *Pol. Degrad. Stab.* **2000**, 69, 73-78.

17. Van der Hoff, B. M. E.; Gall, C.E. *J. Macromol. Sci.-Chem.* **1977**, A11, 1739-1758.

18. Price, G. J.; Smith, P. F. *Eur. Pol. J.* **1993**, 29, 419-424.

19. Price, G. J.; Smith, P. F. *Polymer* **1993**, 34, 4111-4117.

20. Madras, G.; Chattopadhyay, S. *Pol. Degrad. Stab.* **2001**, 71, 273-278.

21. Agarwal, U. S.; Bhargava, R.; Mashelkar R. A. *J. Chem. Phys.* **1998**, 108, 1610-1617.

22. James, D. F. *J. Rheol.* **1995**, 39, 713-724.

23. Agarwal, U. S. *e-Polymers* **2002**, no. 14, 1-15.

24. Yasui, K. *J. Acoust. Soc. Am.* **1995**, 98, 2772-2782.

25. Leighton, T. J. *The Acoustic Bubble*, Academic Press, London, 1994.

26. Wulkow, M. *Macromol. Theory Simul.* **1996**, 5, 393-416.

27. Casale, A.; Porter, R. S. *Polymer Stress Reactions*, Academic Press, New York, 1978.

28. Xue, L.; Agarwal, U. S.; Lemstra, P. J. *Macromolecules* **2002**, 35, 8650.

6 Anti-Solvent effect on Ultrasound-induced Polymer Scission Kinetics

Ultrasound-induced polymer scission is a non-random process, which alters the molecular weight distribution of polymers. However, cavitation and consequently polymer scission is not possible in concentrated polymer solutions, due to the high liquid viscosity. The addition of an anti-solvent can be used to circumvent this problem because the anti-solvent decreases the gyration radius of polymer chains, which induces a reduction in liquid viscosity. To determine the influence of CO_2 as an anti-solvent on the ultrasound-induced scission rate, ultrasonic scission experiments of PMMA have been performed in bulk MMA as well as in CO_2-expanded MMA. Modeling the experimental time-dependent molecular weight distributions has revealed the scission kinetics at different polymer concentrations and CO_2 fractions. At low polymer concentrations, the scission rate is decreased upon an increased CO_2 content. This is a result of the higher vapor pressure of CO_2, which cushions the cavitation. However, at higher polymer concentrations this effect is counteracted by the viscosity reduction induced by CO_2. As a consequence, the scission rate in CO_2-expanded MMA is higher as compared to bulk MMA for solutions with a high polymer concentration. The results show that ultrasound-induced scission in pressurized CO_2 can alter and control the MWD of polymers even in concentrated polymer solutions, whereas ultrasound-induced scission in bulk solutions is limited to relatively low polymer concentrations.

This chapter is based on: M.W.A. Kuijpers, R.M.H. Prickaerts, M.F. Kemmere, J.T.F. Keurentjes *Macromolecules*, submitted.

6.1 Introduction

The molecular weight distribution (MWD) is an important characteristic of polymers. In the polymer industry often a post-processing step is applied to alter the MWD, e.g. peroxide-induced degradation of polypropylene.[1] In this process, fracture of the polymer chains occurs at random sites. An alternative method is ultrasound-induced polymer scission, which involves a much better controlled, non-random process.[2] It can either be used as a post-processing step or can be used during ultrasound-induced polymerizations.[3]

Ultrasound is known to enhance chemical reactions as well as mass transfer at ambient temperatures and pressures. Most of these effects are caused by cavitations, i.e. the collapse of microscopic bubbles in a liquid. The chemical effects of cavitation result from the extreme conditions in the bubble (5000 K and 200 bar)[4] and the high strain rates outside the bubble (10^7 s^{-1})[5] generated upon implosion. Polymer scission arises from the high strain rates near an imploding cavity. The chain is fractured approximately in the middle of the chain, until a limiting molecular weight (M_{lim}) is reached.[6] The M_{lim} is defined as the maximum chain length that does not break by ultrasound. A direct consequence of the non-random scission behavior is that no oligomers are formed by ultrasound-induced scission in contrast to chemical degradation of polymers. Oligomers often have a negative influence on the polymer properties and are thus undesired in the final product. Additionally, an interesting application of ultrasound-induced polymer scission is the production of block copolymers, for which two different methods are possible. The first route involves the dissolution of a homo-polymer in a different monomer.[7] Subsequently, ultrasonic scission of the polymer chains will generate the radicals that initiate the polymerization reaction with the monomer present. In the second method two different homo-polymers are dissolved in a non-reactive solvent.[8] Ultrasound generates polymeric radicals, which will terminate by cross combination. The advantage of this method is that block copolymers can be produced from homo-polymers of which the polymer-monomer systems are immiscible.

The viscosity is an important factor during ultrasound-induced scission.[9] A high viscosity hinders cavitation and consequently the polymer scission rate is reduced. At increasing polymer concentration, the scission process is less effective and eventually stops, as a high viscosity hinders the bubble implosion. This is a drawback for the development of a scission process based on ultrasound, as concentrated polymer systems are favored in industry. The addition of an anti-solvent for the polymer can counteract the increase in viscosity at higher polymer concentrations.[10] At relatively low anti-solvent concentrations, the viscosity reduction is a result of the smaller gyration radius of the dissolved polymer molecules. It is still a one-phase system, due to which the scission rate constant is expected to remain virtually unchanged. At higher CO_2 fractions, the polymer precipitates and as a result a second phase is formed. The precipitated polymer cannot be stretched by cavitation, and subsequently it is no longer susceptible for ultrasound-induced scission. A constant scission rate is thus expected with increasing polymer concentration as the liquid viscosity is unchanged by precipitation of the polymer.

High-pressure CO_2 is an interesting medium for ultrasound-induced polymer scission, because it exhibits an anti-solvent effect for most polymers, whereas most monomers have a high solubility in CO_2.[11] Moreover, CO_2 is regarded as an environmentally friendly compound, which is non-toxic, non-flammable and naturally abundant.[12,13] However, up till now ultrasound is rarely studied at higher pressures, because in most cases a high static pressure hampers the growth of cavities. Recently, we have shown that cavitation is possible in dense-phase fluids.[14] This provides a means for the development of scission processes based on ultrasound and high-pressure CO_2. These types of processes can contribute to a safer and cleaner way to produce polymers with the desired molecular weight distribution. By adjusting the CO_2 fraction in the liquid, the amount of polymer that is dissolved can be controlled and hence the scission rate. Moreover, the CO_2 fraction influences the liquid viscosity and the vapor pressure, which determine the cavitation intensity.[2] Therefore, the cavitational collapse and consequently the fracture rate and the M_{lim} are dependent on the amount of CO_2 in the liquid.

In this work, the influence of the CO_2 anti-solvent effect on the ultrasound-induced polymer scission has been studied. Scission experiments have been performed at different CO_2 fractions and polymer concentrations. With the development of the experimental molecular weight distributions as well as a general scission model based on population balances, the influence of CO_2 and the polymer concentration on the scission kinetics has been determined.

6.2 Ultrasound-induced scission

The breakage of polymer molecules due to ultrasound is a direct result of cavitation, because no polymer fracture occurs when cavitation is suppressed.[15] Upon bubble collapse, the entire molecule will move along with the fluid. Due to the velocity profile near the cavities, friction between the polymer chain and the liquid will occur (Figure 6.1). This friction can result in stretching of the polymer coil and subsequent fracture of the chain. The drag force accumulates in the middle of the chain, due to which scission primarily occurs at the center. The chain is fractured if the accumulated drag force in a chain fragment is higher than the bond strength. This force (Equation 6.1) is dependent on the size of the monomer molecules (a and b), the shielding factor (S), the solvent viscosity (η), the number of monomer units (n) and the strain rate (dε/dt).[16] The strain rate can be calculated from the distance of the polymer chain from the center of the cavity (r), the bubble wall velocity (dR/dt) and the radius of the bubble (R) (Equation 6.2).[17]

$$F_c = \frac{6 \cdot \pi}{8} \eta \; a \; b \; S \frac{d\varepsilon}{dt} n^2 \qquad (6.1)$$

$$\frac{d\varepsilon}{dt} = -2 \frac{R^2 \frac{dR}{dt}}{r^3} \qquad (6.2)$$

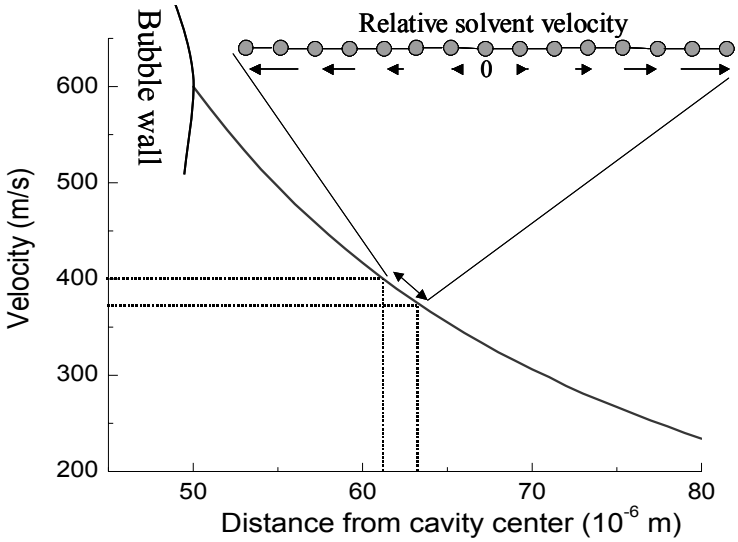

Figure 6.1. Representation of the velocity profile near an imploding bubble and the resulting relative liquid velocity near a stretched polymer chain.

The two most important quantities describing an ultrasound-induced scission reaction are the limiting molecular weight and the scission rate. The first is determined by the maximum strain rate in the liquid, which is obtained at the cavity interface at the moment of implosion. From the cavitation bubble interface towards the bulk liquid, the strain rate decreases rapidly. Polymer chains with a molecular weight slightly higher than M_{lim} can only break in the vicinity of the bubble interface, whereas higher molecular weight polymers can also break further away from the cavitation bubble. The scission rate is thus proportional to the volume around the cavity in which a polymer chain can stretch and break. Since the strain rate and the length of the polymer chain determine this volume, relatively low molecular weight polymers have a small volume in which they can break and hence have a low scission rate. The scission volume increases for polymer chains with a higher molecular weight and for faster imploding bubbles. The kinetics of ultrasonic scission can thus be directly ascribed to the implosion velocity of the cavitation bubbles and the length of the polymer that is fractured. The implosion velocity is dependent on the liquid properties, the content of the bubble, the acoustic pressure and the static pressure, respectively.[18] Therefore, it is important to know the phase composition, density and viscosity of the liquid.

Assuming first-order scission kinetics, the scission rate can be determined as a function of molecular weight and liquid properties. The kinetic scheme of scission by ultrasound reads as follows:[19]

Scission: $P_n \xrightarrow{k_d(n,m)} P_m \bullet + P_{n-m} \bullet$

Termination by recombination: $P_m \bullet + P_{n-m} \bullet \xrightarrow{k_{tc}} P_n$

Termination by disproportionation: $P_m \bullet + P_{n-m} \bullet \xrightarrow{k_{td}} P_m + P_{n-m}$

If a radical scavenger is present, the termination reaction occurs instantaneously and only between a macroradical fragment and a scavenger molecule. Thus, the scheme reduces to:

$$P_n \xrightarrow{k_d(n,m)} P_m + P_{n-m}$$

where $k_d(n,m)$ is an effective scission rate constant. The scission rate constant k_d is chosen as a function of the original chain length n and fragment length m to allow for the non-random character of the scission process. According to the overall scission reaction, the population balance then becomes:

$$\frac{dP_n}{dt} = \sum_{m=n+1}^{\infty} k_d(n,m) P_m - P_n \sum_{m=1}^{n} k_d(n,m) \quad (6.3)$$

This balance equation is solved with the Galerkin finite element (FEM) package PREDICI®.[20] By manipulating the shape of $k_d(n,m)$ – which is anticipated to be Gaussian with a width (σ) – it is possible to obtain a best fit between the MWD predicted by Equation 6.4 and the measured MWD. The overall dissociation constant k_d consists of a Gaussian distribution function and a molecular weight dependent scission function (k_{MW}):

$$k_d(n,m) = \frac{k_{MW}(n)}{\sqrt{2\pi}\,\sigma(n)} e^{\left(-\frac{1}{2\sigma(n)^2}(m-\frac{n}{2})^2\right)} \quad (6.4)$$

As the force in the middle of the chain has a squared dependence in the number of beads (Equation 6.1), an almost quadratic function is used to

describe the dissociation rate as a function of the molecular weight (Equation 6.5). This equation is only valid for polymer chains with a molecular weight higher or equal to the limiting molecular weight. When the dissociation constant k_{MW} is zero, the corresponding limiting molecular weight at these conditions is obtained. This molecular weight is determined by the constants A and B. The scission rate is defined by all three constants in Equation 6.5:

$$k_{MW}(n) = A + B \cdot n^{2 \cdot e^{-n/C}} \quad (6.5)$$

6.3 Experimental

The polymer solutions used for the scission experiments with ultrasound consisted of MMA, CO_2 and PMMA. The composition of the liquid was calculated with the Lee-Kessler-Plöcker (LKP) equation of state (Table 6.1).[21] This equation of state applies to hydrocarbon systems, which include light gases such as CO_2. The LKP-model uses pure component parameters, such as the critical temperature, the critical pressure and the acentric factor (ω), and one binary interaction parameter. The interaction parameter for the MMA/CO_2 system appears to be 1.08 at 20°C.[22] The influence of the polymer on the CO_2 fraction (X_{CO_2}) in the liquid at a certain pressure was assumed to be negligible. The density of the liquid was approximately 0.945 kg/L at 20°C.[21]

Ultrasound-induced scission was studied in a thermostated 175 mL high-pressure vessel at 20°C (Figure 6.2). Sonification of the solution was performed using 20 kHz ultrasound, which was produced by a Sonics and Materials VC-750 generator. A ½-inch full-wave titanium probe was applied to couple the piezoelectric transducer to the liquid. To allow for an accurate comparison, the total configuration and the ultrasound amplitude (75 μm) were kept constant during all the experiments.

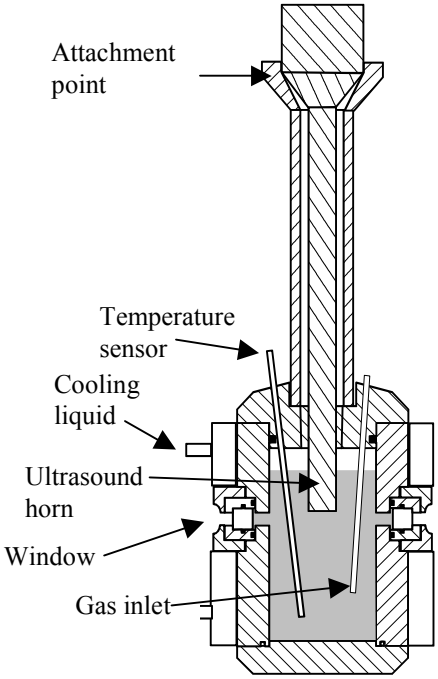

Figure 6.2. High-pressure ultrasound reactor for scission reactions.

The experimental procedure of the ultrasound-induced scission experiments was as follows. The reactor was filled with 150 mL bulk MMA or CO_2-expanded MMA, in which a known amount of PMMA was dissolved. The MMA (Merck) was distilled under vacuum to remove the hydroquinone inhibitor before use. To ensure that no reaction or recombination of polymer radicals could occur during the scission experiments, a radical scavenger (1,1-diphenyl-2-picrylhydrazyl, Aldrich) was added to the solution. The weight average molecular weight (M_w) and polydispersity of the PMMA used for the scission experiments were $2.4*10^6$ g/mol and 2.4, respectively. During the experiments CO_2 (grade 5.0, Hoekloos) was bubbled through a 3 mm tube into the reaction mixture with a flow rate of 2.0 mL/s. As a result of the high solubility of CO_2 in MMA, bubbling CO_2 through bulk MMA at atmospheric conditions already resulted in a CO_2 fraction of 0.02 (Table 6.1).

Table 6.1. Experimental conditions for the ultrasound-induced scission experiments.

T (°C)	P (bar abs)	X_{CO_2} (-)	I_{US} (W/cm²)
20	1.0	0.02	31
20	4.0	0.08	59
20	7.0	0.14	70

During the scission reaction, samples were taken and analyzed by gel permeation chromatography (GPC), which was calibrated against polystyrene standards. The molecular weight distributions of the PMMA samples were calculated with Mark-Houwink parameters (a=0.719 and $K=9.44*10^{-5}$ m^3).[23] By simulating the development of the MWDs in time with PREDICI®, the molecular weight dependent scission rate constants ($k_d(n,m)$) were obtained.

The ultrasound-intensities were determined at an amplitude of 75 μm for the different conditions by calorimetry and are given in Table 6.1. These values give an indication of the ultrasound power transferred to the liquid in the high-pressure reactor. The heat flow (Q) that was generated by ultrasound in the calorimeter was calculated based on the surface area of the reactor wall (A_r), the overall heat transfer coefficient (U) and the difference between jacket (T_j) and reactor temperature (T_r).[24] Subsequently, the ultrasound intensity (I_{US}), was calculated by dividing the heat flow by the surface area of the ultrasound horn (A_{US}), according to Equation 6.6.[25]

$$I_{US} = \frac{Q}{A_{US}} = \frac{U\,A_r\,(T_r - T_j)}{A_{US}} \quad (6.6)$$

6.4 Results and discussion

In this study, the effect of the CO_2 fraction and the polymer concentration on the scission kinetics has been determined by comparing experimentally obtained MWDs with predicted MWDs using PREDICI®. First, the ultrasound-induced polymer scission simulations will be discussed briefly. Next, the influence of the liquid viscosity on the scission kinetics has been determined in bulk MMA. To quantify the influence of CO_2 on the implosion velocity independently from the CO_2 anti-solvent effect, first the influence of the CO_2 fraction on the fracture rate has been measured at low polymer concentrations. Subsequently, the anti-solvent effect of CO_2 on the scission kinetics has been studied also for more concentrated polymer solutions. Finally, the application of CO_2 to control the molecular weight during ultrasound-induced scission is discussed.

Simulations of ultrasound-induced polymer scission

Figure 6.3A shows the development of the molecular weight distribution for a scission experiment in bulk with 4 weight% PMMA. A decrease in polydispersity and molecular weight is obtained by irradiation of the solution with ultrasound. The modeled MWDs for this scission reaction are shown in Figure 6.3B. In a previous study, where mono-disperse polymer samples have been used in bulk MMA, the width of the sigmoidal distribution function (Equation 6.4) has been determined, which appears to be $\sigma(n)=0.13*n$.[26] In general, the model fully describes the scission reaction, as only minor differences between the experimental and the model results can be observed. Table 6.2 presents the limiting molecular weight and the constants and the exponent for the scission rate constant $k_{MW}(n)$ as given in Equation 6.5.

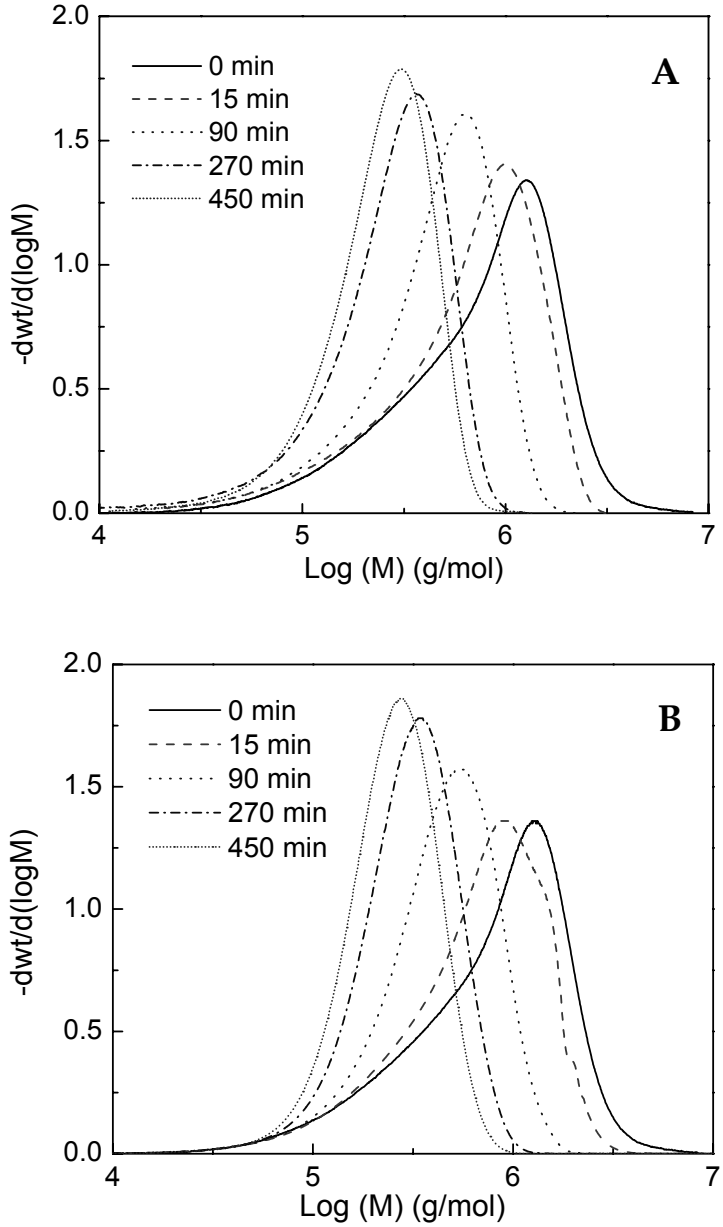

Figure 6.3. Experimental (A) and simulated (B) molecular weight distributions of an ultrasound-induced scission reaction of 4 weight% PMMA in bulk MMA (X_{CO2} = 0.02).

Influence of viscosity on cavitation

The liquid viscosity has a major influence on the implosion velocity and consequently on the scission rate and the limiting molecular weight. The experimentally observed development of M_w at different polymer concentrations in bulk MMA is plotted in Figure 6.4A. Figure 6.4B shows the scission constants (k_d), determined by the simulations, as a function of molecular weight at different polymer concentrations in bulk MMA. It should be noted that with decreasing molecular weights, the reaction time increases. A much lower scission rate constant is observed at higher polymer concentrations, which is a result of the higher viscosity. This decrease is the most distinct between polymer concentrations of 0.1 and 2 wt%, whereas the difference between 2 and 4 wt% dissolved polymer is small. Limiting molecular weights of $1.0*10^5$, $1.9*10^5$ and $1.9*10^5$ g/mol are obtained for scission in bulk MMA for PMMA at concentrations of 0.1, 2 and 4 weight percent, respectively (Table 6.2).

With respect to simulations using PREDICI®, Table 6.2 shows that the calculated M_{lim}-value at low polymer concentration is in good agreement with the experiment, because the viscosity and consequently the cavitation intensity do not change during the experiment. Due to these constant experimental conditions, the scission model accurately predicts the limiting molecular weight at low polymer concentrations. Contrarily, at high polymer concentrations, the calculated M_{lim}-values deviate from the experimentally obtained M_{lim}, approximately by a factor of 2. This is caused by the constant cavitation intensity in time used in the PREDICI® model. This would imply that the viscosity of the solution remains constant during sonification. Experimentally, however, the viscosity changes significantly during the scission experiments of the more concentrated polymer solutions, as a result of which the largest deviation in predicted limiting molecular weight is observed at the 2 and 4 wt% polymer solutions. In contrast to M_{lim}, the scission model accurately predicts the initial scission rate constants at higher polymer concentrations.

Table 6.2. Experimental and modeling results of ultrasound-induced scission in bulk MMA (X_{CO2}= 0.02) at different polymer concentrations.

Weight% PMMA	X_{CO2} (-)	$M_{lim,experiment}$ (10^5 g/mol)	$M_{lim,model}$ (10^5 g/mol)	A (10^{-5} 1/s)	B (10^{-11} 1/s)	C (10^6)	$2e^{-n/C}$ at 10^6 g/mol
0.1	0.02	1.0	0.9	-2	2.4	0.2	1.9
2.0	0.02	1.9	0.9	-0.1	0.13	5	2
4.0	0.02	1.9	1.0	-0.1	0.10	5	2

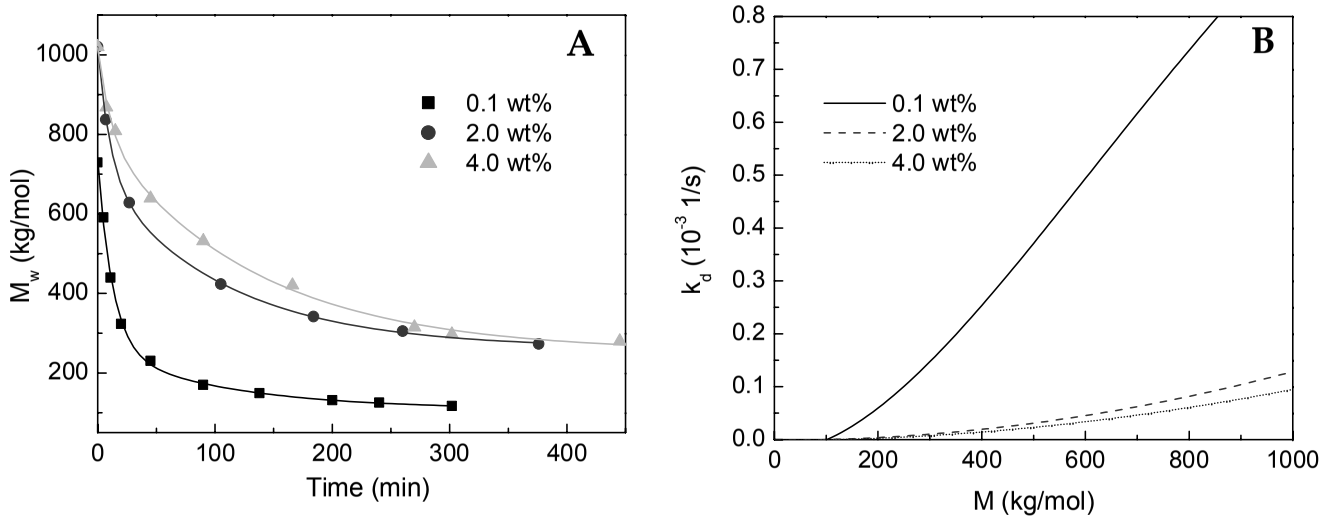

Figure 6.4. Experimentally observed development of the weight average molecular weight (A) and calculated scission rate constants (B) for ultrasound-induced scission at different PMMA concentrations in bulk MMA (X_{CO2} = 0.02).

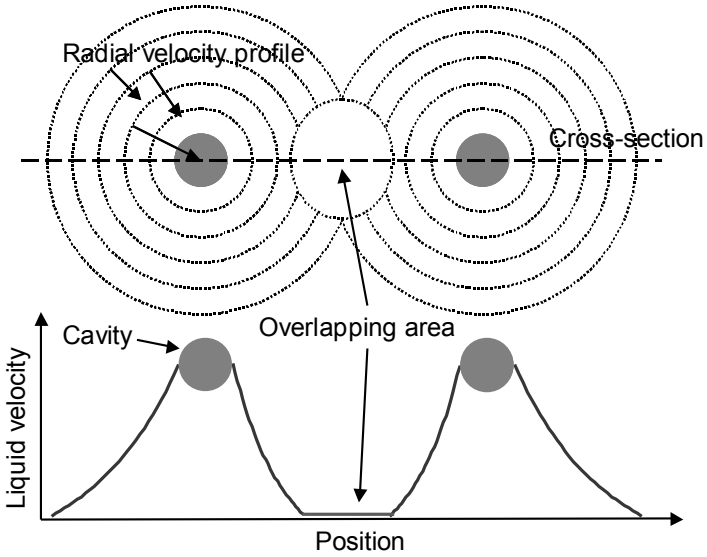

Figure 6.5. Schematic representation of overlapping velocity profiles around two imploding cavitation bubbles and the resulting radial velocity.

In Table 6.2 the molecular weight dependent scission constants at different polymer concentrations are given. The exponent ($2e^{-n/C}$) given in Table 6.2 describes the dependence of the scission rate on the chain length (Equation 6.5). The scission rate is expected to be a quadratic function of the length of the chain (Equation 6.1). Although this is correct for low molecular weight polymers, from the simulations with 0.1 wt% polymer it is concluded that for higher molecular weight polymers (10^6 g/mol), the scission rate depends on the chain length to the power 1.9 (Table 6.2). We assume that this deviance is probably a consequence of overlapping velocity profiles from neighboring cavitation bubbles (Figure 6.5). As a result, the volume in which a polymer with a certain molecular weight can break is reduced. The scission rate of a polymer chain is proportional to this volume, as mentioned in the theoretical section. In general, high molecular weight polymers can fracture further away from the bubble interface and therefore their scission rate will be more susceptible to this volume decrease. Consequently, the deviation from the theory (a quadratic function) is more distinct at higher molecular weights.

Additionally, at higher cavitation intensities (lower viscosities), the radial velocity profile extends further in the liquid, which will cause more overlap with neighboring bubbles and thus a larger decrease in effective volume. As a result, a less than quadratic function is obtained at lower polymer concentrations.

Influence of CO_2 fraction on cavitation

The influence of the CO_2 fraction on the implosion velocity has been measured independently from the anti-solvent effect, by performing the experiments at low polymer concentrations (Table 6.3). At low polymer concentrations, the influence of the CO_2 fraction on the viscosity can be neglected, because the polymer chains are not entangled. Figure 6.6A shows the development of M_w in time for scission experiments with a low polymer concentration at different CO_2 fractions. With an increasing CO_2 fraction, the scission rate decreases (slope of Figure 6.6A) and the limiting molecular weight increases. The change in scission kinetics is a result of the lower strain rate produced upon collapse at higher CO_2 fractions. This is not an anti-solvent effect, because the CO_2 fraction has almost no influence on the viscosity in a 0.1 weight percent polymer solution. However, the lower scission rate and higher M_{lim} at higher CO_2-pressures is a result of the higher vapor pressure in the cavitation bubble, which reduces the implosion velocity (cushioning effect) and consequently reduces the drag force acting on the polymer chain, see Equation 6.1.

Figure 6.6B presents the overall scission constants at different CO_2 fractions as a function of the molecular weight. From the simulations it is concluded that for higher molecular weight polymers (10^6 g/mol) the scission rate depends on the chain length to the power 1.9, 1.93 and 2, at 1, 4 and 7 bar, respectively (Table 6.3). This small deviance from the theory is probably a consequence of overlapping velocity profiles from neighboring cavitation bubbles (Figure 6.5), as mentioned in the previous section. The larger deviation at lower pressures is caused by the higher implosion velocities. At lower CO_2 fractions, the radial velocity profile extends further in the liquid, which will cause more overlap with neighboring bubbles and thus results in a larger decrease in effective volume.

Table 6.3. Experimental and modeling results of ultrasound-induced scission at different CO_2 fractions and 0.1 wt% polymer.

Weight% PMMA	X_{CO_2} (-)	$M_{lim,experiment}$ (10^5 g/mol)	$M_{lim,model}$ (10^5 g/mol)	A (10^{-5} 1/s)	B (10^{-11} 1/s)	C (10^6)	$2e^{-n/C}$ at 10^6 g/mol
0.1	0.02	1.0	0.9	-2	2.4	0.2	1.9
0.1	0.08	1.6	1.6	-4	1.5	0.3	1.93
0.1	0.14	1.8	1.8	-2	0.60	5	2

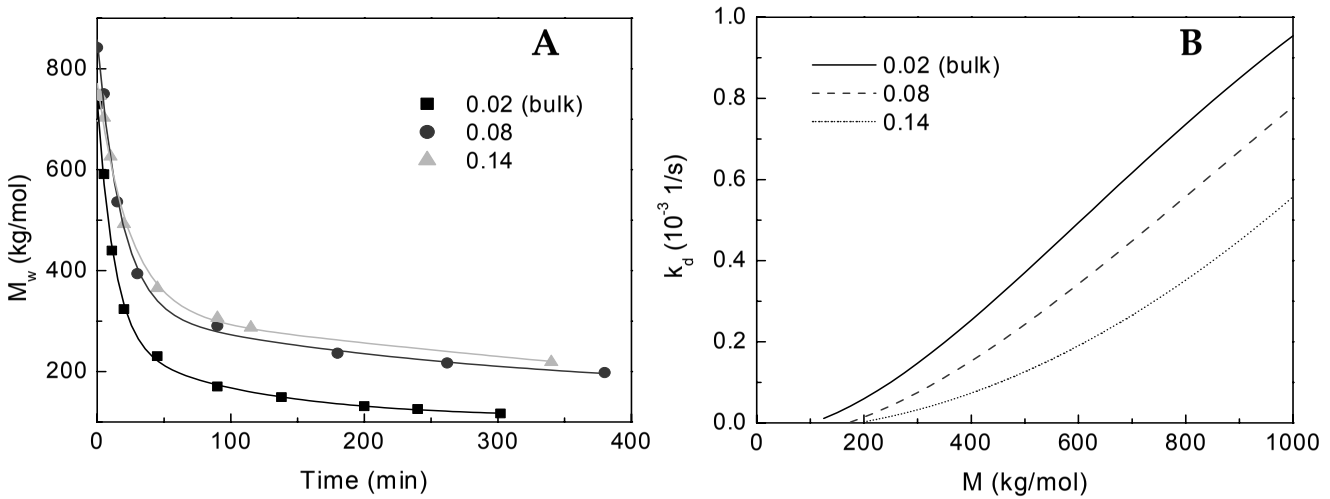

Figure 6.6. Experimentally observed development of the weight average molecular weight (A) and calculated scission rate constants (B) for ultrasound-induced scission at 0.1 wt% polymer and CO_2 fractions of 0.02, 0.08 and 0.14.

Influence of the anti-solvent effect on the scission kinetics

Carbon dioxide reduces the viscosity of concentrated polymer solutions.[11] As a result, the scission rate constant is expected to remain virtually constant at higher polymer concentrations, whereas in bulk the scission rate constant strongly decreases. Figure 6.7A shows the development of M_w in time for scission experiments for a 4 weight% polymer solution at several CO_2 fractions (Table 6.4). All the reaction mixtures are one-phase systems, as no precipitated polymer was observed in a high-pressure view-cell at these conditions. Figure 6.7B shows the scission rate constants for different CO_2 fractions, as obtained from the model. It can be seen that the scission rate constant is initially (right-hand side of point I and II) higher for the CO_2-expanded liquids, in contrast to the bulk experiment (Figure 6.7B vs. 6.6B). The negative influence of the CO_2 fraction on the implosion velocity at low polymer concentrations is thus counteracted at higher polymer concentrations by the CO_2 anti-solvent effect. As no precipitated polymer is observed, the higher scission rate is a consequence of the smaller gyration radius of the polymer chain, which results in a lower liquid viscosity. At the left-hand side of point I in Figure 6.7B, the scission rate in bulk is faster than the scission rate in CO_2-expanded MMA at 7 bar (X_{CO_2} = 0.14). The difference with the right-hand side is caused by the larger viscosity decrease during the scission experiment in bulk MMA, which results in a larger increase in the implosion velocity of the cavitation bubbles. This higher implosion velocity also results in a lower limiting molecular weight for the scission experiment in bulk MMA as compared to scission in CO_2-expanded MMA. The intersection point between CO_2-expanded MMA at 4 bar (X_{CO_2} = 0.08) and bulk MMA (Figure 6.7B, II) occurs at a lower molecular weight, because at 4 bar less CO_2 is dissolved in MMA as compared to 7 bar. Therefore, the cushioning effect will be less pronounced at 4 bar CO_2.

Table 6.4. Experimental and modeling results of ultrasound-induced scission at different CO_2 fractions and 4.0 wt% polymer.

Weight% PMMA	X_{CO_2} (-)	$M_{lim,experiment}$ (10^5 g/mol)	$M_{lim,model}$ (10^5 g/mol)	A (10^{-5} 1/s)	B (10^{-11} 1/s)	C (10^6)	$2e^{-n/C}$ at 10^6 g/mol
4.0	0.02	1.9	1.0	-0.1	0.10	5	2
4.0	0.08	2.6	2.1	-0.7	0.16	∞	2
4.0	0.14	3.0	2.9	-1	0.12	∞	2

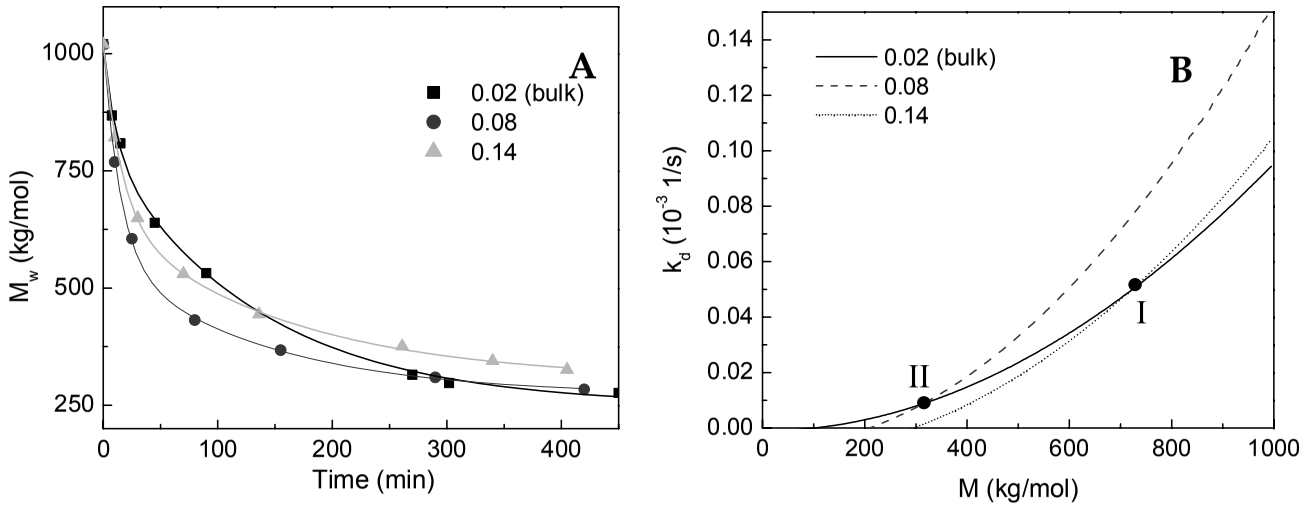

Figure 6.7. Experimentally observed development of the weight average molecular weight (A) and calculated scission rate constants (B) for ultrasound-induced scission at 4.0 wt% polymer and CO_2 fractions of 0.02, 0.08 and 0.14.

Control of molecular weight by ultrasound-induced polymer scission

In general, ultrasound can be applied as a clean alternative method to control polymer properties by tuning the polydispersity and molecular weight distribution, because polymer scission occurs in situ without the addition of peroxides.[1] Especially, for polymers where the high molecular weight part of the distribution has a disadvantageous effect on the product properties, ultrasound has significant application potential. The possibility to perform these reactions at higher polymer concentration by the addition of an anti-solvent makes the ultrasound technique more feasible for industry.

Moreover, by combining ultrasound with CO_2, the scission rate and limiting molecular weight can independently be altered. In comparison with bulk experiments, scission in CO_2-expanded liquids results in a lower viscosity and consequently a higher scission rate as well as a lower limiting molecular weight in concentrated polymer solutions. Above a given CO_2 fraction the polymer starts precipitating, resulting in a constant scission rate. The CO_2 fraction influences the amount of polymer that is dissolved, the limiting molecular weight and the scission rate. Additionally, an increase in the ultrasound intensity will result in a lower limiting molecular weight and a higher scission rate, whereas the sonication area only influences the scission rate. In summary, the ultrasound-intensity, the sonication area and the CO_2 fraction can thus independently influence the limiting molecular weight and the scission rate. Therefore, ultrasound-induced polymer scission in CO_2-expanded liquids allows for an accurate control of the scission kinetics and hence the polymer properties.

6.5 Conclusions

In this work, the influence of the CO_2 anti-solvent effect on the viscosity and the resulting reaction kinetics of ultrasound-induced polymer modification have been studied. For this purpose, ultrasound–induced polymer scission experiments have been performed in CO_2-expanded MMA as well as in bulk MMA at different PMMA-concentrations.

Modeling the development of the experimental MWDs in PREDICI® has revealed the scission kinetics at different polymer and CO_2 concentrations. At low polymer concentrations, the scission rate decreases at higher CO_2-pressures, due to the negative influence of CO_2 on the cavitation velocity. However, at higher polymer concentrations this effect is counteracted by the viscosity reduction induced by the anti-solvent effect of CO_2, which results in faster scission in CO_2-expanded MMA as compared to bulk MMA. Due to this anti-solvent effect, it is possible to alter the MWD of polymers by ultrasound in concentrated polymer solutions.

6.6 References

1. A.V. Machado, J.A. Covas, M. van Duin, *J. Appl. Pol. Sci.* **2001**, 81, 58

2. M.W.A. Kuijpers, M.F. Kemmere M.F., J.T.F. Keurentjes, "*Ultrasound-induced radical polymerization*", in Encyclopedia of Polymer Science and Technology; John Wiley & Sons: New York, 2004

3. G.J. Price, *Ultrason. Sonochem.* **1996**, 3, S229

4. Y.T. Didenko, W.B. Mcnamara III, K.S. Suslick, *Nature* **2000**, 407, 877

5. T.Q. Nguyen, Q.Z. Liang, H.-H. Kausch, *Polymer* **1997**, 38, 3783

6. J.M. Pestman, J.B.F.N. Engberts, F. de Jong, *Recl. Trav. Chim. Pays-Bas* **1994**, 113, 533

7. H. Fujiwara, J. Tanaka, A. Horiuchi, A. *Polymer Bulletin* **1996**, 36, 723

8. H. Fujiwara, *Polymer Bulletin* **2001**, 47, 247

9. G.J. Price, P.J. West, P.F. Smith, *Ultrason. Sonochem.* **1994**, 1, S51

10. M.F. Kemmere, M.W.A. Kuijpers, L.J.M. Jacobs, J.T.F. Keurentjes, *Macromol. Symp.* **2004**, 206, 321

11. K.A. Shaffer, J.M. DeSimone, *Trends Polym. Sci.* **1995**, *3*, 146

12. P.G. Jessop, W. Leitner, *Chemical Synthesis using Supercritical Fluids;* Wiley-VCH: Weinheim, 1999

13. M.A. Abraham, L. Moens, *Clean Solvents, Alternative Media for Chemical Reactions and Processing*; ACS Symposium Series 819: Washington, 2002

14. M.W.A. Kuijpers, D. van Eck, D., M.F. Kemmere, J.T.F. Keurentjes, *Science* **2002**, 298, 1969

15. T.J. Mason, J.P. Lorimer, *Applied Sonochemistry*, Wiley-VCH, Weinheim, 2002

16. J.A. Odell, A. Keller, *J. Pol. Sci. B* **1986**, 24, 1889

17. U.S. Agarwal, *e-Polymers* **2002**, 14, 1

18. T.J. Leighton, *The Acoustic Bubble;* Academic Press: London, 1994

19. A. Casale, A., R.S. Porter, *Polymer Stress Reactions*; Academic Press: New York, 1978.

20. M. Wulkow, *Macromol. Theory Simul.* **1996**, 5, 393.

21. U. Plöcker, H. Knapp, J. Prausnitz, *Ind. Eng. Chem. Process Des. Dev.* **1978**, 17, 324

22. Kuijpers, M. W. A.; Jacobs, L. J. M.; Kemmere, M. F.; Keurentjes, J. T. F., submitted.

23. L. Xue, U.S. Agarwal, P.J. Lemstra, *Macromolecules* **2002**, 35, 8650

24. M.W.A. Kuijpers, M.F. Kemmere, J.T.F. Keurentjes, *Ultrasonics* **2002**, 40, 675

25. U. Hoffmann, C. Horst, U. Wietelmann, S. Bandelin, R. Jung, *Sonochemistry*, in Ullmann's Encyclopedia of Industrial Chemistry; Wiley-VCH: Weinheim, 2003

26. M.W.A. Kuijpers, P.D. Iedema, M.F. Kemmere, J.T.F. Keurentjes, submitted.

7 Calorimetric Study of the Energy Efficiency for Ultrasound-induced Radical Formation

Energy conversion in sonochemistry is known to be an important factor for the development of industrial applications, however, the strong influence of the physical properties of the liquid on the ultrasound characteristics usually prevents an accurate determination of the chemical effects. In this study, the energy efficiency of the ultrasound-induced radical formation from methyl methacrylate has been investigated. The energy yield can be quantified by comparison of the ultrasonic power that is transferred to the liquid and the radical formation kinetics. Based on this method the influence of temperature and amplitude of the ultrasound horn on the energy efficiency has been determined. The energy yield for the formation of radicals from ultrasonic waves appears to be in the order of $5*10^{-6}$ J/J. The energy conversion is the highest at low temperatures and at low amplitudes.

This chapter is based on: M.W.A. Kuijpers, M.F. Kemmere, J.T.F. Keurentjes *Ultrasonics*, **2002,** 40, 675

7.1 Introduction

Sonochemistry comprises all chemical effects that are induced by ultrasound. These effects include the formation of radicals and the enhancement of reaction rates at ambient temperatures[1,2]. Most of the chemical effects of ultrasound are caused by cavitations, i.e. the collapse of microscopic bubbles in a liquid. Cavities are generated when the "negative" pressure during the rarefaction phase of the sound wave is sufficiently large to disrupt the liquid. The implosions of these cavities generate temperatures and pressures of approximately 5000K and 200 bar, due to compression of the gas-phase inside the cavity. These harsh conditions lead to the production of excited states, to bond breakage and the formation of radicals. In general, the acoustic power that is transferred to the liquid is not uniformly available in the total reaction medium. Only in the immediate vicinity of the tip cavitation occurs, so that the majority of the radicals are formed at this location in the reactor. Subsequently, these radicals are dispersed throughout the reactor.

Although the energy conversion from ultrasonic waves to the desired effect is an important factor in the development of an industrial process, it has scarcely been studied in literature[3,4]. The strong dependency of the ultrasound characteristics on the liquid properties is one of the main problems. In this study, the energy efficiency of ultrasound-induced radical formation is determined by a combination of reaction calorimetry and the use of radical scavengers.

7.2 Experimental

Sonification of the solvent was performed in a 1.8 L commercially available reaction calorimeter RC1e (Mettler-Toledo GmbH, HP60 reactor, Switzerland). A detailed description of this equipment is given by Varela de la Rosa et al.[5] and Sáenz de Buruaga et al.[6] (Figure 7.1). Ultrasound with a frequency of 20 kHz was produced using a Sonics and Materials VCX600 ultrasonic generator. A ½-inch full-wave titanium probe was applied to couple the piezoelectric transducer to the liquid. To allow an accurate

comparison, the total configuration of the reactor was exactly kept constant during all the experiments. The RC1e was operated in isothermal mode, i.e. the jacket temperature of the reactor was automatically adjusted to keep the reactor temperature constant. The overall heat transfer coefficients over the reactor wall were determined by calibration. Throughout the experiment the heat flow was constantly calculated, based on the surface area of the reactor wall, heat transfer coefficients and the difference between jacket and reactor temperature. During the reaction argon 6.0 (Hoekloos, The Netherlands) was bubbled through a 3 mm tube into the reaction mixture with a flow rate of 2.0 mL/s. The reactor was filled with 1.5 L methyl methacrylate (MMA), obtained from Aldrich and distilled under vacuum to remove the hydroquinone inhibitor before use.

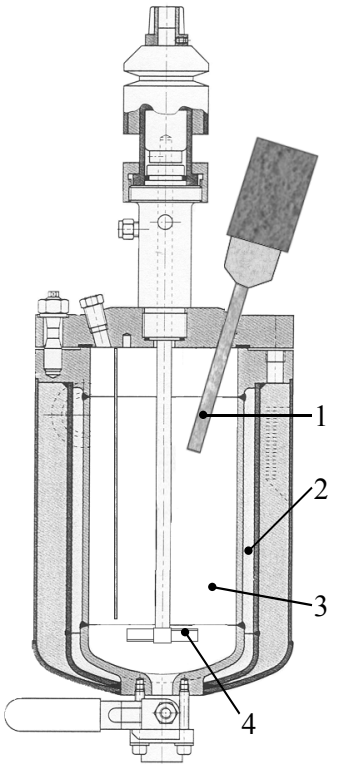

Figure 7.1. Schematic representation of the reactor set-up, with full-wave horn (1), jacket (2), reactor contents (3) and impeller (4).

Bawn et al.[7] reported the use of DPPH (1,1-diphenyl-2-picrylhydrazyl) as a radical scavenger to determine radical formation kinetics. In this work, the concentration profile of the active radical scavenger DPPH during sonification was determined by UV-vis spectrometry. DPPH was obtained from Aldrich and was used as received. It was found that the difference in the molecular absorption coefficients of the active and inactive radical scavenger has a maximum at 519 nm. The coefficients were $1.15*10^4$ L/(mol cm) and $2.28*10^3$ L/(mol cm) for the active and inactive radical scavenger, respectively. The thermal dissociation of DPPH was taken into account by doing the appropriate blank measurements.

By combining calorimetry and radical formation data, the energy conversion (X_{US}) can be calculated according to Equation 7.1:

$$X_{US} = \frac{½ \cdot \Delta H \cdot \frac{dn_{rad}}{dt}}{Q_{US}} \qquad (7.1)$$

in which Q_{US} is the ultrasonic power transfer, dn_{rad}/dt the radical formation rate and ΔH the bond energy, respectively. As the desired effect of ultrasonic irradiation is the formation of radicals, the energy efficiency is exclusively calculated from the energy used for bond breakage. Therefore, the improved mixing due to ultrasound is not taken into account. It is assumed that the radicals are formed by the dissociation of a carbon-hydrogen bond, for which the bond energy equals $3.38*10^5$ J/mol[8].

7.3 Results and discussion

The sonochemical energy efficiency for the formation of radicals is investigated in this study, requiring the calorimetric measurement of the ultrasonic power transfer. The measured influence of the amplitude and the temperature on the input of acoustic power is shown in Figure 7.2. Based on literature, it is expected that the acoustic power input is proportional to the square of the amplitude.[9] As can be seen from Figure 7.2, this is not valid in the case of cavitations under the tip. Additionally, Figure 7.2 shows that the temperature of the reaction medium has no significant influence on the ultrasonic power input.

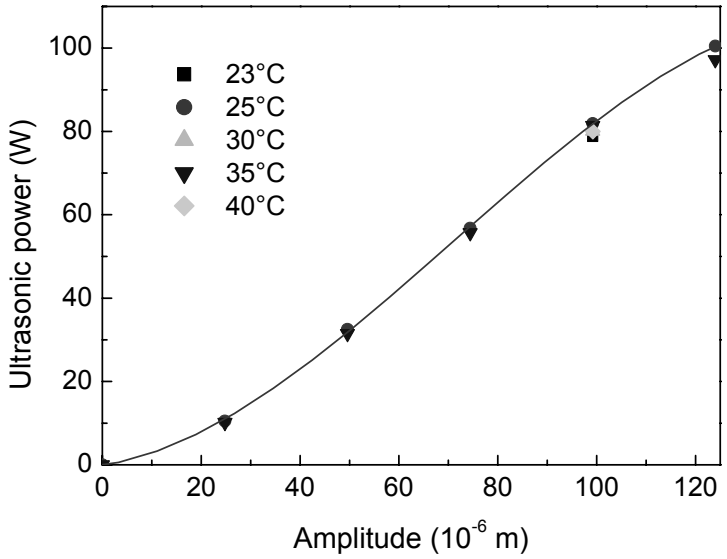

Figure 7.2. Effect of amplitude and temperature on the ultrasonic power transfer in MMA.

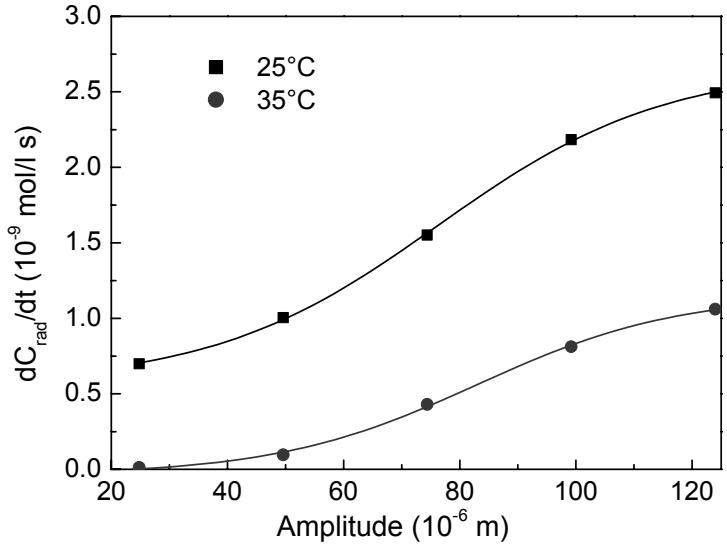

Figure 7.3. Radical formation rate as function of the amplitude at two different temperatures in MMA.

Table 7.1. Energy efficiency of ultrasound-induced radical formation in MMA obtained by reaction calorimetry.

T (°C)	ξ (10^{-6} m)	Q_{US} (W)	dC_{rad}/dt (10^{-10} mol/l s)	X_{US} (10^{-6})
23	99.2	78.8	22.9	7.3
25	24.8	10.5	6.99	16.8
25	49.6	32.5	10.0	7.8
25	74.4	56.8	15.5	6.9
25	99.2	81.9	21.8	6.7
25	124	100.5	24.9	6.3
30	99.2	80.1	14.1	4.4
35	24.8	10.2	0.12	0.3
35	49.6	31.5	0.96	0.7
35	74.4	55.7	4.30	1.9
35	99.2	81.4	8.12	2.5
35	124	97.2	10.6	2.7
40	99.2	80.0	0.74	0.2

Ultrasound-induced radical formation

The amount of radicals formed due to sonification is a function of the number of cavities created and the number of radicals that are formed per cavitation bubble. The extrinsic parameters, e.g. pressure, temperature, ultrasound settings and type of liquid, influence the formation of the radicals in a complex way. Here, the temperature and the amplitude of the sonification tip (ξ) are varied, according to the settings given in Table 7.1. As shown in Figure 7.3, temperature has a significant effect on the formation of radicals, especially at lower amplitudes. Due to the

cushioning effect of the vapour pressure on the implosion of the cavity, the local temperatures generated inside the cavity are lower at higher overall temperatures.[10] As a consequence, fewer radicals are generated. At higher amplitudes, coalescence of cavitation bubbles occurs, which reduces the number of cavitations and therefore the slope of the curve. Up till now, these effects can only be described qualitatively, as quantifying the influence of one single parameter is rather complex due to entwining of the various parameters.

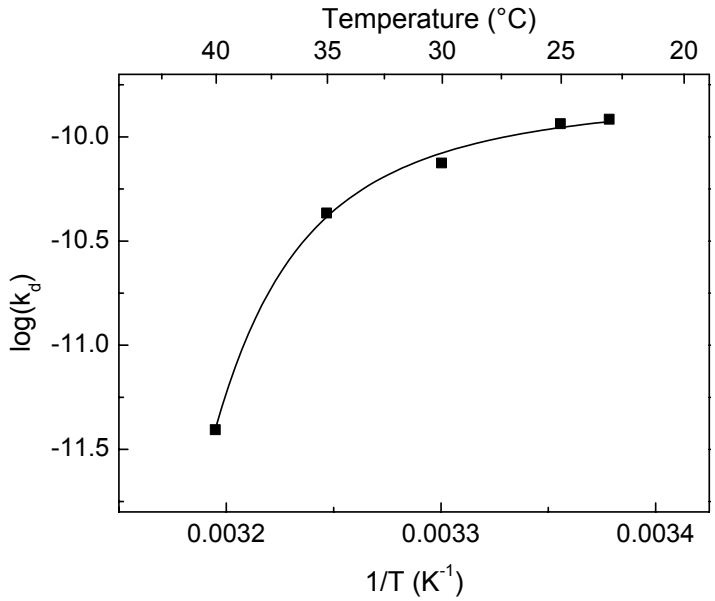

Figure 7.4. Arrhenius plot of the ultrasonically formed radicals from MMA at an amplitude of 99.2 μm.

Subsequently, the dependency of the radical formation kinetics on the temperature has been studied. From these experiments the ultrasound-induced dissociation constants (k_d) of MMA have been calculated from the decomposition rate equation:

$$\frac{dC_{radical}}{dt} = 2 \cdot k_d \cdot C_{monomer} \qquad (7.2)$$

The dissociation constants are shown in Figure 7.4 as an Arrhenius plot. Obviously, the usual Arrhenius behaviour is not obeyed for sonochemical reactions, as the reaction caused by ultrasound is accelerated at lower temperatures. Typically, this is a result of the lower vapour pressure of the liquid at lower temperatures. Price et al. have reported a similar tendency for the radical formation from methyl butyrate[11]. It should be noted, however, that the course of the Arrhenius plot shown in Figure 7.4, is mainly determined by the measurement at 40°C. The inaccuracy is the most substantial at this temperature due to the low radical formation rate as compared to the thermal decomposition rate of DPPH.

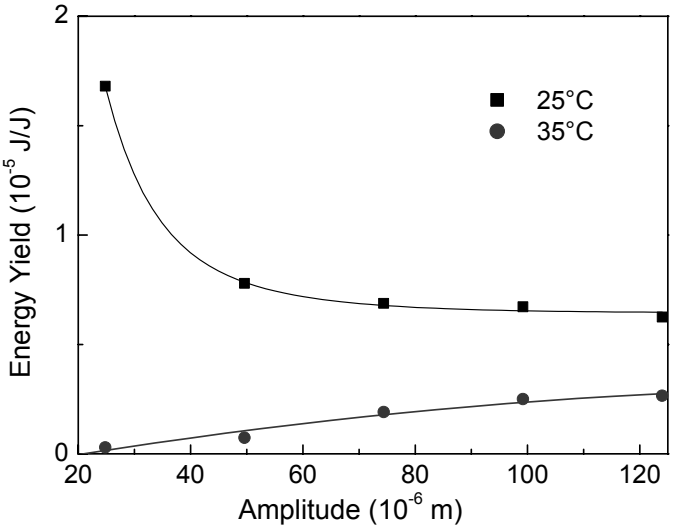

Figure 7.5. Ultrasonic efficiency for the formation of radicals from MMA at different amplitudes and temperatures.

Energy efficiency

From the dissociation rates and the ultrasonic heat input as measured by reaction calorimetry, the energy conversion is calculated according to Equation 7.1. Figure 7.5 shows the ultrasonic efficiency as a function of the amplitude. Typically, the energy conversion appears to be in the order of $5*10^{-6}$ J/J. From Figure 7.5 it can be seen that the two different temperatures

exhibit opposite slopes. This is due to the inefficient production of radicals at higher temperatures and lower amplitudes as explained above. In addition, the results of the 25°C experiment indicate that it is inefficient to use high amplitudes; a larger sonification area should rather be applied instead.

The dependency of the energy conversion on the temperature is presented in Figure 7.6. The energy efficiency decreases at higher temperatures due to the lower radical formation rate as can be derived from the Arrhenius plot (Figure 7.4). As a result of the minor influence of temperature on the ultrasonic power transference, the energy conversion follows the same tendency. Note that the energy conversion is not zero at temperatures above 40°C, as at these temperatures some radicals are still being formed from MMA.

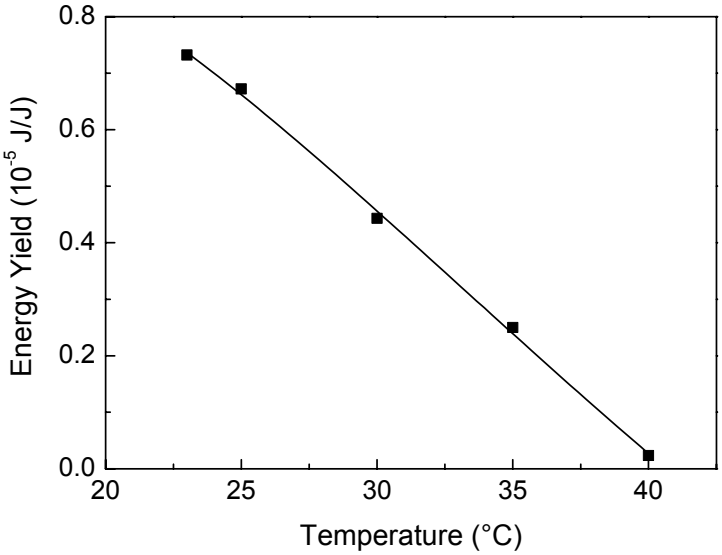

Figure 7.6. Ultrasonic efficiency as function of the temperature at an amplitude of 99.2 μm.

From Figures 7.3-7.6 it will be obvious that the energy efficiency is strongly influenced by the various process conditions. For industrial applications it will be mandatory to explore these influences to their limits to come to feasible ultrasound-based processes.

7.4 Conclusions

In this study reaction calorimetry in combination with the use of radical scavengers has been applied to determine the sonochemical efficiency for ultrasound-induced radical formation. The proposed method has shown to be a versatile tool to obtain the energy efficiency of ultrasound induced radical formation. Typically, the energy yield for the formation of radicals is in the order of $5*10^{-6}$ J/J. In general, the method described in this paper can be applied to any other ultrasonic reaction, provided the reaction kinetics are known.

7.5 References

1. L.H. Thompson, L.K. Doraiswamy, *Ind. Eng. Chem. Res.* **1999**, 38, 1215

2. K.S. Suslick, G.J. Price, *Annu. Rev. Mater. Sci.* **1999**, 29, 295

3. J.-M. Löning, C. Horst, U. Hoffmann, 7th Meeting of the European Society of Sonochemistry, **2000**, 197

4. P.D. Lickiss, *The New Chemistry*; Cambridge University Press: Cambridge, 2000

5. L. Varela de la Rosa, E.D. Sudol, M.S. El-Aasser, A. Klein, *J. Polym. Sci.* **1996**, 34, 461

6. I. Saenz de Buruaga, A. Echevarrío, P.D. Armitage, J.C. de la Cal, J.R. Leiza, J.M. Asua, *AIChE J.* **1996**, 43, 1069

7. C.E.H. Bawn, S.F. Mellish, *Trans. Faraday. Soc.* **1951**, 47, 1216

8. K.P. Huber, G. Herzberg, *Molecular spectra and molecular structure constants of diatomic molecules*; Von Nostrand Reinhold: New York, 1979

9. T.G. Leighton, *The Acoustic Bubble*; Academic Press: London, 1994

10. J.M. Pestman, J.B.E.N. Engberts, F. de Jong, *Recl. Trav. Chim. Pays-Bas* **1994**, 113, 533

11. G.J. Price, D.J. Norris, P.J. West, *Macromolecules* **1992**, 25, 6447

8 Preliminary Design of an Ultrasound-induced Polymerization Process

Based on the results described in the previous chapters, a preliminary design of an ultrasound-induced process for the production of pure PMMA in CO_2-expanded MMA has been developed. This has resulted in a clean, closed-loop process to produce PMMA at a capacity of 10 kg/hour. The possibility to perform the polymerization without any initiators or organic solvents allows for application of the synthesized PMMA as specialty polymer in biomedical materials.

This chapter is partially based on: M.F. Kemmere, M.W.A. Kuijpers, R.M.H. Prickaerts, J.T.F. Keurentjes, A novel process for the ultrasound-induced radical polymerization of MMA in pressurized CO_2, Macromolecular Materials and Engineering/ Macromolecular Reaction Engineering, in preparation.

8.1 Preliminary design of an ultrasound-induced polymerization process in CO_2-expanded MMA

Applications of ultrasound in processing and synthesis are widespread on laboratory scale. However, no industrial plant in which ultrasound initiates a polymerization reaction has been built so far. This is a consequence of the low energy yield of the cavitation process (Chapter 7), which results in a high electrical power consumption. For the development of an economically feasible bulk process (> 5000 kg/hr), the energy conversion still needs to be improved. For specialty products, however, it is expected that an ultrasound-based process can be viable. A product with a high-added value has thus to be produced, e.g. polymers for biomedical applications. These types of polymers have stringent demands concerning impurities, such as catalyst and initiator traces, residual monomer and organic solvents. With the ultrasound-induced polymerization process in CO_2, no initiators and organic solvents are required. In this section, a preliminary process design is developed to produce 10 kg/hour pure PMMA (specialty product, Figure 8.1) in CO_2-expanded MMA by ultrasound-induced initiation.

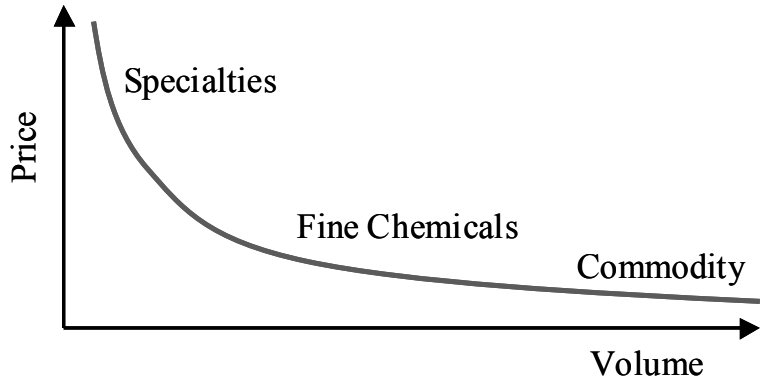

Figure 8.1. Classes of chemicals and their price as function of the production volume.

8.2 Ultrasound-induced polymerization

When ultrasound is used to initiate a radical polymerization reaction, radicals can be formed both from monomer and from polymer molecules. The majority of the radicals in an ultrasound-induced polymerization reaction originate from the polymer chains (Chapter 1). Therefore, the polymer scission rate mainly determines the radical formation rate. The highest polymerization rate is thus obtained when the maximum amount of polymer is dissolved in CO_2-expanded MMA, as the scission rate constant is approximately constant at high polymer concentrations (Chapter 6).[1]

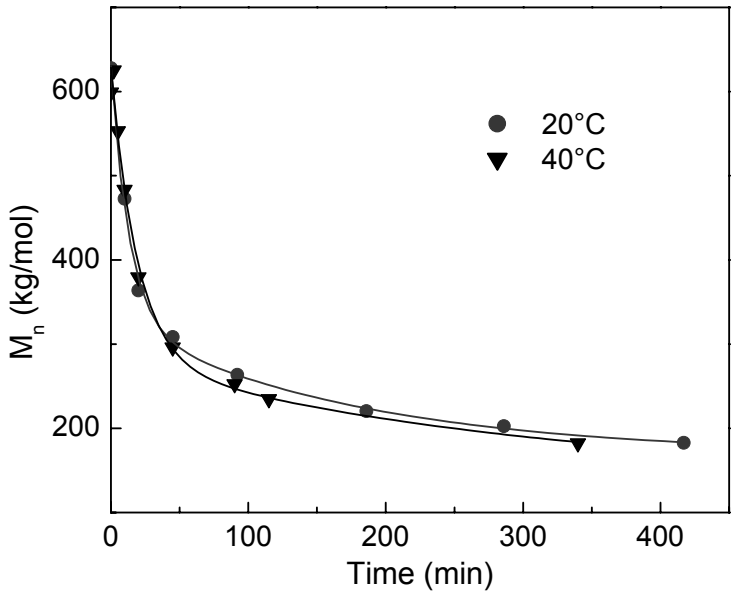

Figure 8.2. Ultrasound-induced polymer scission reactions of 0.1wt% PMMA in CO_2-expanded MMA at 7 bar absolute, at 20°C and 40°C, respectively.

Most ultrasound-induced bulk polymerizations are performed at room temperature. This low temperature is chosen because ultrasound-induced polymer scission in bulk is more efficient at lower temperatures.[2] It should be noted, however, that the propagation rate increases with an increasing temperature. Therefore, a suitable temperature in terms of propagation rate constant and radical formation rate has to be chosen to optimize

ultrasound-induced bulk polymerizations. Apparently this is not the case for polymerizations in CO_2-expanded MMA. Figure 8.2 shows the development of the number-averaged molecular weight (M_n) in time for scission experiments at different temperatures. The scission rate and consequently the radical formation rate are similar at 20°C and 40°C in CO_2-expanded MMA. This is probably caused by the lower CO_2 fraction in the bubble, which compensates the higher MMA-fraction. Because of the higher MMA propagation rate at 40°C, the polymerization at 7 bar will be faster at 40°C than at 20°C.

8.3 Polymerization reactor

Ultrasound-induced polymerization reactions have some characteristics, which require a specific type of reactor:

- The ultrasound-induced polymerization of MMA is rather slow due to the low reaction temperature.[3] As a result a *long residence time* is required in the reactor.
- Due to the low energy yield, a *high ultrasound power input* is needed. This energy has to be removed, otherwise the reaction temperature will increase, which is disadvantageous for the ultrasound-induced initiation step**.** This implies that a *large heat transfer area* and a *turbulent flow* are needed.
- The *maximum amount of polymer* should be dissolved in the reaction medium at every point in the reactor. This ensures that the highest radical formation rate and hence the maximum polymerization rate is obtained
- A *large sonification area* is required in order to achieve a high ultrasound-induced radical formation rate and a relatively high energy efficiency (Chapter 7).

Since a loop reactor satisfies all these requirements, it is considered to be the best reactor choice for an ultrasound-induced polymerization process on an industrial scale. In the proposed loop reactor (Figure 8.3), the

reaction mixture is continuously pumped through the cavitation sections (A) and the cooling sections (B) at a high speed. In this way the radicals that are formed in section A can still react in section B and the heat generated by ultrasound can be removed after each sonification area.

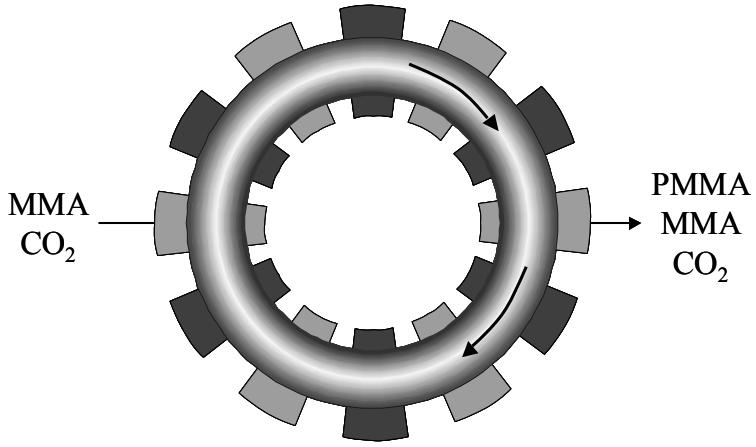

Figure 8.3. A schematic representation of the ultrasound-induced polymerization reactor, with cavitation (A) and cooling sections (B).

Table 8.1. Characteristics of the ultrasound-induced polymerization loop reactor.

Loop reactor	
Volume	168 L
Temperature	40°C
Pressure	7 bar
Concentration PMMA	15 wt%
Molecular weight PMMA	800 kg/mol
Intensity	70 W/cm^2
US-area	0.14 m^2
US-power	96.0 kW

From the previous sections it can be concluded that the highest polymerization rate in this loop reactor is probably obtained at a CO_2-pressure of 7 bar, a temperature of 40°C and a polymer concentration of 15

wt%. This 15 wt% is approximately the maximum solubility of PMMA (M_n = 800 kg/mol) in CO_2-expanded MMA at 40°C and 7 bar. By combining the results from Figure 6.7B and Figure 8.2, the scission rate constant is estimated to be approximately $5*10^{-4}$ 1/s. The radical formation rate from monomer molecules is neglected, as it only contributes for a small part to the overall radical formation rate by ultrasound. The propagation rate and termination rate constants at 40°C are 494 L/mol s and $3*10^7$ L/mol s, respectively.[4] Based on these conditions, a reactor volume of 168 L is required to produce 10 kg PMMA/hour (Table 8.1). In these calculations, the ultrasound intensity and the ratio between reaction volume and ultrasound area are chosen equal to the scission experiments performed in Chapter 6.

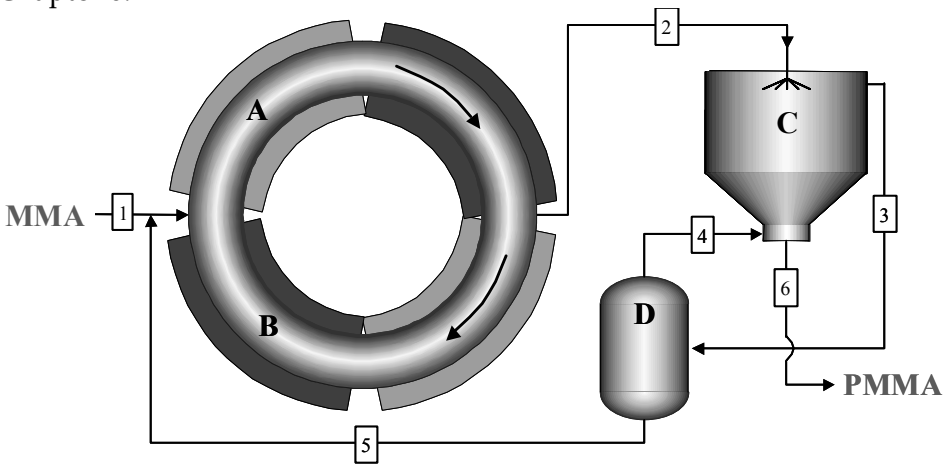

Figure 8.4. Process flow diagram of the ultrasound-induced polymerization of MMA in CO_2-expanded MMA; with, cavitation (A) and cooling areas (B) in a loop reactor, an extraction column (C) and a separation unit (D).

8.4 Flow diagram for ultrasound-induced polymerization

Figure 8.4 shows the process concept with the loop reactor for the ultrasound-induced polymerization of MMA. The MMA fed to the reactor is converted to PMMA till a conversion of 15%. The product stream (2) consisting of PMMA, MMA and CO_2 (Table 8.2), is sprayed into the extraction column, in which it is contacted with supercritical CO_2 counter currently (Table 8.3). The PMMA precipitates and the MMA dissolves in

the supercritical phase. This extraction process is better known as the Supercritical Anti-Solvent process (SAS).[5] Typically, residual monomer concentration in the final product can go down to 10 ppm,[6] because of the significant extraction capacity of CO_2 for MMA. However, in literature no references were found that describe the extraction of large amounts of MMA from PMMA. Therefore, it is assumed that 20 times (molar basis) the amount of CO_2 is required to produce pure PMMA.

The resulting MMA/CO_2-stream from the SAS-column (3) is separated in a flash-drum (D) into almost pure CO_2 (4) and MMA (5). The flash-drum is operated adiabatically at 7 bar, resulting in an operation temperature of -42°C. The cold CO_2 stream has to be recompressed to 80 bar before it can be reintroduced into the extraction column, which requires a compressor of 24 kW. By compression, the CO_2 is heated to 180°C, which has to be cooled down to 40°C. The cold MMA stream (5) can be added directly at multiple places into the loop reactor, which already results in a cooling capacity of approximately 30 kW.

Table 8.2. Process flows for the ultrasound-induced polymerization process.

Streams	Components	Flow (kg/h)	Temperature (°C)	Pressure (bar)
1	MMA	10	20	1
2	PMMA	10	40	7
	MMA	57		
	CO_2	3		
3	MMA	58	40	80
	CO_2	493		
4	MMA	1	-42	7
	CO_2	490		
5	MMA	57	-42	7
	CO_2	3		
6	PMMA	10	40	1

Table 8.3. Process conditions for the process units in the process diagram.

	Temperature (°C)	Pressure (bar)
Loop reactor	40	7
Extraction column	40	80
Flash drum	-42	7

8.5 Conclusions

Based on the obtained results in Chapter 4 and Chapter 6, a process design for the production of PMMA has been developed. The possibility to produce polymers without any initiators or organic solvents has resulted in a clean, closed-loop process. To determine if this process is viable, additional research has to be performed on the extraction column and a cost calculation has to be included. Moreover, it is necessary to determine the optimum reaction conditions in a loop reactor, as scale-up of ultrasound reactors is not straightforward. Both the shape and size of the reactor influence the ultrasound field and consequently the radical formation rate.

8.6 References

1. M. W. A. Kuijpers, R. M. H. Prickaerts, M. F. Kemmere, J. T. F. Keurentjes, submitted

2. M. Ibisi, B. Brown, *J. Acoust. Soc. Am.* **1967**, 41, 568

3. M. W. A. Kuijpers, L. J. M. Jacobs, M. F. Kemmere, J. T. F. Keurentjes, submitted

4. O. F. Olaj, P. Vana, *Macromol. Rapid Commun.* **1998**, 19, 533

5. L. Dan, L. Zhimin, Y. Guanying, H. Buxing, Y. Haike, *Polymer* **2000**, 41, 5707

6. M.F. Kemmere, M. Cleven, M. A. van Schilt, J.T.F. Keurentjes, *Chem. Eng. Sci.* **2002**, 57, 3929

9 Application Potential of Ultrasound Reaction Engineering

In this chapter, several issues with respect to the application of ultrasound technology are addressed. First, the relatively poor energy conversion of ultrasound to the desired chemical reaction is discussed. Subsequently, a number of ultrasound applications are presented, which have a high potential to be developed into sustainable processes, such as the conversion of methane to methanol at ambient temperatures, ultrasound-assisted phase transfer catalysis in CO_2 and the production of polyethylene without initiators.

This chapter is partially based on: M.W.A. Kuijpers, L.J.M Jacobs, M.F. Kemmere, J.T.F. Keurentjes, Ultrasound-induced ethylene polymerization, in preparation.

9.1 Introduction

In this thesis, ultrasound-induced polymerizations and ultrasound-induced polymer scission reactions in high-pressure fluids have been explored, for which both a more fundamental approach and an engineering point of view have been taken. First, ultrasound-induced cavitation in high-pressure fluids has been investigated, including the description of bubble growth and implosion in these fluids with the Blake threshold pressure and a dynamic bubble model based on the Rayleigh-Plesset equation.

In addition, the possibility to perform ultrasound-induced polymerizations and ultrasound-induced polymer scission in CO_2-expanded media have been studied in detail. Experimental results show that it is possible to perform polymerization reactions in CO_2-expanded MMA, yielding high molecular weight polymer. The influence of CO_2 on the viscosity and on the reaction kinetics of ultrasound-induced polymerizations of MMA has been investigated. In contrast to polymerizations in bulk, a low viscosity is maintained during polymerization reactions in CO_2-expanded MMA. As a consequence, a constant or even increasing polymerization rate is observed when pressurized CO_2 is applied. Because of the constant viscosity, it should be possible to obtain higher conversions in CO_2-expanded MMA systems as compared to bulk MMA. In addition, ultrasound-induced polymer scission appears to be a well-controlled process, as fracture occurs approximately in the center of the chain. A mechanism has been proposed for this non-random fracture behavior, from which it can be concluded that complete stretching of the polymer chains is required before breakage can occur. Moreover, it is shown that it is possible to alter the MWD of polymers by ultrasound in concentrated polymer solutions, due to the addition of the anti-solvent CO_2.

Based on the results described in the previous chapters, a process design using ultrasound-induced initiation is presented in Chapter 8. In the current chapter, some remaining issues are discussed, i.e. the energy conversion of ultrasound and several potential ultrasound applications.

9.2 Energy efficiency of ultrasound

In general, the development of an economically feasible process demands the minimization of energy losses. This certainly applies to ultrasound-induced reactions, because of the low energy yield obtained until now. Typically an energy efficiency of 10^{-5} J/J is found (Chapter 7). During ultrasonic reactions, electrical energy is converted in several steps to perform a chemical reaction. First, an ultrasonic system transforms the electrical power into mechanical energy. Subsequently, this mechanical energy is transmitted into the sonicated reaction medium. Finally, the cavities that are formed by the ultrasound waves result in a chemical effect. Energy losses occur in each conversion step, see Figure 9.1. The lowest energy efficiency is observed for the cavitation process. Only a small fraction (10^{-4} J/J)[1] of the potential energy of a cavitation bubble is used for the desired chemical reaction. The largest improvements can thus be obtained at this transformation.

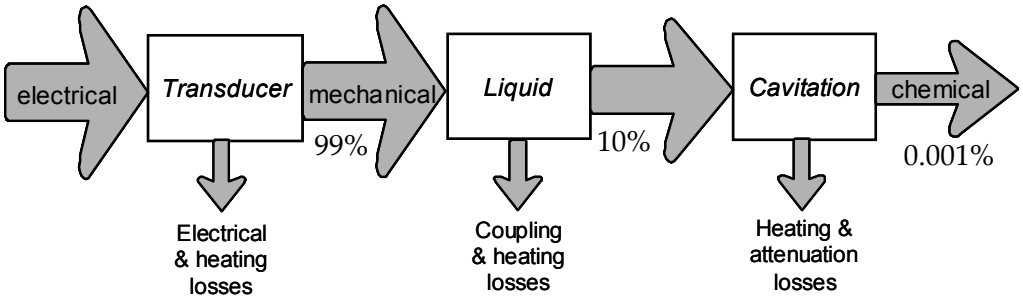

Figure 9.1. A schematic representation of the energy flows in an ultrasound-induced reaction.

It is important that the potential energy of the bubble at its maximum radius is used efficiently for the desired chemical effect. In general, this means that heating of additional non-reacting molecules in the bubble or condensation of compounds at the bubble wall interface has to be prevented. Chemicals that do not contribute to the desired chemical effect should thus not be present in the bubble. Additionally, the drag of the liquid during implosion has to be minimized. Therefore, a low viscosity solvent with a low vapor pressure in which the reactants dissolve is desirable from an energy efficiency point of view. Since ionic liquids have

no vapor pressure, they are interesting fluids to apply in ultrasound-based processes.[2,3] As only part of the bubble cloud is effective for radical formation, it would be worthwhile to investigate the application of multiple single bubble systems. This can be achieved using micro-system technology by constructing micro-transducers that drive the oscillation of one single bubble. This leads to "scaling out" rather then to "scaling up", which in principle would allow for a much higher energy conversion.

9.3 Ultrasound-induced ethylene polymerization

Polyethylene (PE) belongs to the most important products of the polymer industry.[4] PE polymers are tough, flexible plastics, which are used in a wide variety of materials. Applications range from rigid materials for refrigerators, computers and car parts, to soft, flexible fibers for baby's diapers. PE polymers are divided into three categories: low-density polyethylene (LDPE), linear low-density polyethylene (LLDPE) and high-density polyethylene (HDPE). LDPE is formed by radical polymerization of ethylene, the other two polymers require a catalyst to be produced.[4] Therefore, only the polymerization reaction for the production of LDPE can be initiated by ultrasound.

LDPE is manufactured at high pressures (810–2760 bar) and high temperatures (130–330°C) in a tubular or autoclave process.[4] The polymerization reactions are commonly started with free-radical initiators, such as peroxides or oxygen. It is a bulk polymerization process in which ethylene acts both as the solvent and the reactant. A maximum conversion of approximately 30% is obtained, as a result of which the polymer remains dissolved in the pressurized ethylene phase.[6] Another reason for the extremely high pressure in this process is the increase in reaction rate and obtained molecular weight with an increase in pressure (Figure 9.2).

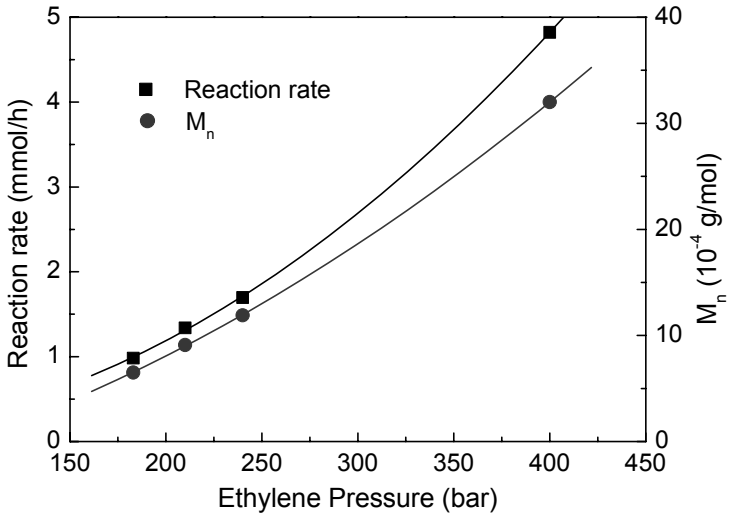

Figure 9.2. Initial polymerization rate and obtained number average molecular weight as a function of the ethylene pressure for the free-radical polymerization of ethylene at 40°C.[5]

The rate-limiting factor in the LDPE production is the heat removal from the reactor. Consequently, a common problem in LDPE production is an overshoot in reaction temperature. As a result of the too high reaction temperature, the initiator added to the reaction mixture degrades very fast and consequently a thermal runaway may occur. Since the reaction is no longer under control, the reactor has to be evacuated. This problem can be circumvented by using ultrasound to initiate the reaction, because it is an external initiation source, which can easily be switched off in the case a runaway might occur.

To determine whether ultrasound can substitute the standard initiators for the polymerization of ethylene, ultrasound-induced polymerizations have been performed in ethylene-expanded octane.

Experimental

Cavitation can only occur in liquids and not in gases or supercritical fluids (Chapter 2). Therefore, the commonly used conditions for the production of LDPE were not used, because ethylene would be a supercritical fluid. Instead, ultrasound-induced polymerization experiments of ethylene were performed in ethylene-expanded n-octane at 20°C and 10 bar. A low ethylene pressure was chosen because of safety considerations. The calculation of the phase behavior of the gas-expanded liquid at increased static pressures requires the use of an equation of state. In this work, the Lee-Kessler-Plöcker equation of state[5] was used to correlate the liquid temperature and static pressure with the liquid composition. The temperature independent interaction parameter for the ethylene/n-octane-system is approximately 1.2 (Figure 9.3).[8]

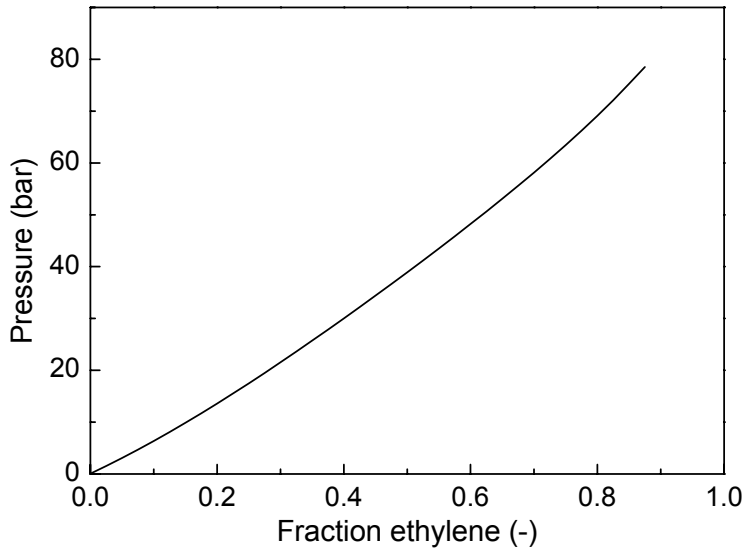

Figure 9.3. Calculated phase diagram of the ethylene/octane-system with the LKP equation of state at 20°C.

The polymerization reactions were investigated in a 1.8 L commercially available reaction calorimeter RC1e (Mettler-Toledo GmbH, HP60 reactor, Switzerland).[9] Sonification of the solution was performed using 20 kHz ultrasound, which was produced by a Sonics and Materials VC-750

generator. A ½-inch full-wave titanium probe was applied to couple the piezoelectric transducer to the liquid. The reactor was first filled with 0.99 kg n-octane (Sigma) and was purged with argon (grade 5.0, Hoekloos) for one hour to remove the dissolved oxygen. Subsequently, the reactor was pressurized up to 10 bar with ethylene (grade 3.5, Hoekloos). This resulted in an ethylene molar fraction of 0.17 in n-octane at 20°C. Finally, the solution was sonicated for 5 hours with a fixed ultrasound probe amplitude of 75 μm. The product, which was obtained after evaporation of the solvent (n-octane), was analyzed with Fourier Transformed Infrared (FTIR).

Results and discussion

The ultrasound-induced polymerization of ethylene in ethylene-expanded octane has resulted in the production of a wax. However, it was not possible to determine the yield of the polymerization experiment due to the low conversion. The low yield was expected, as the polymerization reaction is slow at low ethylene pressures (Figure 9.2). Despite the low yield, it has been possible to make an FTIR-spectrum of the product.

Figure 9.4 shows the FTIR-spectrum of the obtained product and a reference PE-sample. Although a large similarity is found between the two spectra, also some absorbance peaks are found in the obtained product that do not originate from PE. These peaks can be a result of impurities or residual n-octane in the FTIR-sample. The peaks in the 3000-2800 cm^{-1} range result from the stretching of CH_3 and CH_2 bonds.[10] The peaks in the 1400 cm^{-1} range originate from the bending of CH_2 bonds. Obviously, these bonds are also present in the infrared spectrum of n-octane (Figure 9.5). However, the two distinct peaks at 729 cm^{-1} and 719 cm^{-1} in Figure 9.4 for the reference polymer can be ascribed to long chain out-of-plain C-C vibrations. These peaks, which are also found in the product-spectrum, can only be observed when the chain is longer than 30 carbon atoms.[10] This implies that the product contains at least oligomers of ethylene.

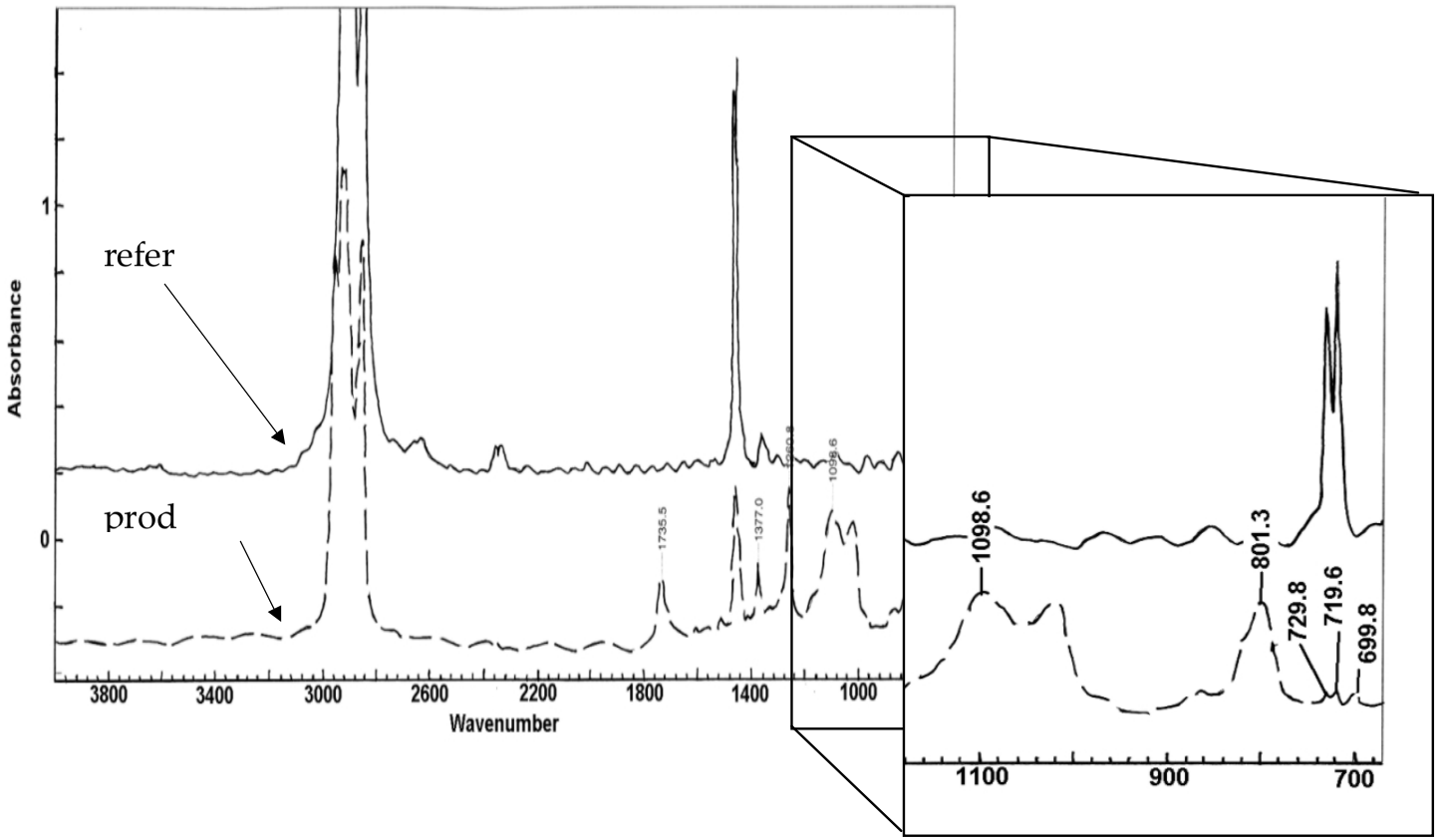

Figure 9.4. FTIR-spectrum of the obtained product and a reference PE-sample.

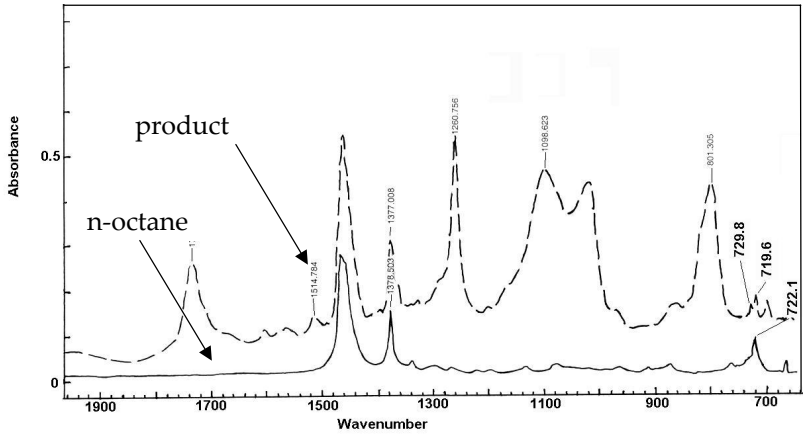

Figure 9.5. FTIR-spectrum of the obtained product and n-octane.

Conclusions

Based on the described results, we can conclude that it is possible to initiate the polymerization of ethylene by ultrasound. Although no conversion could be determined due to the low yield, we expect that the reaction rate and subsequently the conversion can substantially be improved by applying higher ethylene pressures. Moreover, a higher ethylene pressure will also increase the obtained molecular weight of the ultrasound-induced polymerization of ethylene.

9.4 Ultrasound-enhanced PTC

A significant problem in organic synthesis arises from water-soluble reagents used for reactions with water-insoluble organic substrates. Most of these reactions involve the reaction of an ionic species from an aqueous or solid phase with an organic phase. Due to mass transfer limitations, the concentration of the reactants at the reaction locus is too low for an efficient process.[11] A number of methods are available to avoid this low reaction rate, such as the use of a co-solvent, rapid stirring and employing a phase transfer catalyst.[12] Usage of a co-solvent is normally not preferred because of environmental considerations.

Phase transfer catalysis (PTC)

Phase transfer catalysts are used to enhance or enable the reaction of compounds that are immiscible. The phase transfer catalyst increases the concentration of chemicals in a liquid in which they would normally not dissolve (Figure 9.6). Especially quaternary ammonium salts are used for enhancing two-phase reactions, such as substitution, condensation and polymerization reactions.[13] Other phase transfer catalysts are for instance crown ethers, micelles and dendrimers.[14]

Ultrasound-induced phase transfer catalysis

Stirring of the reaction mixture provides mass and heat exchange in the system. In two-phase systems, stirring also influences the interface by breaking up droplets or solid particles. Consequently, improved hydrodynamics in a heterogeneous reaction mixture lead to a larger mass transfer area and hence directly influences the reaction rate of PTC-reactions. An approach to improve this mass transfer area is by applying ultrasound technology.

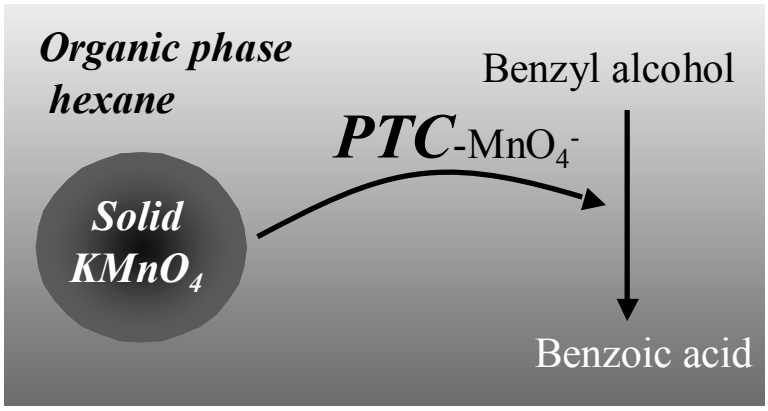

Figure 9.6. A schematic representation of a phase transfer catalyst (PTC) enabling the reaction of benzyl alcohol with permanganate.

Ultrasound has shown to have positive effects on both homogeneous and heterogeneous reactions.[15] The chemical effects induced by ultrasound are caused by the implosion of microscopic bubbles in a liquid. When solid

particles are present in a liquid, the cavitation bubble can implode symmetrically or asymmetrically. If solid particles are in the proximity of the bubble, the cavity implodes asymmetrically and a micro-jet is formed. This jet can break up the particles resulting in a larger contact area. Symmetric cavitations create shock waves that propagate in the surrounding liquid, causing microscopic turbulences. This so-called micro-streaming, results for instance in smaller liquid droplets and hence higher mass transfer rates.[16] Additionally, micro-streaming increases the liquid renewal rate at the surface interface. The phase transfer rate can thus significantly be enhanced by ultrasound. For this reason, it is expected that ultrasound can substitute a phase transfer catalyst.

To determine the influence of ultrasound on the reaction rate of immiscible reactants, the reaction of benzyl alcohol with potassium permanganate ($KMnO_4$) has been studied in hexane, with and without ultrasound.

Experimental

Ultrasound-induced phase transfer catalysis in hexane was investigated in a thermostated 200 mL vessel (Figure 5.2). Sonification of the solution was performed using 20 kHz ultrasound, which was produced by a Sonics and Materials VC-750 generator. A ½-inch full-wave titanium probe was applied to couple the piezoelectric transducer to the liquid. The amplitude of the ultrasound probe was fixed at 62 μm.

Phase transfer experiments of $KMnO_4$ (Merck) with benzyl alcohol (Fluka) were performed with and without ultrasound. In the experiments without ultrasound, a magnetic stirrer was used to homogeneously distribute the solid $KMnO_4$-particles in the reactor. The reactor was filled with hexane (Merck) or CO_2 (Hoekloos, Grade 5.0) to which 3.8 g $KMnO_4$, 1.6 g benzyl alcohol and 0.7 g n-decane (Fluka) were added. The decane was used as internal standard for the GC-analysis, with which the

conversion to benzoic acid was determined. The particle size distributions of the $KMnO_4$-particles were measured with static light scattering.

Results and discussion

Figure 9.7 shows the conversion history of the oxidation of benzyl alcohol with solid $KMnO_4$ in hexane. In this reaction, ultrasound is used as a substitute for a phase transfer catalyst. The observed reaction rate of the sonicated experiment is a factor 1.5 higher than the stirred experiment. This difference can be a result of the improved mixing by ultrasound or a larger surface area. Therefore, the particle size distributions of the $KMnO_4$-particles have been measured after 5 hours of stirring or sonification, without reaction. Figure 9.8 shows the surface averaged particle diameter distribution. The size distributions are almost similar from which it can be concluded that the particles are too hard to be fractured by cavitation at these conditions in hexane. This implies that the higher reaction rate with ultrasound is the result of the improved hydrodynamics.

In Chapter 2, we have shown that cavitation is possible in liquid CO_2.[17] As a result, it is interesting to combine ultrasound-induced phase transfer catalysis with high-pressure CO_2 in order to avoid the use of organic solvents. Unfortunately, the experiments performed in liquid CO_2 with ultrasound did not result in the appropriate product, due to experimental difficulties. Because of severe vibrations in the reactor, the reactions in liquid CO_2 had to be interrupted. Although the experiments did not yet succeed, it is a promising and sustainable concept to combine ultrasound-induced phase transfer catalysis with liquid carbon dioxide.

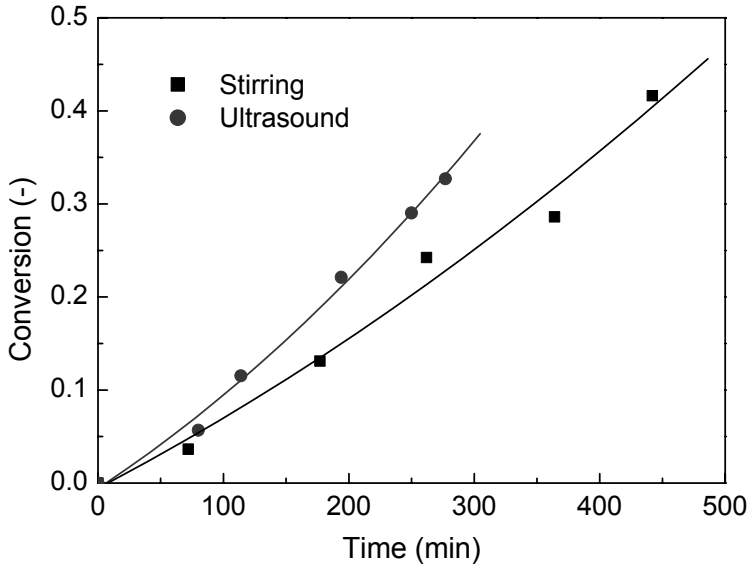

Figure 9.7. Conversion history of the oxidation of benzyl alcohol with potassium permanganate in hexane, with and without ultrasound.

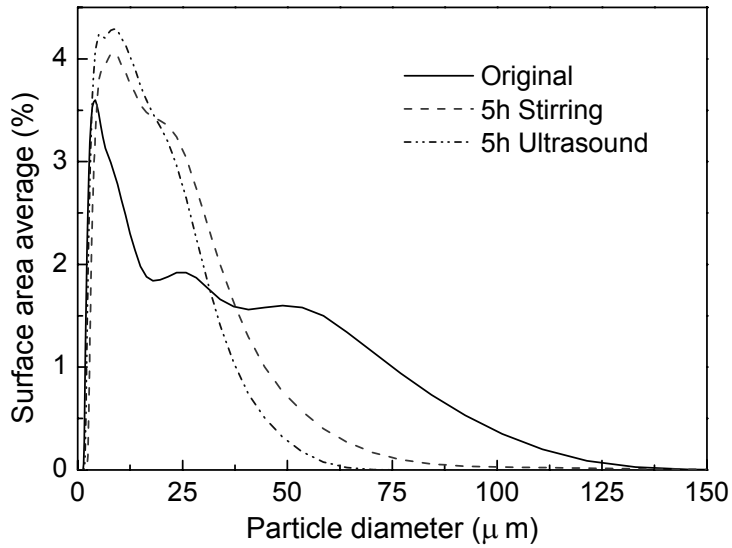

Figure 9.8. Surface averaged particle diameter of potassium permanganate after 5 hours of stirring or sonification in hexane.

9.5 Methane conversion at ambient temperature

Methane is the main component of natural gas, which can be found all over the world. Most of the methane is discovered in regions that are far removed from industrial complexes, such as offshore locations. The transportation of methane from the platform to the consumer is expensive.[18] Liquefaction of methane by converting it to methanol, the initial product of methane oxidation, forms a possible solution. However, these oxidation processes typically occur at elevated pressures and temperatures of approximately 250 bar and 1200 K, respectively.[19] These extreme conditions are required to dissociate the methane molecules and as a consequence this process is not suitable for offshore platforms. For this reason, research is performed on the synthesis of methanol from methane at milder conditions. Recently, results have been reported of methane conversion at 373 K and 10 bar, by a photo-catalytic reaction with the help of methane hydrates.[20]

In potential, ultrasound can also induce this methane conversion at ambient temperatures, because of the high temperatures and pressures that are generated locally in the cavities.[21] Kruus et al. have shown that ammonia can be produced from nitrogen and hydrogen by sonification,[22] which is a good indication for the possibility of ultrasound-induced methanol synthesis. The most probable reaction scheme for the methanol synthesis is given below, resulting in methanol and hydrogen:

$$CH_4 \longrightarrow CH_3\bullet + H\bullet$$

$$CH_3\bullet + H_2O \longrightarrow CH_3OH + H\bullet$$

$$CH_4 + H_2O \longrightarrow CH_3OH + H_2$$

Experimental

Experiments to produce methanol from methane and water were performed in a high-pressure ultrasound reactor[23] at 10°C. The reactor was filled with 150 mL water and was pressurized with 3 bar of methane (Hoekloos, grade 4.5). Ultrasound with a frequency of 20 kHz was

produced using a Sonics and Materials VC-750 ultrasonic generator. A ½-inch full-wave titanium probe was applied to couple the piezoelectric transducer to the liquid. The amplitude of the ultrasound probe was fixed at 75 μm. During sonification, methane was bubbled through a 3 mm tube into the reaction mixture with a flow rate of 2.0 mL/s. The conversion of the reaction was determined by GC-analysis.

Results and Discussion

Figure 9.9 shows the GC-analysis of the ultrasound-induced methanol synthesis. The retention times of methane and methanol are 46 and 92 seconds, respectively. From these graphs, it can be concluded that no measurable amount of methanol has been formed in 270 min of sonification. This is probably a result of the limited quantity of methane present in water. Only a methane molar fraction of approximately 10^{-5} in water dissolves at these conditions. Another disadvantageous effect is the presence of large amounts of water vapor in the bubble; water degrades at lower temperatures than methane. Consequently, the obtained hot-spot has a too low temperature to degrade methane. A possible solution is to use a non-volatile solvent in which both methane and water dissolve, e.g. perfluor liquids. To determine if cavitation-induced methane conversion is possible, more ultrasound experiments are required.

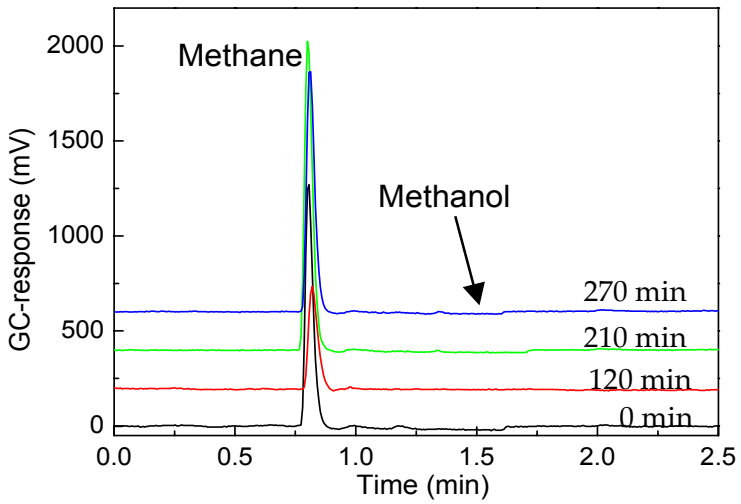

Figure 9.9. GC-chromatograms of the ultrasound-induced methanol synthesis from water and methane.

9.6 Concluding remarks

In this thesis, the potentials and challenges of ultrasound-induced reactions in high-pressure fluids have been explored for which the emphasis has been on ultrasound-induced polymerizations. The polymerization reactions in gas-expanded liquids have been addressed both fundamentally and from an engineering point of view for application in industry. The possibility to produce polymers without any initiators or organic solvents has resulted in a clean, sustainable process. However, the energy consumption and the relatively low polymerization rates make it a relatively expensive way to produce polymers. An improved energy efficiency and polymerization rate will enable the development of an commercial ultrasound-induced polymerization process without any additional chemicals.

Besides polymerization reactions, ultrasound-induced phase transfer catalysis and methane conversion at ambient pressure have been addressed in this last chapter. Other potential applications are dying, sterilization and washing of textiles in CO_2,[24] in which ultrasound can accelerate these processes due to micro streaming. Moreover, gas-expanded liquids can be used in combination with ultrasound to carry out oxidation or hydrogenation reactions, because of the high solubility of hydrogen and oxygen in these types of fluids.

Although no large-scale industrial polymerization processes based on ultrasound exist yet, commercial applications in other fields such as ultrasound cleaning and sterilization prove that ultrasound is a readily available technique on larger scale. Nevertheless, the application of ultrasound for polymerization purposes requires a thorough multidisciplinary understanding of both ultrasound parameters and liquid properties, including aspects from physics, chemistry and engineering.

9.7 References

1. Y. T. Didenko, K. S. Suslick, *Nature* **2002**, 418, 394

2. J. D. Oxley, T. Prozorov, K. S. Suslick, *J. Am. Chem. Soc.* **2003**, 125, 11139

3. J.-M. Leveque, J.-L. Luche, C. Petrier, R. Roux, W. Bonrath *Green Chemistry* **2002**, 4, 357

4. N. Maraschin, Ethylene Polymers, *Encyclopedia of Polymer Science and Technology*, John Wiley & Sons: New York, 2004

5. S. Machi, T. Sakai, F. Suganuma, T. Kagiya, *Bull. Chem. Soc. Japan* **1968**, 41, 897

6. P. van den Heuvel, Industrial polyethylene production, *Polymer Reaction Engineering Course* **2001**, Eindhoven University of Technology.

7. U. Plöcker, H. Knapp, J. Prausnitz, *Ind. Eng. Chem. Process Des. Dev.* **1978**, 17, 324

8. W. L. Weng, M. J. Lee, *J. Chem. Eng. Data* **1992**, 37, 213

9. L. Varela de la Rosa, E. D. Sudol, M. S. El-Aasser, A. Klein, *J. Polym. Sci.* **1996**, 34, 461

10. D. O. Hommel, F. Scholl, *Atlas der Kunstoff-Analyse*, Hanser: München, 1968

11. M. M. Varma, *Chem. Eng. Sci.* **1998**, 43, 1749

12. Y. Sasson, R. Neumann, *Handbook of phase transfer catalysis*, Blackie A&P: London, 1997

13. M. Halpern, Phase Transfer Catalysis, *Ullmann's Encyclopedia of Industrial Chemistry*, John Wiley & Sons: New York, 2004

14. M. W. P. L. Baars, P. E. Froehling, E. W. Meijer, *Chem. Commun.* **1997**, 20, 1959

15. L. H. Thompson, L. K. Doraiswamy, *Ind. Eng. Chem. Res.* **1999**, 38, 1215

16. L. C. Hagenson, L. K. Doraiswamy, *Chem. Eng. Sci.* **1998**, 53, 131

17. M. W. A. Kuijpers, D. van Eck, M. F. Kemmere, J. T. F. Keurentjes, *Science* **2002**, 298, 1969

18. J. H. Lunsford, *Cat. Today* **2000**, 63, 165

19. E. Fiedler, G. Grossman, D. Brukhard, G. Weis, C. Witte, Methanol, *Ullmann's Encyclopedia of Industrial Chemistry*, John Wiley & Sons: New York, 2004

20. C. E. Taylor, *Cat. Today* **2003**, 84, 9

21. K. S. Suslick, *Science* **1990**, 247, 1439

22. Supeno, P. Kruus, *Ultrason. Sonochem.* **2002**, 9, 53

23. M. W. A. Kuijpers, R. M. H. Prickaerts, M. F. Kemmere, J. T. F. Keurentjes, submitted

24. M.-W. Park, H.-K. Bae, *J. Supercrit. Fluids* **2002**, 22, 65

Dankwoord

Zonder mensen om mee samen te werken en overige activiteiten te doen is het werk natuurlijk niet half zo gezellig. Daarvoor wil ik iedereen danken en een aantal in het bijzonder. Allereerst, *Jos* en *Maartje* voor de uitstekende en leuke begeleiding op de momenten dat ik het nodig had en dat was nog wel eens tijdens het schrijven. De vrijheid die jullie mij gegeven hebben, heb ik zeer gewaardeerd. Volgens mij zijn jullie nooit de snelheidsbepalende stap geweest tijdens mijn promotie, dus jullie mogen best wel wat meer ontspannen. Dat heb ik ook elke keer gedaan toen de journalisten langskwamen!

De mensen waar ik donderdag om 4 uur op kon rekenen om mee te vergaderen in de F.O.R.T., *Willy*, *Joop*, *Chris L.*, *Bram*, *Jaco*, *Chris S.*, *Joost*, *Stefan*, en het geadopteerde wiskundekindje *Rob*. Ik zal er alleen niet meer zo vaak zijn. *Zwannet* (Barcelona/ Granada en Parijs), *Henny* (Sardinië en Biaritz) en *Marcus* (Parijs en Halkidiki) voor de zeer leuke tijd tijdens de werkvakanties rond de congressen en cursussen. Ik hoop dat ik in mijn toekomstige werk ook zulke leuke en begripvolle (*Zwannet*) reisgenoten heb om mee op werkvakantie te gaan! De mensen die bij me op de kamer wilden zitten en toch allemaal vertrokken zijn, *Dick*, *Dirk* en *Roger*. Door hen was ik genoodzaakt twee surrogaatkamergenoten (Ali en Mowgli) te nemen, maar als jullie er waren was het wel gezellig. De mensen met wie ik naar Mamma Mia in Londen ben geweest, ben wezen wadlopen of sporten, *Ana*, *Frank*, *Johan*, *Thijs* en *Xaviera*.

Zeker niet te vergeten mijn afstudeerders *Diana*, *Leon* en *Ramona* en researchstagair *Arno*. Dankzij deze vier heb ik er veel langer over gedaan om alles op te schrijven, maar heb ik wel 6 hoofdstukken extra. Het was zeer leuk om met jullie samen te werken. Zonder de hulp van de technische dienst konden ook zij hun werk niet doen. Daarvoor ben ik vooral *Chris Luyk* veel verschuldigd die de reactor ontworpen en gebouwd heeft en altijd voor me klaar stond. Gelukkig wordt je baan nu ook gewaardeerd

door het management. Ook niet te vergeten, *Vincent* en *Anton* voor hun technische hulp. *Wieb* bedankt voor de honderden GPC-monsters die je hebt gemeten.

Naast de mensen op het werk zijn er natuurlijk ook nog mensen in het dagelijks leven die me gesteund hebben. Eerst de mensen die al bijna 29 jaar voor me klaar staan, *mijn ouders* en mijn kleine broertje *Stefan*, die er toch ook al 26 jaar bij is. *Ma* en *Pa,* jullie hebben de optimist toch een aantal maal versteld doen staan. Het komt goed.

Alle huisgenoten waarmee ik de laatste acht jaar heb samengewoond in de *Wittegijt* (als ik niet weg was) wil ik bedanken voor de gezellige tijd en het leegeten van hun bordjes. *Roel* en *Ronald,* nog even doorzetten dan lukt het jullie ongetwijfeld ook. *Bart*, *Meta* en *Ronald* dankzij de reis naar Zuid-Afrika ben ik verslaafd geraakt aan lange reizen naar verre landen. *Robbie*, het was gezellig in Costa-Rica en Brazilië. In Costa-Rica heb ik voor het eerst echt mijn ogen uitgekeken onder water. *Bart* je weet niet wat je meemaakt als je onder een gigantische manta ray zweeft of met haaien zwemt, moet je echt een keer doen. En natuurlijk nog alle mensen van de *Stiefel* vereniging met wie ik behoorlijk wat stiefels heb genoten en lekker heb gevolleybald. We kunnen nog wel één keer de ONCS winnen!

Martijn

Publications

1. *Calorimetric Study of the Energy Efficiency for Ultrasound-induced Radical Formation.* M.W.A. Kuijpers, M.F. Kemmere, J.T.F. Keurentjes, Ultrasonics, 2002, 40, 67.
2. *Cavitation-induced Reactions in High-Pressure Carbon Dioxide.* M.W.A. Kuijpers, D. van Eck, M.F. Kemmere, J.T.F. Keurentjes, Science, 2002, 298, 1969.
3. *Cavitation in Pressurized Carbon Dioxide: a Clean and Safe Way to Perform Reactions.* M.F. Kemmere, M.W.A. Kuijpers, D. van Eck, J.T.F. Keurentjes, NPT Procestechologie, 2003, 10, 23.
4. *Catalytic and Multiphase Reactors for the Future.* J.T.F. Keurentjes, E.L.V. Goetheer, F.C. Gielens, M.W.A. Kuijpers, J.H.M. Heijnen, L.J.P. van den Broeke, M.F. Kemmere, M.A.G. Vorstman, Chem. Eng. & Tech., 2003, 26, 835.
5. *Ultrasound-induced Polymerizations in High-Pressure Fluids.* M.W.A. Kuijpers, M.F. Kemmere, J.T.F. Keurentjes, 6th ISASF-meeting, Versailles (France), 2003, 1367.
6. *Ultrasound-induced Radical Polymerization.* M.W.A. Kuijpers, M.F. Kemmere, J.T.F. Keurentjes, in *Encyclopedia of Polymer Science and Technology*, Wiley, July 2004.
7. *Ultrasound-induced Polymerization of Methyl Methacrylate in Liquid Carbon Dioxide.* M.F. Kemmere, M.W.A. Kuijpers, L.J.M. Jacobs, J.T.F. Keurentjes, Macromol. Symp, 2004, 206, 321.
8. *The Mechanism of Cavitation-induced Polymer Scission*. M.W.A. Kuijpers, P.D. Iedema, M.F. Kemmere, J.T.F. Keurentjes, submitted to Polymer.
9. *Influence of CO_2 on Ultrasound-induced Polymerizations in High-Pressure Fluids.* M.W.A. Kuijpers, L.J.M. Jacobs, M.F. Kemmere, J.T.F. Keurentjes, submitted to AIChE Journal.
10. *Influence of the CO_2 Anti-Solvent Effect on Ultrasound-induced Polymer Scission Kinetics.* M.W.A. Kuijpers, R.M.H. Prickaerts, M.F. Kemmere, J.T.F. Keurentjes, submitted to Macromolecules.

11. *Cavitation Threshold in Gas-Expanded Liquids at Elevated Pressures.* M.W.A. Kuijpers, D. v. Eck, M.F. Kemmere, J.T.F. Keurentjes, submitted to J. Phys. Chem. A.
12. *Ultrasound-induced Ethylene Polymerizations*. M.W.A. Kuijpers, L.J.M. Jacobs, M.F. Kemmere, J.T.F. Keurentjes, in preparation.
13. *A novel Process for the Ultrasound-induced Radical Polymerization of MMA in Pressurized CO_2*. M.F. Kemmere, M.W.A. Kuijpers, R.M.H. Prickaerts, J.T.F. Keurentjes, in preparation.

Parts of the work described in this thesis have been presented at the following meetings: Annual AIChE Meeting (Reno, United States, 2001); Ultrasonics International Conference (Delft, The Netherlands, 2001); 8th Conference of the European Society of Sonochemistry (Villasimius, Italy, 2002); Workshop on Applications of Ultrasound Technology (Eindhoven, The Netherlands, 2002); 6th ISASF Symposium (Versailles, France, 2003); 30th Meeting of the Foundation of Emulsion Polymerization (Eindhoven, The Netherlands, 2003); 4th European Congress of Chemical Engineering (Granada, Spain, 2003); Polymer Reaction Engineering V (Quebec, Canada, 2003); Annual AIChE Meeting (San Francisco, United States, 2003); DECHEMA (Frankfurt, Germany, 2003); CERC3-Meeting (St. Malo, France, 2004); 9th Conference of the European Society of Sonochemistry (Badajoz, Spain, 2004).

About the Author

Martijn Kuijpers was born on November 20th, 1975 in Breda. In 1994 he graduated from the Katholieke Scholengemeenschap Etten-Leur (VWO high school). He subsequently started his university study in Chemical Engineering and Chemistry at the Eindhoven University of Technology. In August 1999 he graduated on the emulsion copolymerization in a pulsed packed column. The work was performed in the Process Development Group of prof. dr. ir. A.A.H. Drinkenburg. In October of that year he started his PhD-project in the Process Development Group at the Eindhoven University of Technology, supervised by dr. ir. M.F. Kemmere and prof. dr. ir. J.T.F. Keurentjes.